The Dissertation Committee for Matthew M. Ramsey Certifies that this is the approved version of the following dissertation:

The Effects of Polymicrobial Metabolism on Pathogenesis and Survival in *Aggregatibacter actinomycetemcomitans*

Committee:

Marvin Whiteley, Supervisor

Edward Marcotte

Richard Meyer

M. Stephen Trent

James Walker

The Effects of Polymicrobial Metabolism on Pathogenesis and Survival in *Aggregatibacter actinomycetemcomitans*

by

Matthew M. Ramsey, B.S.; M.S.

Dissertation

Presented to the Faculty of the Graduate School of

The University of Texas at Austin

in Partial Fulfillment

of the Requirements

for the Degree of

Doctor of Philosophy

The University of Texas at Austin

August, 2011

Dedication

This work is dedicated to the survivors of Hurricane Katrina and especially those who did not. Father and friends, you are truly missed. I can only hope that whatever life I have left will make you proud.

Acknowledgements

I would like to thank Marvin Whiteley for years of advice and an infinity of patience. I would also like to thank my parents for more things than I could ever write. I love you both. I thank my brother and sisters for being good examples and inspirations. I thank my friend Kelli Palmer, for always listening and being a constant source of encouragement. I thank Zach Stump and Marc Stoll for always being friends who kept me in touch with who I am as a person and not just a scientist; you both have my absolute trust and admiration. I thank my oldest friend Ryan Price, for keeping so many memories alive and for consistently proving that any friendship can be renewed with just a few words. I thank Stacie Brown for always being helpful when it counted, here's to another trip to Italy. I thank all of my professors and teachers along the way, I am grateful to have learned from all of you. To Aimee, Aishwarya, Apollo, Greg, Holly, Jeff, Katie, Lauren, Lindsay, Megan, Pete and Tina I thank all of you for not only for being great lab mates and coworkers, but for putting up with me as many times as you had to, especially Greg. I know it wasn't always easy. To Roxana, thanks for being such a bright spot in a difficult year, I love you. To everyone else I did not mention and should have, you have my apologies and gratitude. I've been nothing short of blessed to work with and be friends with as many good people as I have.

The Effects of Polymicrobial Metabolism on Pathogenesis and Survival in *Aggregatibacter actinomycetemcomitans*

Matthew M. Ramsey, Ph.D.

The University of Texas at Austin, 2011

Supervisor: Marvin Whiteley

In this dissertation I describe a model system to characterize the response of an oral bacterial pathogen, *Aggregatibacter actinomycetemcomitans* to the metabolic byproducts of a representative member of the oral flora, *Streptococcus gordonii*. *A. actinomycetemcomitans* is a causative agent of periodontal infections in humans. To cause infection, *A. actinomycetemcomitans* must overcome numerous challenges, including the host immune system and toxic metabolite production from other microbes. The most numerically dominant flora in the oral cavity are oral streptococci, which are well known for their ability to produce copious amounts of lactic acid and H_2O_2. By studying the response to H_2O_2 and lactic acid in pure and co-cultures, I have demonstrated that *A. actinomycetemcomitans* responds to these metabolites by several novel mechanisms that both enhance its survival in the presence of the host immune system and in the presence of the model oral streptococci *S. gordonii*. These studies have demonstrated that metabolites produced by normal flora can impact the survival of a single species *in vivo* as much as previously known virulence factors have done. In addition, I present a new method for measuring metabolite production in an attached cell population. This method is a novel application of scanning electrochemical microscopy (SECM) and I used this technique to study H_2O_2 production in the three dimensional space surrounding a multispecies biofilm in real time. In a related study I present the use of SECM to discover a novel redox chemistry phenomenon in the opportunistic pathogen *Pseudomonas aeruginosa*.

Table of Contents

List of Figures

Chapter 1: Introduction

1.1 *AGGREGATIBACTER ACTINOMYCETEMCOMITANS AND ITS ENVIRONMENT*

Properties of *Aggregatibacter actinomycetemcomitans*

A. actinomycetemcomitans is a Gram-negative, non-motile, facultatively anaerobic opportunistic pathogen of the mammalian oral cavity. *A. actinomycetemcomitans* was first isolated in 1912 and has been implicated as a causative agent of localized aggressive periodontitis [1, 2]. In addition to periodontal disease, *A. actinomycetemcomitans* has been detected in endocardial infections, and a correlation between periodontal health and endocardial infections has been observed [3]. *A. actinomycetemcomitans* is found primarily in the mammalian sub-gingival crevice and on the buccal epithelial cells and thought to compose part of the sub-gingival plaque in some individuals [4, 5]. *A. actinomycetemcomitans* is detected in a significant portion of individuals not symptomatic periodontal infections, but its numbers increase dramatically during periodontitis [2].

A. actinomycetemcomitans metabolism

A. actinomycetemcomitans is a facultative anaerobe that is able to utilize only a limited number of carbon sources. These carbon sources include glucose, fructose and L-lactate [6, 7], although lactate utilization had been debated in the literature previously [2, 6]. Glucose, fructose and lactate are present in gingival crevicular fluid (GCF) at millimolar concentrations and likely serve as *in vivo* carbon sources for *A. actinomycetemcomitans* [8]. Based on sequence data, *A. actinomycetemcomitans* is

predicted to utilize aerobic respiration. Anaerobically *A. actinomycetemcomitans* is a mixed acid fermenter of fructose [9] and likely other hexose sugars including glucose.

The sub-gingival crevice

The sub-gingival crevice, or gingival sulcus, is the area of the oral cavity where the tooth surface meets the gumline. This area is persistently colonized in healthy individuals primarily by Gram-positive facultative anaerobes and Gram-negative fusiform bacterium [4, 5]. These bacteria grow as biofilms and comprise what is known as the sub-gingival plaque, which is spatially and compositionally distinct from supra-gingival plaque [5]. The sub-gingival crevice is fed by the serum exudate gingival crevicular fluid, which contains carbohydrates and serum proteins such as complement and IgG [8, 10]. Often, bacteria of the sub-gingival plaque are present in healthy individuals, yet many have been shown to be involved in the transition to periodontitis.

Oxidative stress in *A. actinomycetemcomitans*

In the sub-gingival crevice, *A. actinomycetemcomitans* colonizes cell and tooth surfaces that are coated with a previously established bacterial plaque comprised of oral streptococci. Oral streptococci produce lactate and copious H_2O_2. Besides bacterially produced H_2O_2, *A. actinomycetemcomitans* encounters host-derived H_2O_2 due to neutrophil turnover [11]. *A. actinomycetemcomitans* engulfed by neutrophils will also have to tolerate additional reactive oxygen species and superoxide anions. To cope with oxidative stress, *A. actinomycetemcomitans* produces a cytoplasmic catalase (KatA) that has been shown to be the primary means for H_2O_2 resistance [12]. Additionally, *A. actinomycetemcomitans* contains both Cu-Zn and Mn superoxide dismutases to detoxify damaging superoxide free radicals. Previous data suggests that *A.*

actinomycetemcomitans is relatively resistant to phagocytic killing, and that superoxide dismutase activity may account for this resistance [13].

Periodontitis

Periodontitis is an inflammatory disease characterized by the loss of alveolar bone in a patient. Periodontitis is largely caused by bacterial infections and is preceded by gingivitis, an inflammation of the gum tissue. Typically a periodontal infection progresses as bacterial plaque, a multispecies attached, sessile "biofilm" community in the gingival crevice increases. The buildup of gingival plaque leads to local increases in inflammation that cause the redness and bleeding characteristic of gingivitis. Chronic inflammation leads to tissue destruction and bone desorption, ultimately leading to tooth loss [14]. During the transition from gingivitis to periodontitis, many Gram-negative species such as *A. actinomycetemcomitans* increase in number and produce virulence factors that can exacerbate the disease [2, 15, 16]. *A. actinomycetemcomitans* is particularly notorious due to its association with localized aggressive periodontitis, an acute form of periodontal infection that can manifest at a much earlier age than typically observed with periodontitis.

***A. actinomycetemcomitans* biofilm formation**

Biofilms are surface-attached cell populations encased in an extracellular matrix composed of exopolysaccharides, DNA, and proteins (reference). *A. actinomycetemcomitans* is a highly adherent bacterium that readily forms biofilms on an array of surfaces. This property can be attributed to a number of genes involved in attachment, invasion, and biofilm development. Biofilm formation is mediated by

fimbriae and pili, which are encoded by the *flp* and *tad* operons, respectively [16]. *A. actinomycetemcomitans* synthesizes a substantial amount of the exopolysaccharide poly-beta-1,6-N-acetyl-D-glucosamine (beta-1,6-GlcNAc; PGA) by products of the *pga*ABCD operon [17]. The *aae* gene product allows specific attachment to mammalian buccal epithelial cells, the *emaA* gene product facilitates attachment to collagen, and the *apiA* gene product, aids in autoaggregation, cell invasion, and resistance to host serum complement [16]. Together, these factors play likely confer a synergistic effect on resistance against host immunity.

1.2 POLYMICROBIAL ASPECTS OF PERIODONTAL DISEASE

Oral streptococci

The oral streptococci are some of the most numerous bacteria in the sub-gingival plaque and, with the exception of *Streptococcus mutans*, are thought to be primarily commensal or opportunistic pathogens. Oral streptococci are separated into 4 groups: mutans, salivarius, anginosus and mitis [18]. The mitis-group streptococci are the most numerous in the human oral cavity and colonize tooth epithelial cell surfaces in both the sub- and supra-gingival plaque. Unlike the mutans-group streptococci, mitis-group streptococci do not normally cause tooth decay, but are opportunistic pathogens that have been isolated from endocardial and septic infections [18]. Mitis-group streptococci, such as *Streptococcus gordonii*, are known for their ability to ferment sugars into lactic acid as well as generate H_2O_2 [19]. *S. gordonii* has also been shown to be one of the initial colonizers on the tooth surface by attachment studies on saliva-coated hydroxyapatite

surfaces. In addition, *S. gordonii* co-aggregates with other oral bacteria, notably *Fusobacterium nucleatum* and *A. actinomycetemcomitans* [20].

Multi-species biofilms and immune resistance

During some infections, bacteria persist as biofilms, which are more resistant to antibiotic therapy and host innate immune factors compared to planktonic cells [21, 22]. There is evidence that host mechanisms may attempt to limit biofilm development [23], and that initiation of terminal steps in acute inflammation may induce more robust biofilm formation in response [24]. It has also been proposed that biofilm growth allows for recruitment of phagocytic cells to infection foci but frustrates attempts at phagocytosis, which can cause damage to neighboring tissue due to phagocytic release of toxic products [21]. Another interesting observation is the presence of increased numbers of eosinophils in the sub-gingival crevice during periodontitis [25]. Eosinophils are typically recruited to sites of parasitic infection and are able to eliminate foreign organisms larger than themselves by extracellular secretion of toxic granules. This response may, in fact, be one way to deal with large multi-cellular biofilms, although this has not been studied in detail.

These results, combined with the fact that *A. actinomycetemcomitans* forms robust biofilms, raise the possibility that immune resistance of *A. actinomycetemcomitans* may be increased in the oral cavity by growth within biofilms. Notably, oral streptococci such as *S. gordonii* produce lactic acid, the preferred carbon source utilized by *A. actinomycetemcomitans* [7]. Thus, in addition to the obvious growth benefit to *A. actinomycetemcomitans*, mixed culture biofilms of *A. actinomycetemcomitans* and *S. gordonii* may further enhance the immune resistance of both species. *S. gordonii* may

growth may be enhanced by having *A. actinomycetemcomitans* in close proximity as it could detoxify H_2O_2 while not directly competing for hexose sugars. Additionally, it may be possible that *A. actinomycetemcomitans* anti-immune factors such as ApiA activity and production of a leukotoxin could afford cross-protection to *S. gordonii*. Such a possibility is attractive due to the fact that synergistic effects have been observed in multi-species biofilms previously [26, 27]. Both *in situ* and *in vitro*, species diversity in bacterial biofilms seems to correlate well with biofilm fitness. There may be other properties of biofilms that affect immune resistance, such as exopolysaccharide production and the possibility that inter-species quorum sensing increases biofilm formation and leukotoxin expression. These types of interactions have been observed in a previous study using *S. gordonii* and *Veillonella atypica* that demonstrated diffusible metabolites affect biofilm architecture and inter-species gene expression [28]. *S. gordonii* has also been shown to make co-culture biofilms with another periodontal pathogen, *Porphyromonas gingivalis*, which indicated wild-type biofilm architecture depends on the AI-2 quorum signal produced by both organisms.

1.3 IMMUNOLOGY OF PERIODONTITIS

Innate immunity in periodontitis

As gingival plaque proliferates, the host inflammatory response increases, causing the influx of innate immune factors such as serum complement and phagocytic cells, ultimately leading to gingivitis [10, 14]. Stimulation of the inflammatory response dictates that microbial flora in this environment respond to innate immune factors such as

complement and phagocytic cells. Alternative and classical complement activation can lead to the direct lysis and opsonization of Gram-negative bacteria or the opsonization of Gram-positive bacteria. In either pathway, serum proteins accumulate at the bacterial cell surface and aid the host in clearing bacteria by phagocytosis. *A. actinomycetemcomitans* posesses both the ability to block host opsonization and enter into host epithelial cells to prevent clearance by innate immunity [16]. These abilities likely help *A. actinomycetemcomitans* proliferate during periodontal infections [29].

A. actinomycetemcomitans produces multiple factors to resist host innate immunity

A. actinomycetemcomitans has been shown to be highly resistant to serum killing. One of the primary factors responsible for serum resistance is the *apiA* gene, which encodes for a 33kD protein that composes the trimeric outer membrane complex formerly known as omp100. ApiA has been shown to be expressed by *A. actinomycetemcomitans* in clinical samples, and heterologous expression in *E. coli* enhances serum resistance in that organism [30]. Mechanistically, ApiA binds the host complement regulatory protein factor H, which destabilizes the formation of C3 convertases at the bacterial cell surface. This function prevents further deposition of the C3b opsonin at the cell surface and also inhibits downstream effects of the complement cascade, such as membrane attack complex formation. Studies described in this dissertation and by others have demonstrated that increased ApiA production decreases *A. actinomycetemcomitans* killing by the alternative complement pathway [30, 31]. ApiA has also been shown to aid *A. actinomycetemcomitans* in translocation into epithelial cells, which would hypothetically allow *A. actinomycetemcomitans* to escape phagocytosis by host neutrophils.

Another method of innate immune evasion used by *A. actinomycetemcomitans* is dependent on the leukotoxin LtxA, an RTX toxin similar to *E. coli* α-hemolysin and *Mannheimia haemolytica* leukotoxin [32]. *A. actinomycetemcomitans* leukotoxin has been shown to kill human leukocytes, which should protect *A. actinomycetemcomitans* by destroying host phagocytic cells. At this time it is unclear to what extent leukotoxin expression affects *A. actinomycetemcomitans* pathogenesis and immune resistance, but there is a positive correlation between highly leukotoxic *A. actinomycetemcomitans* strains and more aggressive periodontal infections [33].

Notable aspects of innate immune defense by other oral microbes

Periodontal infections typically correlate with the presence of more than one species of periodontal pathogen. Quite often several pathogenic species are co-isolated from periodontal lesions and much effort has gone into characterization of different groups associated with periodontal infections. As periodontal infections increase in severity, the periodontal "pocket" or opening of gum tissue between the tooth and gums, deepens. As the "pocket" deepens, specific groups of pathogens are found together with a very high frequency. These pathogens include *Bacteroides forsythus*, *Porphyromonas gingivalis*, *Treponema denticola*, *Fusobacterium nucleatum*, *Prevotella intermedia*, *A. actinomycetemcomitans* and others [34].

Despite the fact that many of these organisms are well studied, the ways in which they evade the human immune system are mostly unknown. The ability of *A. actinomycetemcomitans* to evade complement lysis by *apiA* expression has been demonstrated [30, 31]. It has been shown that *P. gingivalis* uses membrane associated extracellular proteases, or Gingipains, to lyse numerous host targets [35]. Gingipains

have been shown to be significant for pathogenesis *in vivo*, where they may inhibit leukocyte activation [36]. Other proteases have also been identified that are useful for *P. gingivalis* pathogenesis [37]. In a similar manner, *P. intermedia* employs a cell-surface associated protease that degrades IgG in serum, which is thought to help assist in host immune resistance [38]. Additionally, *P. intermedia* can bind the Fc fraction of immunoglobulins, which can additionally confound the host immune response [39]. Several specific factors have been identified for the other organisms, most of which involve either cytolytic toxins or other extracellular proteases. It is likely that these organisms alone can initiate and maintain a periodontal infection with great difficulty; however, when present together in an infection site may enjoy a synergistic resistance to host immunity.

1.4 *STREPTOCOCCUS GORDONII* AND H_2O_2 MEASUREMENT

Common methods for measurement of H_2O_2

As mentioned, oral streptococci produce H_2O_2, and this potent metabolic ability is thought to function as a way to limit competition for resources in the oral cavity. Oral streptococci can inhibit neighboring organisms and by doing so also may inhibit select periodontal pathogens, especially of the strict anaerobe variety, from forming an infection foci [40]. The measurement of H_2O_2 has been performed by a few techniques, namely fluorometric and colorimetric reagent assays as well as direct absorbence measurements at 330 nm [41]. Fluorometric assays for H_2O_2 are rapid, cheap and sensitive compared to direct absorbance. However all of these techniques require either an aliquot of sample to

be removed or the presence of a dye substrate within the sample. Such constraints are detrimental to measuring H_2O_2 in real-time.

One method utilized for H_2O_2 measurement in real-time is electrochemical detection [42-47]. Electrochemical detection involves the use of a conducting surface held at a potential that is set based on the oxidation or reduction potential of the substrate of interest. The current, or flow of electrons, to or from the surface is measured and calibrated back to a standard curve of current yielded from known concentrations of the substrate. This allows for near instantaneous detection of H_2O_2 in solution and can be used to study H_2O_2 production in real time.

Scanning electrochemical microscopy

To study the production of H_2O_2 by *S. gordonii* biofilms, we used an application of electrochemical detection known as scanning electrochemical microscopy (SECM). SECM is a sensitive and non-invasive technique that allows us to measure H_2O_2 concentration in real-time and 3 dimensional space, unlike previously described techniques. SECM uses the properties of electrochemical detection, current changes at an electrode by oxidation or reduction of a substrate, and couples these properties to a 3-dimensional manipulator (Figure 1.1). To enhance resolution, an ultramicroelectrode (UME) is used instead of much larger electrodes often used for electrochemical studies. The UME employed in our experiments is 25 μm in diameter, similar to the size of many UMEs. By slaving electrochemical detection to 3-dimensional control, it is possible to measure substrate concentration in real-time in 3 dimensions around a sample. Thus, the production of metabolites and metabolite flux can be measured as other compounds are introduced into the system. This method of detection was the primary method used in a collaborative study in chapters 4 and 5.

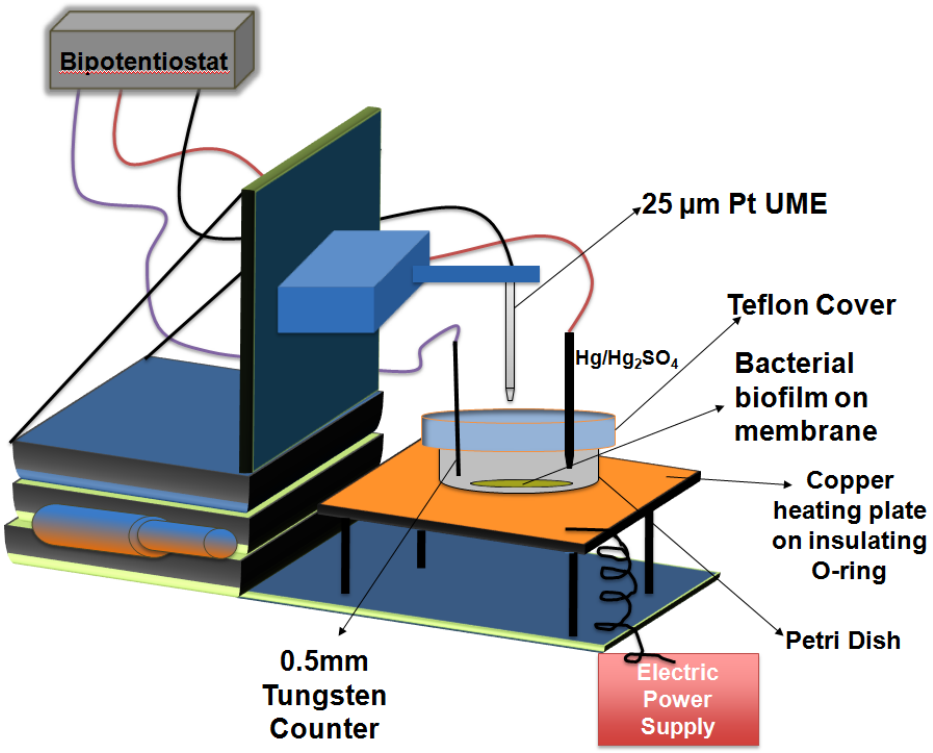

Figure 1.1. A representative SECM apparatus, adapted from [48].

1.5 DISSERTATION OBJECTIVES

In this dissertation I sought to characterize how an invading pathogen, *A. actinomycetemcomitans*, can co-exist and/or compete with numerically dominant oral streptococci using *S. gordonii* as a representative model organism. The actual number of polymicrobial interactions that can occur between *A. actinomycetemcomitans* and the host oral flora is nearly infinite in number. Thus, by taking a reductionist approach I have endeavored to explain how *A. actinomycetemcomitans* could thrive in the face of bacterial competitors. As oral streptococci comprise a majority of the population in the subgingival crevice where *A. actinomycetemcomitans* is found, I proposed that oral strepcoccci metabolite production would be a significant factor that *A.*

actinomycetemcomitans must respond to. By observing the response of *A. actinomycetemcomitans* to the two primary oral streptococci metabolites L-lactate and H_2O_2, I was able to demonstrate several unique facets of *A. actinomycetemcomitans* physiology and immune resistance.

Chapter two details the *A. actinomycetemcomitans* response to *S. gordonii*-produced H_2O_2. In this chapter I present entirely novel data demonstrating that *A. actinomycetemcomitans* responds to H_2O_2 by upregulating genes whose products serve to detoxify H_2O_2 and also increase the resistance of *A. actinomycetemcomitans* to host innate immune factors. The microbial induction of factors for innate immune resistance is a novel finding that may have implications for many other polymicrobial infection sites.

Chapter three studies carbon source metabolism in *A. actinomycetemcomitans* and elaborates on previous work in our laboratory conducted by Dr. Stacie Brown. In this chapter I demonstrate that the preferential use of L-lactate by *A. actinomycetemcomitans* has implications for survival *in vivo*. I also demonstrate that the L-lactate preference of *A. actinomycetemcomitans* is maintained only in the presence of O_2 and is due to O_2 reduction by the CydAB cytochrome oxidase. A major revelation from this study was that *A. actinomycetemcomitans* does not require L-lactate catabolism to survive *in vivo*, however it is crucial for its survival when oral streptococci are present. These novel findings have implications for drug targets and treatment strategies for polymicrobial infections.

Chapter four is the result of a collaborative effort between Dr. Alan Bard's laboratory at the University of Texas Department of Chemistry and our own. We utilized

the scanning electrochemical microscopy (SECM) technique for the 1st time in history to observe metabolite production directly from a bacterial biolfilm. Dr. Bard's laboratory provided the SECM collection data, and I prepared all biological samples, media and assisted in experimental design. This study measured H_2O_2 production from a *S. gordonii* biofilm and demonstrated that H_2O_2 concentrations in close proximity to the biofilm were almost 100x greater than those in bulk phase solution surrounding the biofilm. This study is the first of its kind to directly measure H_2O_2 production from living bacterial cells in close proximity and in real-time. We also demonstrated that the addition of *A. actinomycetemcomitans* in co-culture was sufficient to remove most H_2O_2 produced by adjacent *S. gordonii*.

Chapter five extends the collaboration in chapter four and applies SECM technology to another biofilm-forming bacterium, *Pseudomonas aeruginosa*. It bears mentioning that this work has no relation to oral microbiology but stemmed from our initial collaboration of using SECM on bacterial biofilms. Our primary goal was to study the production of the quorum sensing regulated molecule pyocyanin by *P. aeruginosa*. Our studies demonstrated that pyocyanin, a long recognized antimicrobial, exists almost entirely in a reduced form near actively respiring *P. aeruginosa* biofilms. We demonstrated that this reduced form of pyocyanin was able to generate large amounts of soluble Fe (II) even in the presence of O_2. This has immediate clinical relevance as Fe acquisition by pathogens is a key factor for establishing an infection. Additionally we demonstrated that certain respiratory chain components were necessary for reduced pyocyanin production and that the inhibitions of these components lead to a decrease in Fe (II) production.

Chapter 2: Multispecies interactions stimulate resistance to human innate immunity through metabolite perception[1]

2.1 INTRODUCTION

The Gram-negative bacterium *Aggregatibacter actinomycetemcomitans* is a common commensal of the human oral cavity and is a causative agent of localized aggressive periodontitis [1]. *A. actinomycetemcomitans* inhabits the mammalian oral cavity beneath the gum line in an area between the tooth surface and the gingival epithelium known as the sub-gingival crevice [49]. A consistent supply of nutrients is provided to the sub-gingival crevice by a serum exudate referred to as crevicular fluid [10] that passes through the gingiva and flows along the teeth [8, 50-52]. Oxygen levels within the sub-gingival crevice vary greatly, from microaerophilic conditions (2.1 kPa) in the 'moderate' pockets (5-6 mm in depth) to near anaerobic conditions (1.6 kPa) in the 'deep' pockets (>6mm in depth) [53]. *A. actinomycetemcomitans* resides in the moderate pockets of the sub-gingival crevice and exhibits enhanced growth under microaerophilic conditions [54].

The mammalian oral cavity is home to a robust microbial community composed of many specialized microbes that are well-adapted to growth in this environment. As with many complex communities, interactions between individual community members in the oral cavity significantly impact phenotypic aspects of the individuals as well as the

[1] Ramsey, M.M. and M. Whiteley, *Polymicrobial interactions stimulate resistance to host innate immunity through metabolite perception*. Proc Natl Acad Sci U S A, **2009**. 106(5): p. 1578-83.

group [20]. When *A. actinomycetemcomitans* is present it grows in the sub-gingival plaque which includes several species from the genus *Streptococcus*, including *S. oralis*, *S. sanguis*, *S. mitis* and *S. gordonii* [5, 20, 29, 55]. These oral streptococci are typically non-pathogenic and rapidly consume sugars within the sub-gingival crevice producing the metabolites lactic acid and hydrogen peroxide (H_2O_2). This physiological ability renders oral streptococci extremely competitive in the oral environment as they consume high energy carbon sources and excrete metabolites that inhibit growth of neighboring microbes [56].

Our laboratory has pursued the idea that since it co-habitates environments with oral streptococci [5, 29], *A. actinomycetemcomitans* has adapted survival strategies for exposure to lactic acid and H_2O_2. Indeed, previous studies demonstrated that *A. actinomycetemcomitans* preferentially utilizes lactic acid over high energy carbon sources such as glucose, despite the fact that this bacterium grows significantly more slowly with lactic acid [7]. The ability to utilize lactic acid preferentially not only eliminates caries-causing lactic acid from the oral environment but also eliminates the need for *A. actinomycetemcomitans* to compete with the more numerous and rapidly growing oral streptococci for carbon [20]. Instead, *A. actinomycetemcomitans* has evolved to utilize the streptococcal metabolic waste product lactic acid for carbon and energy.

Although our previous studies provided insight into the *A. actinomycetemcomitans* response to lactic acid, essentially nothing is known about how *A. actinomycetemcomitans* responds to the other primary metabolite of streptococci, H_2O_2. In this study, we examined the *A. actinomycetemcomitans* response to H_2O_2 by performing a transcriptome analysis of *A. actinomycetemcomitans* biofilms exposed to

H_2O_2. In sharp contrast to other bacterial species, only two *A. actinomycetemcomitans* genes, *katA* and *apiA*, were differentially regulated upon H_2O_2 exposure. In addition, these genes were regulated in a H_2O_2-dependent fashion during co-culture with the oral bacterium *S. gordonii*. Induction of the outer membrane protein ApiA during co-culture provided protection of *A. actinomycetemcomitans* from killing by human serum. Mechanistically, this enhanced protection was enacted by increased binding of the serum protein factor H by ApiA. These results indicate that bacterial resistance to killing by host innate immunity is enhanced during co-culture and suggest that *A. actinomycetemcomitans* utilizes a streptococcal metabolite as a cue to an impending immune response.

2.2 MATERIALS AND METHODS

Strains and media

A. actinomycetemcomitans strains VT1169 [57], Y4 [12], *Streptococcus gordonii* strain Challis DL1.1 (ATCC 49818), *E. coli* DH5α, and *E. coli* SM10 were used in this study. *A. actinomycetemcomitans* strains were grown in Brain Heart Infusion (BHI) medium, Tryptic Soy Broth + 0.5% Yeast Extract (TSBYE) or Chemically Defined Medium (CDM) with 20 mM glucose [7]. Culture conditions were at 37ºC in a 10% CO_2 atmosphere with shaking at 165 RPM unless otherwise indicated. *E. coli* strains were grown on Luria-Bertani (LB) medium at 37ºC. Where applicable, antibiotics were used at the following concentrations: Chloramphenicol 2 μg/ml for selection and maintenance in *A. actinomycetemcomitans*, 20 μg/ml for selection and maintenance in *E. coli*. In both *A. actinomycetemcomitans* and *E. coli*, spectinomycin was used at 50 μg/ml for selection and 10 μg/ml for maintenance, and streptomycin was used at 50 μg/ml for selection and 20 μg/ml for maintenance.

DNA and plasmid manipulations

DNA and plasmid isolations were performed using standard methods [58].

GeneChip and RT-PCR analysis

For flowcell biofilm experiments, cells were grown in 20% TSBYE medium in a once-flow-through biofilm flowcell as described in [59]. Biofilms were allowed to mature for 18 hours, and then TSBYE, with or without 1 mM H_2O_2, was added for 30 min. To harvest biofilm cells, the coverslip was removed from the flowcell with a razorblade and vortexed for 1 min in 20ml of RNALater to remove attached cells. For colony biofilms,

10^5 cells were spotted onto a UV sterilized 0.2 μm polycarbonate membrane on 10 ml CDM solid medium containing 1.5% agarose in a 100 mm Petri dish. Cells were then grown for 32 hours at 37ºC in a 10% CO_2 atmosphere. The membranes were transferred to identical Petri plates and incubated for 2 h before being transferred to another Petri plate containing CDM with or without the addition of 1 mM H_2O_2. After 20 min, the membranes were transferred into 20 ml of RNALater. Cells were harvested from the membranes by gentle vortexing in the RNALater solution for ~2 min until no cells visibly remained on the membrane. RNA isolation, preparation of labeled cDNA, and processing of the *A. actinomycetemcomitans* GeneChip microarrays was performed as described previously [60]. Data analysis was performed using GeneChip Operating Software version 1.4 (GCOS). RT-PCR was performed as described [59] with the following changes: 100 ng of RNA was used for cDNA synthesis; 1 ng of cDNA was used as a template in the *katA* and *apiA* PCR reactions; and 5 ng of cDNA was used as a template in the *clpX* PCR reaction. RT-PCR primers are included in SI Text. Planktonic *A. actinomycetemcomitans* were grown to mid-exponential phase (A_{600} = 0.4) and mixed 1:1 with RNALater prior to RNA purification.

Primer extension

Primer extension was performed as previously described [61]. Primers used were *apiA*-PE (5' – tctttagcccaatgcattgacaga – 3') and *katA*-PE (5' – catggtgttgtcattatcca – 3'). The sizes of primer extension products were determined at the University of Oklahoma Health Science Center sequencing core facility.

Luminescence reporter assays

10^7 *A. actinomycetemcomitans* carrying either the *apiA-luxCDABE* or *katA-luxCDABE* reporter were spread evenly over the surface of a TSBYE agar plate and grown overnight at 37ºC. Two 0.6 cm paper discs containing 10^7 *S. gordonii* were added to each *A. actinomycetemcomitans* coated TSBYE agar plate. 1 disc received 10,000 U of bovine catalase (Sigma) and the other disc received 10,000 U of heat killed catalase. The plates were incubated for an additional 4 h at 37ºC prior to imaging each for 15 min with a Syngene G:Box (Syngene) imaging system.

***luxCDABE* reporter fusion construction**

To study *katA* and *apiA* promoter activity in *A. actinomycetemcomitans*, the vectors pMR310-*katA* and pMR310-*apiA* were constructed. pMR310 incorporates a 5.8 kb region containing the *Photorabdus luminescens luxCDABE* operon from the vector pCGLS1 [62]. This region was PCR amplified with the addition of BamHI, NotI restriction sites at the 5` end and a SalI site at the 3` end. Transcriptional TGA stop codons were also added to the 5` primer in all 3 frames using the following primers: LuxCE-for (5'- atacgggccgctgaatgaatgaggcaaatatgactaaa-3') and LuxCE-rev (5'-acgcgtcgacatatcaactatcaaacgcttcgg-3'). This promoterless fragment was cloned into the BamHI and SalI restriction sites in the spectinomycin resistant cloning vector pDMG4 [63], creating the promoterless *luxCDABE* expression vector pMR310. The *A. actinomycetemcomitans katA* promoter region was PCR amplified with the addition of the BamHI and NotI restriction sites at the 5` and 3` ends, respectively, using the primers katApro-5' (5'- cgggatcctaatcggtcagaaaaaacaccgt-3') and katApro-3' (5'-ataagaatgcggccgcgctgacataatcgtttccttaat-3'). The *apiA* promoter region was amplified with identical restriction sites using the primers apiApro-5' (5'-

cgggatccctcggcaggtaactattttaacc-3') and apiApro-3' (5'-ataagaatgcggccgcgcaacgaggtggtgtttaaataa-3'). Amplified fragments were restriction digested and ligated into pMR310 to create the *katA* reporter vector pMR310-*katA* and *apiA* reporter vector pMR310-*apiA*. Plasmids were transformed into *E. coli* DH5α cells and then electroporated into *A. actinomycetemcomitans* [64].

Construction and complementation of an *oxyR*- mutant in *A. actinomycetemcomitans*

Construction of the *oxyR*⁻ mutant was performed as previously described [7] using the primers oxyRKO-for (5'- cggaattcggattcttgtcatgtaagccaac-3') and oxyRKO-rev (5'-cggaattcgttggacttcaataaaggcttca-3') to amplify a 413bp internal fragment of the *oxyR* gene. This fragment was digested with EcoRI and ligated into the suicide plasmid pVT1461 [65] to generate the vector pVT1461-oxyRko. Plasmids were transformed and screened as described [7], and insertion into *oxyR* was confirmed using PCR. Complementation of *oxyR in trans* was performed using the *A. actinomycetemcomitans* streptomycin resistant expression vector pYGS [66]. The 1068bp *oxyR* containing fragment was amplified using the primers oxyRPro-full-for (5'-cccaagcttccatattagacatgatttttctcc-3') and *oxyR*-full-rev (5'-cggaattcccattaagaagataagatagatttaacc-3') and cloned into HindIII/EcoRI digested pYGS to yield the complement vector pYGS-OxyRC, which was introduced into *A. actinomycetemcomitans* by electroporation. Construction of the constitutive *apiA* expression vector was carried out using the primers and methods given by Yue *et al* [67].

Serum sensitivity and factor H binding

For all serum sensitivity assays, bacteria were grown in 10% CO_2. Fig. 2.6 experiments were carried out under microaerophilic conditions. Microaerophilic medium was prepared by injecting 10 ml of aerobic BHI broth into rubber-stopper sealed Balch tubes and flushed with N_2 gas. Cultures were allowed to grow overnight and then diluted at least 1:5 into N_2 flushed Balch tubes containing 4 ml BHI broth. Cultures were grown two hours to an A_{600} of 0.2 for *A. actinomycetemcomitans* and 0.4 for *S. gordonii* prior to treatment. 200 µl of 5000 U/ml catalase (Sigma) or catalase that had been boiled for 10 min @ 95 ºC (heat inactivated) was added to an N_2 flushed sealed Balch tube. Two ml of *S. gordonii* culture or 2 ml sterile media was then added to each tube. Two ml *of A. actinomycetemcomitans* culture was added to each tube and incubated at 37ºC for 15 min. Another 200 µl of heat-inactivated or untreated 5000 U/ml catalase was added to each culture and allowed to incubate for an additional 15 min. An equal volume of normal human serum (2 ml) (Valley Biomedical) or complement-inactivated serum was added to each culture and allowed to incubate for 2 h. 1 ml of culture was removed prior to serum addition for factor H staining and 1 ml was removed for serial dilution and plate counting. Cells removed for factor H staining were collected by centrifugation at 5,000xg for 10 minutes and cell pellets were resuspended in 100% ice-cold methanol and fixed at -20ºC for 2 h. After fixing, cells were stained as described in [68] using 1:1000 mouse anti-human factor H antibody (Santa Cruz Biotechnology) and 1:1000 Alexa-488 goat anti-mouse (Invitrogen) secondary antibody. Images were captured at 1000x magnification using a Nikon 50i microscope, 100x 1.4NA PLAN APO lens and Nikon DS-2MBW digital camera and Nikon NIS-Elements D 3.0 software.

2.3 RESULTS

A. actinomycetemcomitans transcriptional response to H_2O_2

For gene expression analyses, *A. actinomycetemcomitans* was grown in a liquid-phase once flow-through biofilm flowcell [69] and a solid phase membrane-associated colony biofilm [70]. A custom Affymetrix GeneChip microarray [7] was used to monitor gene expression of *A. actinomycetemcomitans* biofilms in the presence or absence of a sub-lethal concentration of H_2O_2. Of the approximate 1800 genes (>90% of the total genes in *A. actinomycetemcomitans*) that exhibited detectable expression on the GeneChip, only two showed statistically significant, reproducible changes in both models upon H_2O_2 exposure (Fig. 2.1A), and these results were verified using reverse transcription PCR (Figure 2.1B). This is in stark contrast to similar studies with other bacteria in which 140-520 genes were differentially expressed upon H_2O_2 exposure [71-76].

The *katA* gene, which encodes a cytoplasmic catalase (KatA) that directly detoxifies H_2O_2 into O_2 and H_2O, was significantly up-regulated in *A. actinomycetemcomitans* biofilms upon exposure to H_2O_2. This was not surprising as *katA* homologs in other bacteria are induced upon exposure to H_2O_2 [71, 73, 76]. More surprising was the H_2O_2-mediated induction of *apiA*. ApiA is a 33kD trimeric outer membrane protein (also referred to as Omp100) [77] that is 55% identical (using pairwise pBLAST) to the non-fimbrial adhesin protein YadA in *Yersinia pestis* and *Yersinia enterolitica* [78]. Similar to YadA function in *Yersinia*, ApiA stimulates *A. actinomycetemcomitans* auto-aggregation, assists translocation into host cells, and binds the human serum protein factor H [30, 67]. Binding factor H inhibits serum complement activity and protects *A. actinomycetemcomitans* from killing by the alternative

complement pathway [30]. Although similar in function, *yadA* and its homologues in other organisms have not been shown to be induced by H_2O_2 at this time.

A **Colony Biofilms**

Fold Change	St. Dev.	ORF #	Description
7.2	1.6	AA0223	catalase *(katA)*
7.0	1.3	AA2485	adhesin invasin, putative *(apiA)*

Flowcell Biofilms

Fold Change	St. Dev.	ORF #	Description
11.1	1.5	AA0223	catalase *(katA)*
6.4	1.1	AA2485	adhesin invasin, putative *(apiA)*

B

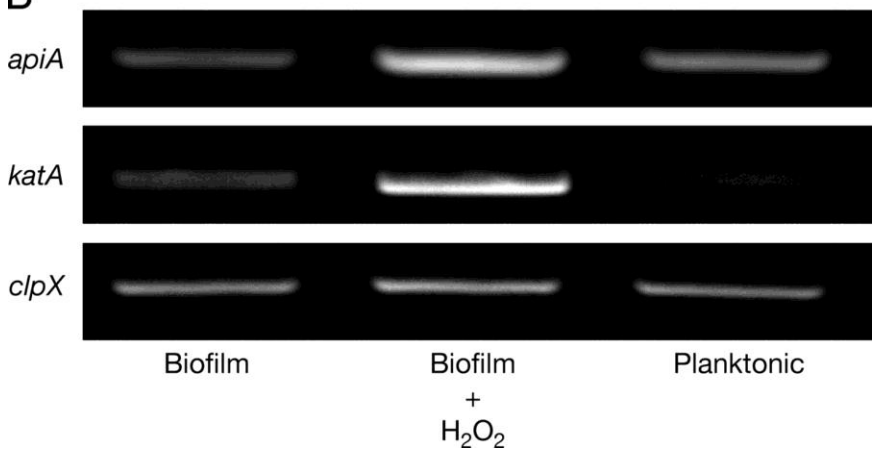

Figure 2.1. A. *actinomycetemcomitans katA* and *apiA* are induced on H_2O_2 exposure

(A) A custom Affymetrix GeneChip was used to examine gene expression of *A. actinomycetemcomitans* colony and flow cell biofilms in the presence and absence of 1 mM exogenous H_2O_2. Fold changes were determined from 4 pairwise comparisons and determined to be statistically different for *katA* and *apiA* ($P < 0.05$) using GeneChip Operating Software version 1.4. (B) RT-PCR was used to verify *katA* and *apiA* induction in colony biofilms on following exposure to H_2O_2. The constitutively expressed gene *clpX* was used to standardize cDNA template levels, and planktonic-grown bacteria were used to assess the impact of enhanced aeration on basal transcript levels.

katA and *apiA* are induced during co-culture with *S. gordonii*

Although our results clearly show induction of *katA* and *apiA* by direct addition of the streptococcal metabolite H_2O_2, it was not clear if these genes were inducible during co-culture with oral streptococci. To examine this, transcriptional fusions of the promoter regions of *katA* and *apiA* with the luminescence reporter genes *luxCDABE* were constructed. These reporter fusions allow for the transcriptional activity of *katA* and *apiA* to be assessed by monitoring light production. To examine the impact of oral streptococci on *katA* and *apiA* transcription, *A. actinomycetemcomitans* carrying *katA-luxCDABE* and *apiA-luxCDABE* were spread on agar plates and light production examined upon exposure to discs containing the oral streptococci *S. gordonii*. To ensure that any luminescence induction was due to *S. gordonii* H_2O_2 production, 10,000 units of exogenous catalase (or heat inactivated catalase as a control) was added to each disc. The presence of *S. gordonii* elicited an increase in both *katA* and *apiA* expression by *A. actinomycetemcomitans* (Fig. 2.2). This induction was dependent on H_2O_2 as addition of exogenous active catalase mitigated this response (Fig. 2.2). Induction of each reporter was also observed in planktonic co-culture (Fig. 2.3).

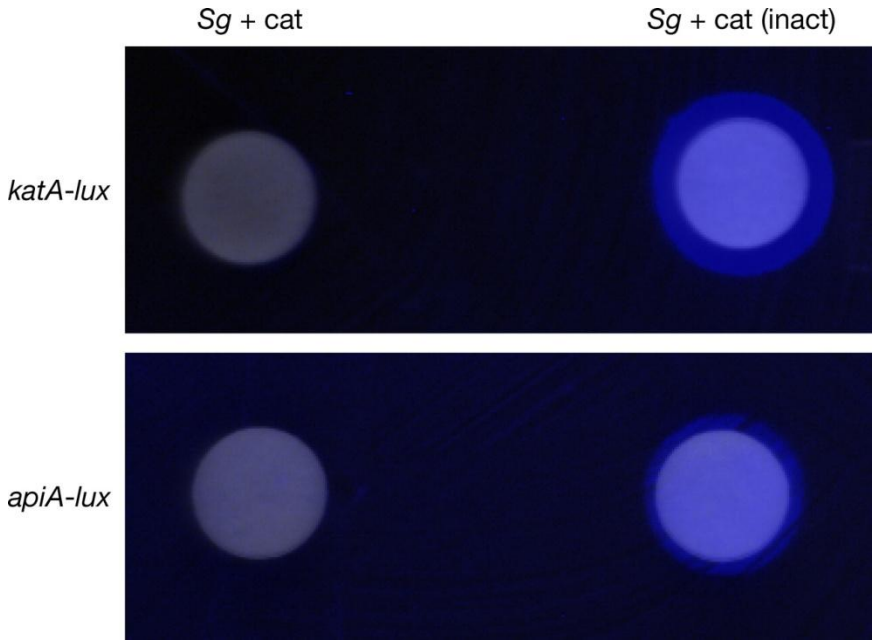

Figure 2.2. *katA* and *apiA* are induced during coculture with *S. gordonii*

A. actinomycetemcomitans containing the *katA-luxCDABE* or *apiA-luxCDABE* reporter fusion was spread on agar Petri plates and exposed to *S. gordonii*–soaked disks containing active catalase (*Sg* + cat) or heat-inactivated catalase (*Sg*). Light production was examined using a Syngene imaging system. The image is a composite of visible light and luminescence (blue) photographs. Sterile paper disks did not induce light production by either reporter fusion (not shown).

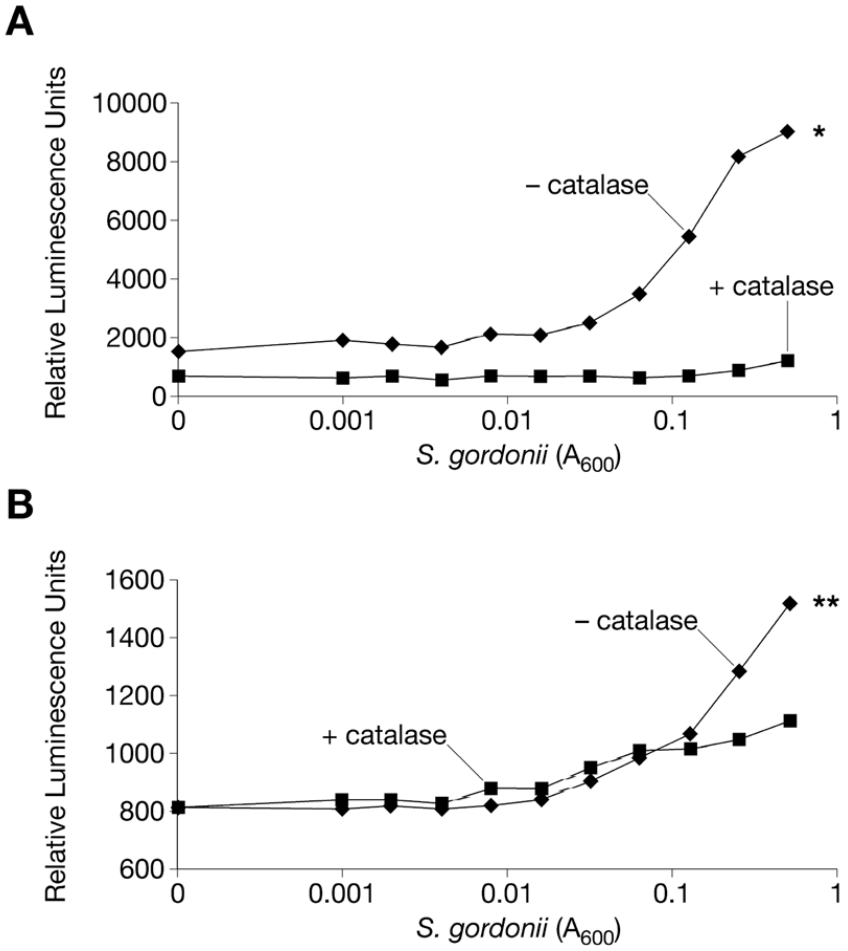

Figure 2.3. Quantification of *katA* and *apiA* induction in co-culture

Light production (relative luminescence units) by *A. actinomycetemcomitans* carrying *katA-luxCDABE* (A) or *apiA-luxCDABE* (B) during coculture with differing concentrations of *S. gordonii* in the presence of heat-inactivated (- catalase) or active catalase (+ catalase). SEM was < 6% for all measurements and error bars were omitted for clarity. *P < 0.0007, **P < 0.01 via Student's t test, n = 4

OxyR is required for H_2O_2-mediated induction of *katA* and *apiA*

Many H_2O_2 responsive promoters possess operator sequences that bind the LysR-type transcriptional regulator OxyR [79]. OxyR exhibits DNA binding activity after oxidation of two reactive cysteine residues by H_2O_2 and can act as an inducer or a

repressor of transcription. The *A. actinomycetemcomitans* genome contains an *oxyR*-like sequence (ORF AA1513) that putatively encodes a protein with 72% identity (assessed by pairwise pBLAST) to *Escherichia coli* OxyR and shows conservation of both reactive cysteine residues (C199, C208). To determine if the *katA* and *apiA* promoter regions contain potential OxyR binding sequences, primer extension was used to map the transcriptional start sites of these genes. The results indicate that the promoters of *katA* and *apiA* possess sequences, centered 46.5 and 58 bp upstream of the transcriptional start sites respectively (Fig. 2.4 A&B), with significant similarity to the consensus OxyR binding sequence (Fig. 2.4 C), ATAG-n7-CTAT-n7-ATAG-n7-CTAT [80, 81]. These sequences suggested that OxyR was a regulator of *katA* and *apiA* transcription. To test this, *oxyR* was insertionally inactivated in *A. actinomycetemcomitans* and transcript levels of *apiA* and *katA* were measured in response to H_2O_2. Inactivation of *oxyR* abrogated the induction of *apiA* and *katA* by H_2O_2, and this activation was restored by expression of *oxyR in trans* (Fig. 2.5 A&B insets).

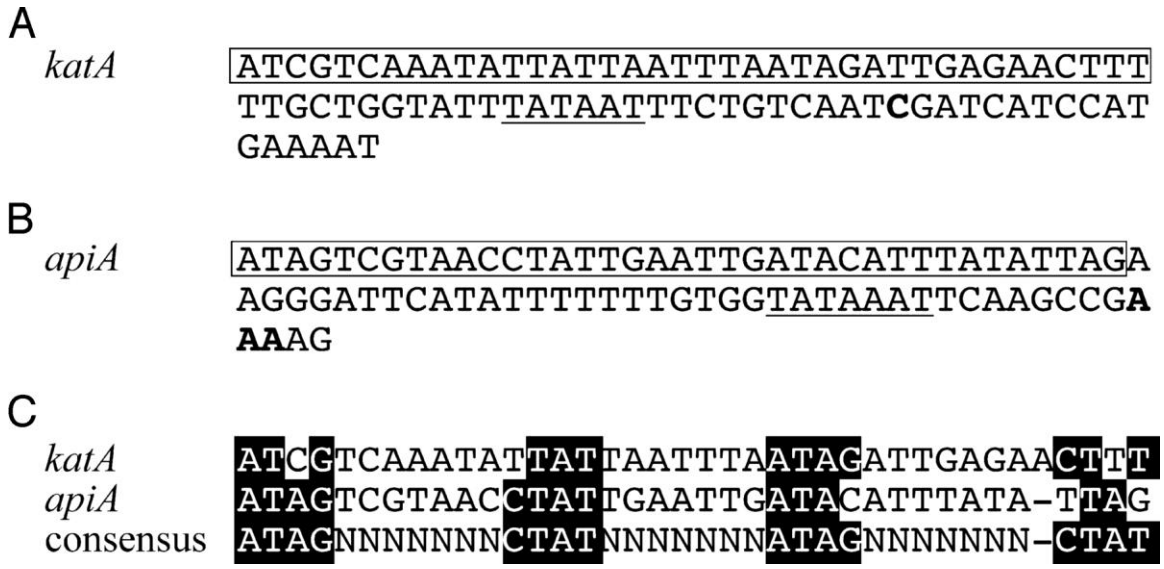

Figure 2.4. DNA sequences of the *katA* (base pairs 154293–154374) (A) and *apiA* (base pairs 1724157–1724078) (B) promoter regions

Transcription start sites are in boldface, putative −10 regions are underlined, and *oxyR*-like binding elements are boxed. (C) Alignment of the putative *katA* and *apiA* OxyR binding sequences with the consensus binding sequence [80, 81].

OxyR is critical for resistance to H_2O_2 and human serum

Based on the observation that OxyR regulates *katA* and *apiA*, we hypothesized that inactivation of *oxyR* would have a profound effect on *A. actinomycetemcomitans* survival upon exposure to H_2O_2 or human serum. To test this hypothesis, we measured the survival of wild-type *A. actinomycetemcomitans* and the *oxyR*$^-$ mutant following exposure to H_2O_2 and human serum. Deletion of *oxyR* significantly decreased survival of *A. actinomycetemcomitans* upon exposure to H_2O_2 and human serum and expression of *oxyR in trans* restored survival to wt levels (Fig. 2.5 A&B). While it is clear that *katA* is a critical component of H_2O_2 resistance in numerous bacteria [71-76, 80], it was not known

if the decrease in serum resistance was due to decreased levels of *apiA*. To test this possibility, *apiA* was constitutively expressed in the *oxyR*$^-$ mutant [67]. Constitutive expression of *apiA* restored serum survival of the *oxyR*$^-$ mutant to wildtype levels (Fig. 2.5 B), suggesting that *apiA* deregulation was responsible for enhanced serum killing in this mutant. As expected, expression of *apiA* had no effect on the sensitivity of the *oxyR*$^-$ mutant to H_2O_2 (data not shown). These results demonstrate that the oxidative stress regulator OxyR is necessary for induction of a gene involved in complement defense in *A. actinomycetemcomitans*.

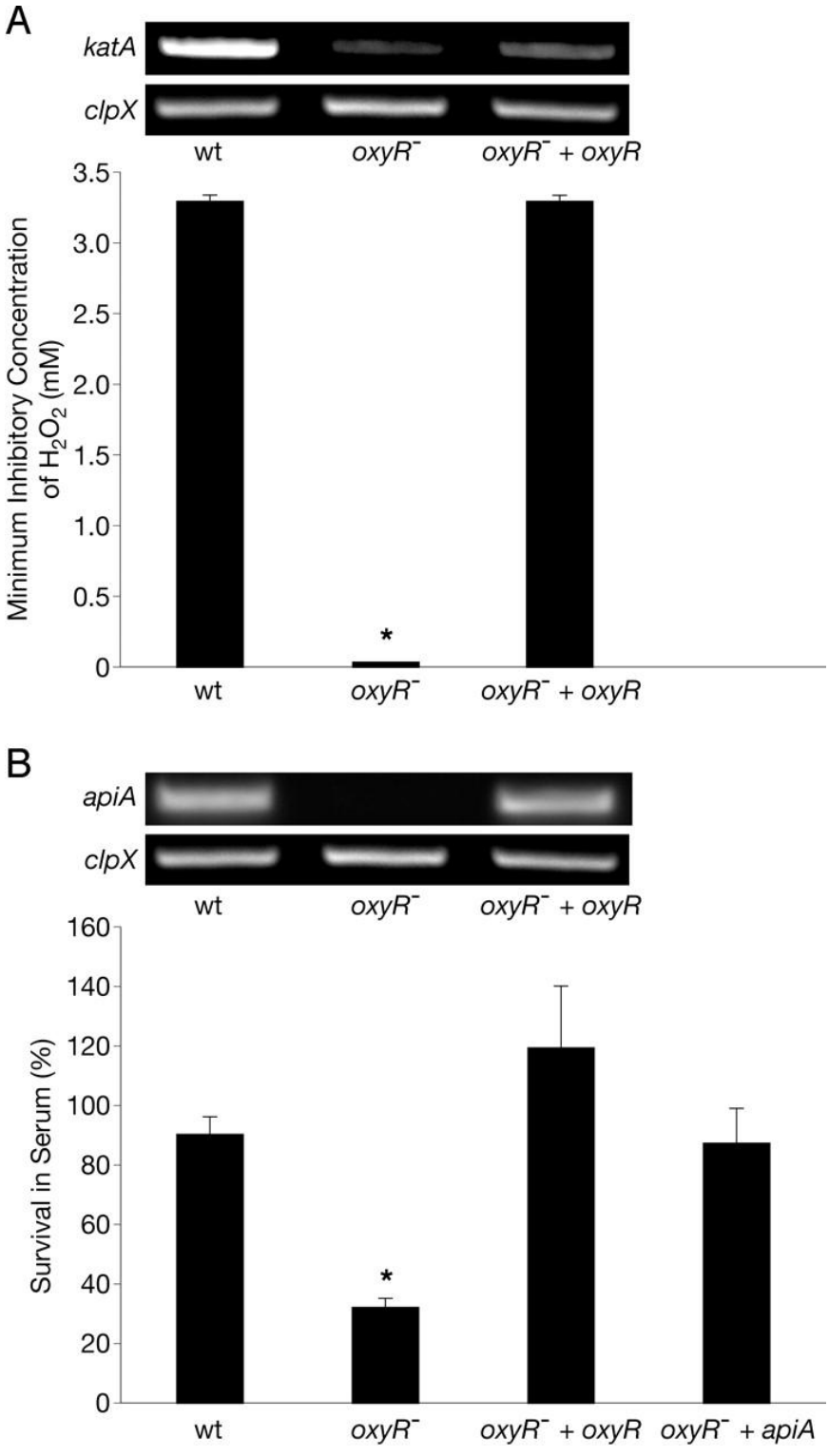
A
katA
clpX
wt
oxyR⁻
oxyR⁻ + oxyR
Minimum Inhibitory Concentration of H2O2 (mM)
3.5
3.0
2.5
2.0
1.5
1.0
0.5
0
*
wt
oxyR⁻
oxyR⁻ + oxyR
B
apiA
clpX
wt
oxyR⁻
oxyR⁻ + oxyR
Survival in Serum (%)
160
140
120
100
80
60
40
20
0
*
wt
oxyR⁻
oxyR⁻ + oxyR
oxyR⁻ + apiA

Figure 2.5. The *A. actinomycetemcomitans oxyR*− mutant is hypersusceptible to killing by H_2O_2 and human serum

(A) The H_2O_2 minimum inhibitory concentration (lowest concentration necessary to inhibit visible growth of an organism) of WT *A. actinomycetemcomitans* (wt), the *A. actinomycetemcomitans oxyR*− mutant (*oxyR*−), and the genetically complemented *A. actinomycetemcomitans oxyR*− mutant (*oxyR*− + *oxyR*). (Inset) RT-PCR analysis of mRNA levels of *katA* and the *clpX* constitutively expressed control in the wt *oxyR*−, and *oxyR*− + *oxyR* after H_2O_2 exposure. (B) Survival of wt, *oxyR*−, *oxyR*− + *oxyR*, and *oxyR*− constitutively expressing *apiA* (*oxyR*− + *apiA*) in the presence of 50% (vol/vol) normal human serum. Percent survival was calculated as follows: number of cells recovered from normal human serum treatment/number of cells recovered from heat-inactivated serum treatment. (Inset) RT-PCR analysis of mRNA levels of *apiA* and the *clpX* constitutively expressed control in the wt, *oxyR*−, and *oxyR*− + *oxyR* after H_2O_2 exposure. As a control, exogenous catalase was added to serum to ensure that any phenotype observed was not attributable to endogenous H_2O_2 within serum. Error bars represent SEM. *$P < 0.004$ via Student's t test, $n = 3$.

Co-culture enhances resistance of *A. actinomycetemcomitans* to alternative complement pathway killing

Based on the observation that *apiA* transcription was enhanced during co-culture, we hypothesized that co-culture with *S. gordonii* would enhance *A. actinomycetemcomitans* resistance to serum killing. To test this, *A. actinomycetemcomitans* serum survival was assessed during co-culture with S. *gordonii* in the presence of heat-inactivated or active catalase. Co-culture with *S. gordonii* enhanced survival of *A. actinomycetemcomitans* to human serum by approximately 7-fold (Fig. 2.6), clearly demonstrating enhanced survival of *A. actinomycetemcomitans* during co-culture. The presence of active catalase mitigated this increase in survival, implicating *S. gordonii* H_2O_2 production as the key mediator of this phenotype (Fig. 2.6).

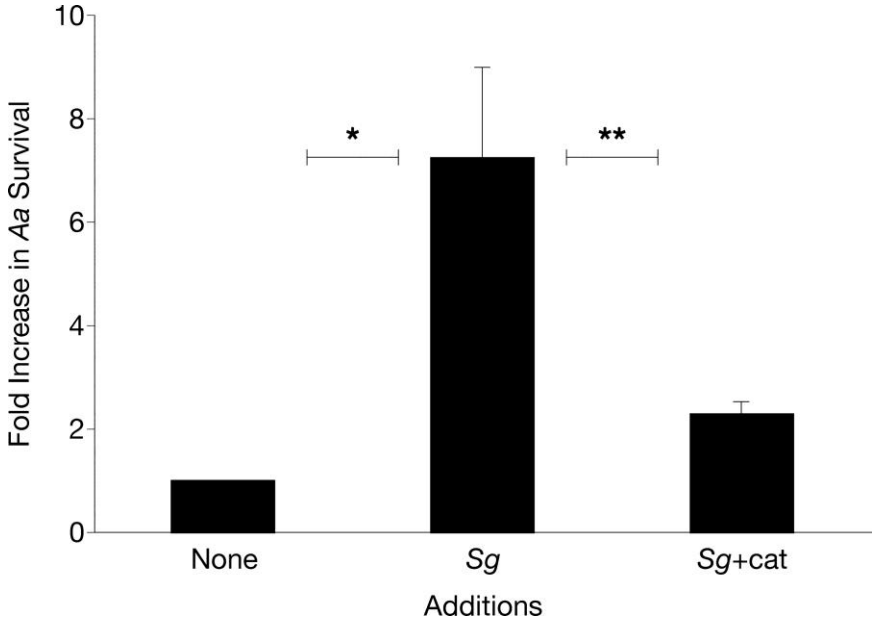

Figure 2.6. Coculture with *S. gordonii* enhances *A. actinomycetemcomitans* resistance to killing by human serum

Fold increase in survival of *A. actinomycetemcomitans* on exposure to 50% (vol/vol) normal human serum when grown in monoculture (*Aa*), coculture with *S. gordonii* + heat-inactivated catalase (*Aa*+*Sg*), and coculture with *S. gordonii* + catalase (*Aa*+*Sg*+cat). Ratios were calculated as follows: colony-forming units present after serum

treatment/colony-forming units present after heat-inactivated serum treatment. Error bars represent SEM. It is important to note that cell numbers were similar with and without catalase in the heat-inactivated complement cultures. *P < 0.01, **P < 0.05 via Student's t test, n = 3.

Co-culture enhances factor H binding to the *A. actinomycetemcomitans* cell surface

From a mechanistic standpoint, it was not clear how induction of *apiA* expression during co-culture enhanced resistance to serum. Clues were provided by Asakawa *et al* who recently demonstrated that ApiA binds the human complement regulatory protein factor H [30]. Factor H is a complement control protein that circulates in human serum, and when bound to cells, inhibits the alternative pathway of complement activation. Since *apiA* is induced during co-culture, we reasoned that the levels of factor H bound to the *A. actinomycetemcomitans* outer surface would be increased during co-culture with *S. gordonii*. To examine this, immunofluoresence staining with an anti-factor H antibody was used to quantify the levels of factor H bound to the *A. actinomycetemcomitans* outer surface during mono-culture and co-culture growth. Our results revealed that approximately 4-fold more factor H was bound to *A. actinomycetemcomitans* during co-culture with *S. gordonii* as compared to mono-culture conditions (Fig. 2.7 A&B). This enhanced binding of factor H during co-culture was mitigated by the addition of active catalase, indicating that as expected, H_2O_2 was the critical cue mediating increased binding.

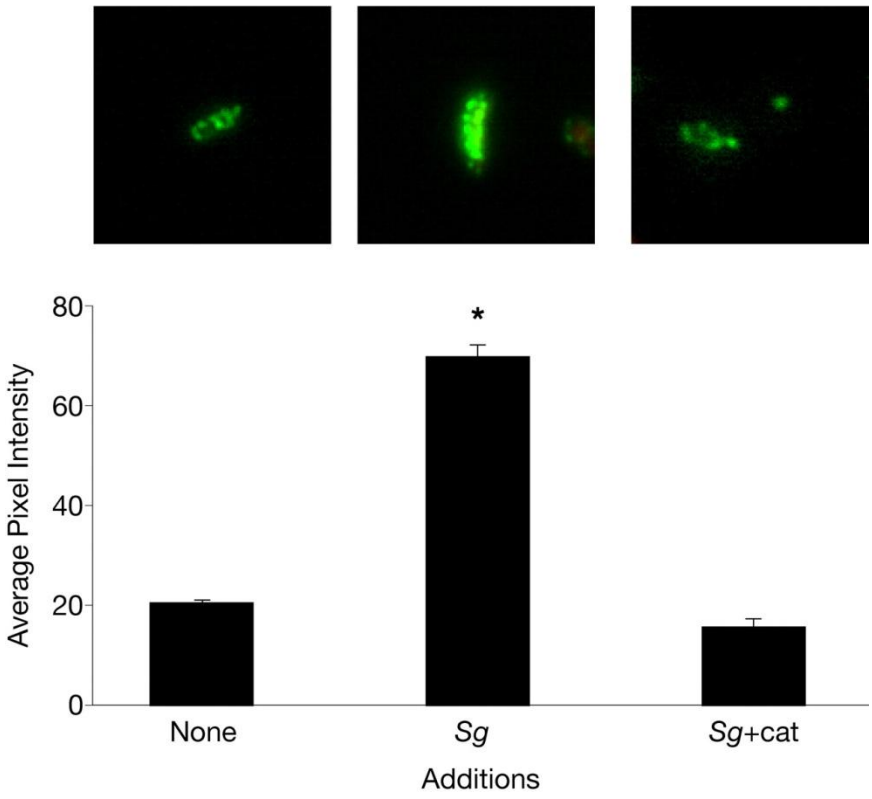

Figure 2.7. Factor H displays enhanced binding to *A. actinomycetemcomitans* during coculture with *S. gordonii*

(A) Immunofluorescent micrographs of factor H attachment to the surface of *A. actinomycetemcomitans* during monoculture (*Aa*), coculture with *S. gordonii* + heat-inactivated catalase (*Aa*+*Sg*), and coculture with *S. gordonii* + catalase (*Aa*+*Sg*+cat). Images were recorded at magnification ×1,000. (B) Average green channel fluorescence intensity per cell. Averages were calculated from 40 independent measurements. Error bars represent SEM. *P < 0.0001 via Student's t test.

2.4 DISCUSSION

A. actinomycetemcomitans is a common commensal of the mammalian oral cavity where it resides in a complex microbial community within the sub-gingival crevice. The sub-gingival crevice is distinct from the exposed tooth surface and poses several challenges for *A. actinomycetemcomitans* growth and survival including: competition with faster growing bacteria for nutrients; the presence of anti-microbial serum proteins such as immunoglobins, complement, and anti-microbial peptides [25, 51, 82]; and the presence of high levels of metabolites produced by other members of the microbial community. Two of the most prominent microbial metabolites produced in the oral cavity are lactic acid and H_2O_2. As observed with lactic acid [7], our results demonstrate that *A. actinomycetemcomitans* displays a unique response to H_2O_2 exposure. It is intriguing that only two *A. actinomycetemcomitans* genes exhibited a significant change in gene expression upon exposure to H_2O_2 (Fig. 2.1). This contrasts with transcriptome studies in many other aerobically/microaerophilically-grown bacteria which have shown large numbers of genes (from 140 to 520) differentially regulated in response to H_2O_2 [71-76]. Many of the H_2O_2-responsive genes identified in these previous studies such as DNA repair proteins and superoxide dismutases are expressed by *A. actinomycetemcomitans* but are not responsive to H_2O_2, suggesting that these genes may be constitutively expressed in *A. actinomycetemcomitans* as an adaptation to frequent H_2O_2 exposure.

The H_2O_2 response was observed not only upon exogenous addition of H_2O_2, but also during co-culture with the H_2O_2 producing oral bacterium *S. gordonii* (Fig. 2.2 and 2.3). Not surprisingly, *A. actinomycetemcomitans* displayed enhanced production of the H_2O_2-consuming enzyme catalase during co-culture. This response has been observed

previously in several bacterial species and serves to enhance resistance to H_2O_2 [71-76, 80]. More intriguing was the finding that *A. actinomycetemcomitans* also induces the outer membrane protein ApiA during co-culture. As ApiA provides protection from killing by the alternative complement component of innate immunity [30], our data represent the first demonstration of a metabolic cue produced by one bacterium mediating enhanced resistance to a component of host innate immunity by another. It should be noted that the mechanism of complement inhibition, namely enhanced binding of the serum protein factor H (Fig. 2.7), will not only protect the bacterium from the alternative complement pathway, but will also significantly decrease complement-mediated opsonic uptake and killing by host phagocytic cells [83]. Thus, it is likely that the impact of co-culture on *A. actinomycetemcomitans* resistance to innate immune effectors will extend beyond our observations of protection from the alternative complement pathway.

Based on murine studies it is likely that *A. actinomycetemcomitans* is exposed to H_2O_2 produced by oral streptococci in the oral cavity [56]. Why would *A. actinomycetemcomitans* respond to H_2O_2 by enhancing resistance to complement killing? While the answer is unknown, in vitro studies reveal that as oral streptococci numbers increase, the levels of streptococcal H_2O_2 increase due to the accumulation of lactic acid [19]. This has been shown to have critical consequences in several non-oral in vivo models, as H_2O_2 produced by streptococci [84, 85], in combination with other factors such as lipoteichoic acids [86, 87], induce significant inflammation. Inflammation leads to increased vascular permeability, influx of serum, and recruitment of neutrophils to the sub-gingival crevice [10]. In the context of these previous studies, we propose a model (Fig. 2.8) where enhanced levels of streptococcal H_2O_2 produced during early inflammation stimulate a more robust immune response, followed by an influx of innate

immune modulators. *A. actinomycetemcomitans* responds to rising H_2O_2 by enhancing resistance to innate immune effectors. In this sense, *A. actinomycetemcomitans* utilizes H_2O_2 as an anticipatory signal for an enhanced immune response.

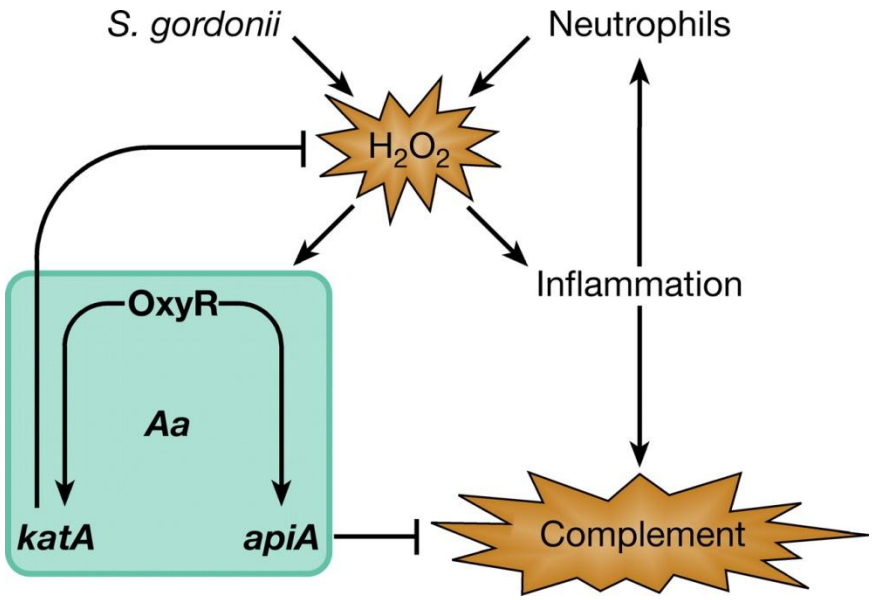

Figure 2.8. Model for the role of H_2O_2 as a mediator of *A. actinomycetemcomitans* resistance to innate immunity

Enhanced levels of H_2O_2 produced by *S. gordonii* during plaque growth stimulate inflammation, leading to an influx of innate immune modulators, including complement and neutrophils. *A. actinomycetemcomitans* responds to rising H_2O_2 by induction of *katA* and *apiA*, which, in turn, enhance resistance to innate immune effectors. On recruitment to the site of inflammation, neutrophils increase the levels of H_2O_2 and further stimulate induction of *katA* and *apiA*.

Of course streptococci are not the only source of H_2O_2 in the sub-gingival crevice. Another source is host tissues which produce endogenous H_2O_2 from the mitochondria during aerobic respiration [88, 89]. Based on the fact that host tissues produce significantly lower levels of H_2O_2 compared to *S. gordonii* [19, 88, 89] and most of the host peroxide is likely scavenged by host catalase, we predict that endogenous H_2O_2 production has little impact on *A. actinomycetemcomitans* gene expression. This is likely

not the case for neutrophils which produce high levels of H_2O_2 upon recruitment to the site of inflammation [11, 90]. Thus, during gingival inflammation, *A. actinomycetemcomitans* will also face high levels of neutrophil-produced H_2O_2. Our model (Fig. 2.8) predicts that before significant neutrophil recruitment to the sub-gingival crevice, neutrophil H_2O_2 likely has little impact on *A. actinomycetemcomitans* gene expression. Instead we predict that during early inflammation, streptococcal H_2O_2 will be the primary stimulant for enhanced production of ApiA and KatA. This initial stimulation by streptococcal H_2O_2 will augment the inflammatory response [84, 85] and stimulate recruitment of neutrophils to the sub-gingival crevice. We propose that the initial *A. actinomycetemcomitans* response to streptococcal H_2O_2 not only provides resistance to the influx of alternative complement during inflammation but likely provides resistance to neutrophil produced H_2O_2. During these latter stages of inflammation, neutrophil H_2O_2 may also serve as an additional stimulus to *A. actinomycetemcomitans* to enhance expression of *katA* and *apiA*. Of course this model requires vigorous *in vivo* testing in the future; however these studies are significantly hampered by the lack of a robust primate model.

Our results demonstrate that *A. actinomycetemcomitans* uses the *S. gordonii* metabolite H_2O_2 as a cue to induce expression of *katA* and *apiA*, whose products aid in defense against host innate immunity. These findings suggest that *A. actinomycetemcomitans* may utilize H_2O_2 as an indicator of an impending host innate immune response in vivo and provide the first description of a polymicrobial interaction that impacts resistance to host innate immunity. There is considerable interest in understanding how pathogenic microbes evade host innate immunity. In fact, there is substantial effort aimed at developing therapeutics to enhance the effectiveness of the

innate immune response [91]. Such studies have focused on treatment of mono-culture infections, despite the observation that many infections are polymicrobial. Our results clearly show that interaction between two prominent oral bacteria significantly affect killing by host innate immunity and reinforce the idea that understanding how polymicrobial interactions affect resistance to innate immunity is critical when examining interactions with the host immune system.

Chapter 3: Metabolite cross-feeding enhances virulence in an in vivo model multispecies infection[2]

3.1 INTRODUCTION

The survival of pathogens in the human body has been rigorously studied for well over a century. The ability of bacteria to colonize, persist and thrive *in vivo* is due to an array of capabilities including the ability to attach to host tissues, produce extracellular virulence factors, and evade the immune system. Invading pathogens must also obtain carbon and energy from an infection site, and specific carbon sources are required for several pathogens to colonize and persist in the host [92]. Although mono-culture infections provide interesting insight into pathogenesis, many bacterial infections are not simply the result of colonization with a single species, but are instead a result of colonization with several [15, 93-95]. The mammalian oral cavity is an excellent environment to study polymicrobial interactions as it is persistently colonized with diverse commensal bacteria as well as opportunistic pathogens. Our lab has utilized a two-species model system composed of the opportunistic pathogen *Aggregatibacter actinomycetemcomitans* and the common commensal *Streptococcus gordonii* to provide mechanistic insight into how specific carbon sources impact disease pathogenesis in polymicrobial infections [7, 31].

A. actinomycetemcomitans is a Gram-negative facultative anaerobic bacterium that inhabits the human oral cavity and is a proposed causative agent of localized aggressive periodontitis [96]. *A. actinomycetemcomitans* is found between the gums and tooth surface in the subgingival crevice [1, 49], an area restricted for O_2 depending on

[2] Ramsey, M.M., Rumbaugh, K.P., and Whiteley, M. *Metabolite cross-feeding enhances virulence in a model polymicrobial infection*. (**2011**) PLoS Pathog 7: e1002012.

tissue depth [53] and irrigated by a serum exudate called gingival crevicular fluid (GCF). GCF not only contains serum proteins such as complement and immunoglobulin [10], but also glucose from 10 to 500 μM in healthy patients [52] and as high as 3 mM in patients with periodontal infections [97]. L-lactate is produced by host lactate dehydrogenase in GCF [98, 99] and resident oral streptococci. Together glucose and L-lactate represent two of the small number of carbon sources that *A. actinomycetemcomitans* is able to catabolize [100]. *A. actinomycetemcomitans* has been proposed to primarily inhabit the aerobic [49] "moderate" pockets (4 to 6 mm in depth) of the gingival crevice as opposed to deeper anaerobic subgingival pockets [101].

In addition to *A. actinomycetemcomitans*, the subgingival crevice is home to a diverse bacterial population, including numerous oral streptococci [102], that reside in surface-associated biofilm communities [20]. Oral streptococci, aside from *Streptococcus mutans*, are typically non-pathogenic and depending upon the human subject and method of sampling, comprise approximately 5% [103] to over 60% [55] of the recoverable oral flora. Through fermentation of carbohydrates to L-lactate and sometimes H_2O_2, acetate, and CO_2, oral streptococci such as *S. gordonii* have been shown to influence the composition of oral biofilms [20, 28, 102, 104]. Additionally, *S. gordonii*-produced H_2O_2 influences interactions between *A. actinomycetemcomitans* and the host by inducing production of ApiA, a factor H binding protein that inhibits complement-mediated lysis [30, 31]. Thus, streptococcal metabolites are important cues that influence the growth and population dynamics of oral biofilms and how oral bacteria interact with the host.

A. actinomycetemcomitans preferentially catabolizes L-lactate over high energy carbon sources such as glucose and fructose in multiple strains, despite the fact that this

bacterium grows more slowly with L-lactate [7]. Given this preference for a presumably inferior carbon source and the observation that *A. actinomycetemcomitans* resides in close association with oral streptococci [105, 106], we hypothesize an *in vivo* benefit exists for *A. actinomycetemcomitans* L-lactate preference. To test this hypothesis, we investigated the importance of *A. actinomycetemcomitans* L-lactate catabolism during mono-culture and co-culture with *S. gordonii in vitro* and in a murine abscess model of infection. Our results reveal that co-culture with *S. gordonii* enhances colonization and pathogenesis of *A. actinomycetemcomitans*, and the ability to utilize L-lactate as an energy source is essential for these co-culture benefits. Surprisingly, inactivation of L-lactate catabolism had no impact on mono-culture growth *in vitro* and *in vivo* suggesting that *A. actinomycetemcomitans* L-lactate catabolism is only critical for establishing co-culture infections. Taken together, these results provide compelling mechanistic evidence that the metabolic properties of human commensals such as *S. gordonii* can alter the course of pathogenesis in polymicrobial communities.

3.2 MATERIALS AND METHODS

Ethics statement

This study was carried out in strict accordance with the recommendations in the Guide for the Care and Use of Laboratory Animals of the National Institutes of Health. The protocol was approved by the Institutional Animal Care and Use Committee of Texas Tech University Health Sciences Center (Protocol Number: 09039).

Strains and media

A. actinomycetemcomitans strains VT1169 [57], *Streptococcus gordonii* strain Challis DL1.1 (ATCC 49818), *S. gordonii spxB*$^-$ [107], *Escherichia coli* DH5α-λpir, and *E. coli* SM10-λpir were used in this study. *A. actinomycetemcomitans* and *S. gordonii* were routinely cultured using Tryptic Soy Broth + 0.5% Yeast Extract (TSBYE). For resting cell suspension *A. actinomycetemcomitans* metabolite analysis, a Chemically Defined Medium (CDM) [7] lacking nucleotides, amino acids, pimelate and thioctic acid (to eliminate further cell growth) containing either 20 mM glucose or 40 mM L-lactate was used. For co-culture experiments, complete CDM with 3 mM glucose was used. Aerobic culture conditions were 37ºC in a 5% CO_2 atmosphere shaking at 165 RPM, and anaerobic culture conditions were static growth at 37ºC in an anaerobic chamber (Coy, USA) with a 5% H_2, 10% CO_2 and 85% N_2 atmosphere. *E. coli* strains were grown on Luria-Bertani (LB) medium at 37ºC. Where applicable, antibiotics were used at the following concentrations: chloramphenicol, 2 μg/ml for *A. actinomycetemcomitans* and 20 μg/ml for *E. coli*; spectinomycin, 50 μg/ml for selection and 10 μg/ml for maintenance for *A. actinomycetemcomitans* and *E. coli* and 100 μg/ml for selection and maintenance

for *S. gordonii spxB*$^{-}$; kanamycin, 40 μg/ml for selection and 10 μg/ml for maintenance; naladixic acid, 25 μg/ml; streptomycin, 50 μg/ml for selection and 20 μg/ml for maintenance. For quantifying CFU/ml in co-culture assays, vancomycin (5 μg/ml) was added to agar plates to enumerate *A. actinomycetemcomitans* and streptomycin (100 μg/ml) was added to agar plates to enumerate *S. gordonii*.

DNA and plasmid manipulations

DNA and plasmid isolations were performed using standard methods [58]. Restriction endonucleases and DNA modification enzymes were purchased from New England Biolabs. Chromosomal DNA from *A. actinomycetemcomitans* was isolated using DNeasy tissue kits (Qiagen), and plasmid isolations were performed using QIAprep spin miniprep kits (Qiagen). DNA fragments were purified using QIAquick mini-elute PCR purification kits (Qiagen), and PCR was performed using the Expand Long Template PCR system (Roche). DNA sequencing was performed by automated sequencing technology using the University of Texas Institute for Cell and Molecular Biology sequencing core facility.

***A. actinomycetemcomitans apiA* mutant construction**

Allelic replacement of *apiA* (AA2485) was carried out by double homologous recombination. For construction of the knockout construct, 856 bp and 842 bp DNA fragments flanking *apiA* were amplified and combined with the *aphA* gene (encoding kanamycin resistance) from pBBR1-MCS2 [108] by overlap extension PCR [109]. The construct was prepared so that *aphA* was positioned between the upstream and downstream regions. Primers used were: Kan-5` (ATGTCAGCTACTGGGCTATCTG)

and Kan-3` (ATTTCGAACCCCAGAGTCCCGC) for the 1074 bp *aphA*-containing fragment; ApiA-UF (CCGATAACAGTAAGATCTTCTAC) and ApiA-UR (CAGATAGCCCAGTAGCTGACATCCTTTTCGGCTTGAATTTATACC) for the upstream *apiA* fragment; and ApiA-DF (GCGGGACTCTGGGGTTCGAAATGCGGTCAGAATTTTAGGTGTTTT) and ApiA-DR (CGAAACCAACGAACTCTTTATTC) for the downstream *apiA* fragment. Underlined sequences indicate overlapping DNA sequences between the *apiA* fragments and *aphA*. The overlap extension product was TA-cloned into the pGEM-T Easy vector (Promega, USA) and excised by EcoRI digest. The EcoRI fragment containing the overlap extension product was ligated into the unique EcoRI site within the λpir-dependent suicide vector pVT1461 [65]. The cloned construct, pVT1461-apiA-KO, was first transformed into *E. coli* DH5α-λpir then into *E. coli* SM10-λpir for conjugation into *A. actinomycetemcomitans*. Conjugation was performed as described [57] and potential mutants were plated onto TSBYE agar plates containing kanamycin to select for recombinant *A. actinomycetemcomitans* and naladixic acid to kill the *E. coli* donors. Kanamycin resistant, spectinomycin sensitive double recombinants were selected and verified by PCR. Enhanced susceptibility of the *apiA* mutant to serum was verified as described previously [31].

A. actinomycetemcomitans cydB mutant construction

Insertional mutagenesis of the *cydB* gene was performed by single homologous recombination using a 543 bp internal piece of the *cydB* (AA2840) gene amplified using the primers cydB-KO5` (GAAGATCTTTATGATTAATACTATCGCGCCG) and cydB-KO3` (GAAGATCTCAAAACCATCTTTGAAAGATAACCA). Underlined sequences represent

BglII restriction sites. The internal *cydB* fragment was digested with BglII and ligated into the *A. actinomycetemcomitans* suicide vector pMRKO-1 (see below) to generate pMRKO-cydB. pMRKO-cydB was transformed into *E. coli* SM10-λpir and conjugated into *A. actinomycetemcomitans*. *A. actinomycetemcomitans* recombinants were grown anaerobically on TSBYE agar containing spectinomycin and naladixic acid. Colonies were subcultured anaerobically on liquid medium at the same antibiotic concentrations and insertion into *cydB* was verified by PCR.

pMRKO-1 suicide vector construction

The spectinomycin resistance gene from pDMG4 [63] was amplified by PCR using the primers: 5`Spec-cass-NotI (ATAAGAATGCGGCCGCCGATTTTCGTTCGTGAATACATG) and 3' Spec-cass-EcoRI (CGGAATTCCATATGCAAGGGTTTATTGTTT), digested with NotI-EcoRI and ligated into NotI-EcoRI digested pmCherry (Clontech) underlined sequences indicate NotI and EcoRI restriction sites. The 3105 bp region containing the pUC origin of replication, plac:mCherry and the spectinomycin resistance gene were PCR amplified using the primers: 5'pMcher-trunc (GAAGATCTGACCAAGTTTACTCATATATACT) and 3' Spec-cass-EcoRI (CGGAATTCCATATGCAAGGGTTTATTGTTT). Underlined sequences indicate BglII and EcoRI restriction sites. This fragment was digested with BglII and EcoRI and ligated into the 2780bp fragment from BglII-EcoRI digested pVT1461. The resulting plasmid (pMRKO-1, submitted to Genbank) is a suicide vector for *A. actinomycetemcomitans* and contains *oriT*, *mob*, and *tra* genes from pVT1461 along with the pUC origin of replication, mCherry expressed from plac, and a spectinomycin resistance cassette.

Resting cell suspensions

A. actinomycetemcomitans was grown in CDM overnight either aerobically or anaerobically in the presence of 20 mM glucose or 40 mM L-lactate. Bacteria were then subcultured in 30 ml of medium and exponential phase cells (OD_{600} = 0.4) were collected by centrifugation (5,000 x g for 15 min) at 25°C. Cell pellets were resuspended in an equal volume of CDM lacking nucleotides, amino acids and any carbon source. Cells were incubated at 37°C aerobically or anaerobically depending on the test conditions for 1 hr. Cells were collected again by centrifugation as described above and resuspended to an OD_{600} of 2 in 3ml of CDM without nucleotides, amino acids, pimelate and thioctic acid containing either 20 mM glucose or 40 mM lactate. Cells were incubated for 4 h at 37°C either aerobically or anaerobically. After incubation samples were stored at -20°C for HPLC analysis.

D-Lactate assay

D-lactate assays were performed as described [110] with modifications. Glycylglycine buffer was replaced with an equal concentration of Bicine (Fisher, USA) buffer and enzymatic assays were monitored by spectrophotometry at 340 nm for 4 hours.

Co-culture experiments

A. actinomycetemcomitans and *S. gordonii* were grown overnight in CDM containing 3 mM glucose. 3 mM glucose was used to ensure that the medium was limited for catabolizable carbon. Cells were diluted 1:50 in the same medium and allowed to grow to exponential phase (OD_{600} of 0.2). Cells were then diluted 1:100 ($2x10^6$ *S. gordonii*/ml and $1x10^7$ *A. actinomycetemcomitans*/ml) as mono-cultures or co-cultures in

3 ml CDM containing 3 mM glucose. Cultures were allowed to grow for 10 h aerobically or 12 h anaerobically, after which cells were serially diluted, plated on either TSBYE agar + vancomycin for *A. actinomycetemcomitans* enumeration or TSBYE agar + streptomycin for *S. gordonii* enumeration. Colonies were counted after incubation at 37°C for 48 h. An aliquot of the culture was also stored at -20°C for HPLC metabolite analysis.

HPLC Analysis

Metabolite levels were quantified using a Varian HPLC with a Varian Metacarb 87H 300 × 6.5 mm column at 35°C. Samples were eluted using isocratic conditions with 0.025 N H_2SO_4 elution buffer and a flow rate of 0.5 ml/minute. A Varian refractive index (RI) detector at 35°C was used for metabolite enumeration by comparison with acetate, ethanol, formate, glucose, L-lactate, D-lactate, pyruvate and succinate standards.

***In vivo* murine abscess growth**

Murine abscesses were generated essentially as described previously [111]. Briefly, 6-8 week-old, female, Swiss Webster mice were anesthetized with an intraperitoneal injection of Nembutal (50 mg/kg). The hair on the left inner thigh of each mouse was shaved, and the skin was disinfected with 70% alcohol. Mice were injected subcutaneously in the inner thigh with 10^7 CFU *A. actinomycetemcomitans*, *S. gordonii* or both. At 6 days post- infection, mice were euthanized and intact abscesses were harvested, weighed and placed into 2 ml of sterile PBS (or water for pH measurements). Tissues were homogenized, serially diluted and plated on Brain Heart Infusion (BHI) agar + 20 μg/ml Na_2CO_3 + vancomycin for *A. actinomycetemcomitans* enumeration or BHI

agar + 20 μg/ml Na_2CO_3 + streptomycin for *S. gordonii* enumeration, to determine bacterial CFU/abscess. Experimental protocols involving mice were examined and approved by the Texas Tech University HSC Institutional Animal Care and Use Committee.

3.3 RESULTS

A. actinomycetemcomitans metabolism of glucose and L-lactate

Within the gingival crevice, host-produced glucose and L-lactate are present [52, 97-99, 112] and likely serve as *in vivo* carbon sources for *A. actinomycetemcomitans*. However in contrast to glucose, L-lactate is also produced by the oral microbial flora, primarily oral streptococci [20]. Indeed, the ability of *A. actinomycetemcomitans* to catabolize streptococcal-produced L-lactate has been demonstrated previously [7], and it was proposed that *A. actinomycetemcomitans* consumes streptococcal-produced L-lactate during co-culture. To assess the importance of *A. actinomycetemcomitans* L-lactate catabolism in polymicrobial communities *in vitro*, we examined the metabolic profile during catabolism of L-lactate and glucose under aerobic and anaerobic conditions. Aerobically, *A. actinomycetemcomitans* primarily produced lactate and acetate from glucose (Fig. 3.1A) while acetate was the sole metabolite produced by L-lactate-grown bacteria (Fig. 3.1C). It was intriguing that lactate was produced, but not consumed, by *A. actinomycetemcomitans* during aerobic catabolism of glucose. We hypothesized that the lactate produced by *A. actinomycetemcomitans* was likely D-lactate, which is not catabolized by *A. actinomycetemcomitans* [113]. Using an enzymatic assay [110], we were able to verify that >99% of the lactate produced by *A. actinomycetemcomitans* was indeed D-lactate.

Anaerobically from glucose, *A. actinomycetemcomitans* primarily produced the mixed acid fermentation products formate and acetate along with lactate, succinate, and trace amounts of ethanol (Fig. 3.1B). Surprisingly, *A. actinomycetemcomitans* was unable to catabolize L-lactate anaerobically (Fig. 3.1C), even if the potential alternative electron acceptors nitrate or dimethyl sulfoxide were added, suggesting that L-lactate oxidation

was O_2 dependent. This is distinct from other oral bacteria including members of the genus *Veillonella* [28, 114], in which L-lactate is an important anaerobic carbon and energy source. If O_2 respiration was indeed required for *A. actinomycetemcomitans* growth with L-lactate, we hypothesized that elimination of the terminal respiratory oxidase, which is required for aerobic respiration, would abolish L-lactate utilization by *A. actinomycetemcomitans* aerobically. To test this hypothesis, *cydB*, which encodes a component of the sole putative *A. actinomycetemcomitans* respiratory oxidase, was insertionally inactivated. The *cydB* mutant was unable to catabolize L-lactate aerobically supporting the hypothesis that L-lactate oxidation requires O_2 respiration (Fig. 3.1C). Interestingly when grown with glucose aerobically, the *cydB* mutant doubled much slower (6.6 hr) than the wt (1.9 hr) and cell suspensions produced a metabolite profile that differed from the wt (Fig. 3.1A) indicating that while not required for aerobic growth on glucose, O_2 respiration is the primary means by which glucose is catabolized by wt *A. actinomycetemcomitans*. As expected, the *cydB* mutant exhibited identical growth rates anaerobically on glucose (not shown) and produced similar metabolites as the wt (Fig. 3.1B). Collectively, these data indicate that O_2 respiration is required for L-lactate oxidation in *A. actinomycetemcomitans*.

As the ultimate goal of this study is to assess the importance of *A. actinomycetemcomitans* L-lactate catabolism for establishing co-culture with oral streptococci, it was important to assess whether eliminating the ability of *A. actinomycetemcomitans* to utilize L-lactate affected growth with glucose. To examine this, we examined growth and metabolite production in an *A. actinomycetemcomitans* strain in which the catabolic L-lactate dehydrogenase, LctD, present in all strains sequenced to date [115, 116], was insertionally inactivated [113]. LctD oxidizes L-lactate

to pyruvate and is required for *A. actinomycetemcomitans* growth with L-lactate as the sole energy source [113]. As expected, the *lctD* mutant was unable to catabolize L-lactate aerobically or anaerobically (Fig. 3.1C); however, metabolite production from glucose was not affected (Fig. 3.1A&B) nor was the growth rate with glucose (not shown). These data indicate that L-lactate catabolism can be eliminated in *A. actinomycetemcomitans* without affecting growth and metabolite production with glucose.

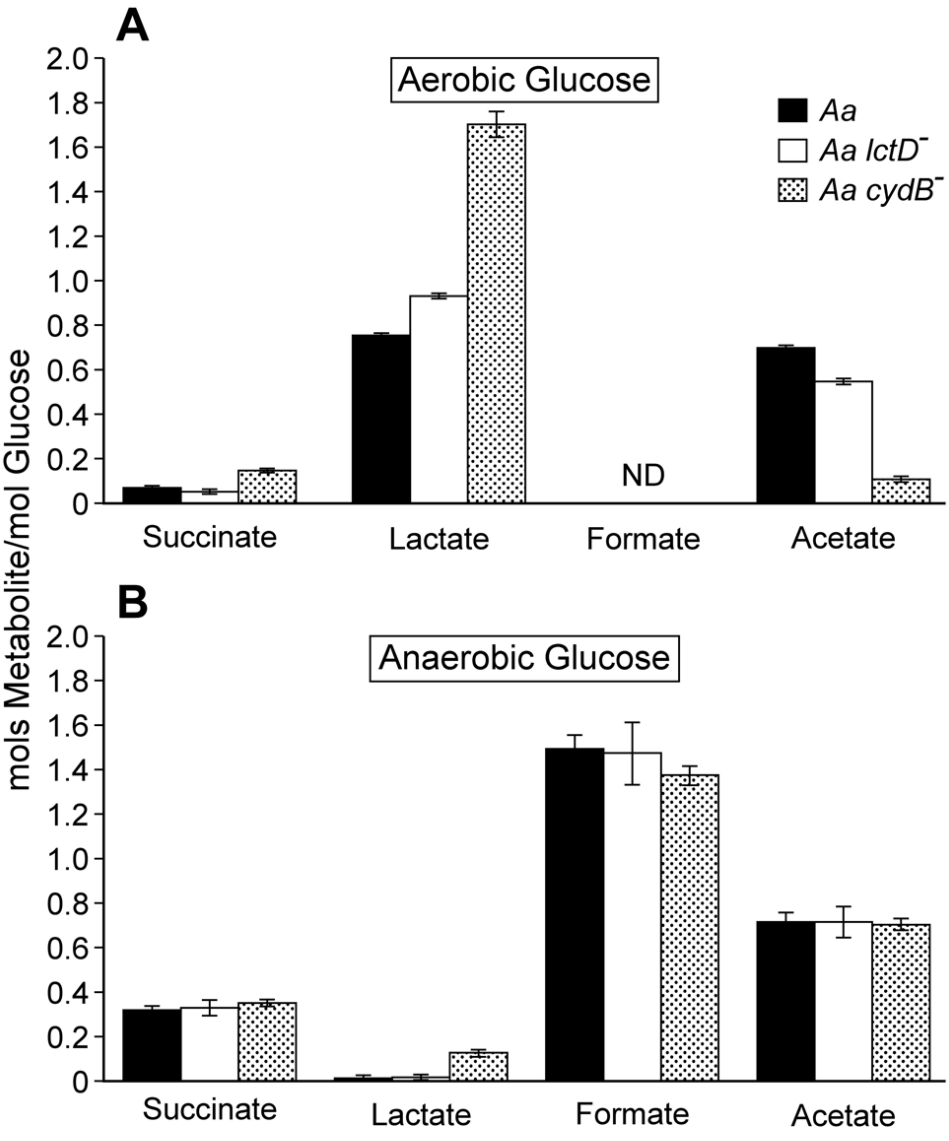

C

	Acetate Produced*	
	Aerobic	Anaerobic
Aa	1.24 mM	<100 μM
Aa lctD$^-$	<100 μM	<100 μM
Aa cydB$^-$	<100 μM	<100 μM

Figure 3.1. Aerobic and anaerobic metabolites produced by *A. actinomycetemcomitans*, *A. actinomycetemcomitans lctD*- and *A. actinomycetemcomitans cydB*-

Resting cell suspensions of each culture were incubated (A) aerobically in glucose; (B), anaerobically in glucose; (C), aerobically or anaerobically in lactate. Metabolite concentrations were measured by HPLC. Data in A and B are presented as moles of metabolite produced/mole of glucose consumed. Only trace concentrations (<50 μM) of ethanol were observed in anaerobic suspensions. Error bars represent 1 standard error of the mean, n = 3. * Acetate concentrations are shown per mM of L-lactate consumed. The detection limit for acetate was 100 μM.

Utilization of L-lactate enhances co-culture growth

Because *A. actinomycetemcomitans* preferentially catabolizes L-lactate in lieu of hexose sugars [7], we hypothesized that L-lactate cross-feeding was important for establishing co-culture with oral streptococci grown on glucose. To test this hypothesis, we examined growth of glucose-grown *A. actinomycetemcomitans* and *S. gordonii* during *in vitro* co-culture aerobically and anaerobically. Aerobically, wt *A. actinomycetemcomitans* co-culture cell numbers were similar to those observed in mono-culture while the *A. actinomycetemcomitans lctD* mutant exhibited an approximate 25-fold change in cell number during co-culture with *S. gordonii* (Fig. 3.2). Anaerobically, both wt *A. actinomycetemcomitans* and *A. actinomycetemcomitans lctD*$^{-}$ cell numbers changed nearly 10-fold in co-culture compared to mono-culture (Fig. 3.2), likely due to the inability to catabolize *S. gordonii*-produced L-lactate.

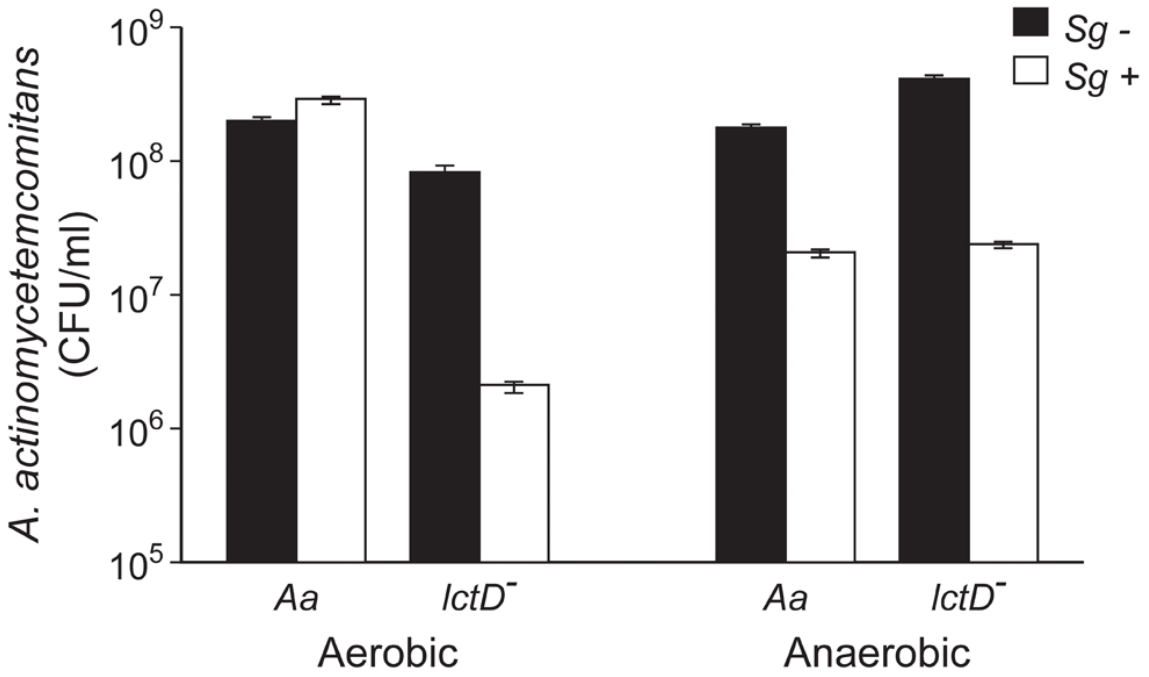

Figure 3.2. Growth of *A. actinomycetemcomitans*, *A. actinomycetemcomitans lctD*-, and *S. gordonii* in aerobic and anaerobic co-cultures on glucose

Strains were grown as mono- or co-cultures in 3 mM glucose aerobically or anaerobically for 10 or 12 h respectively, serially diluted and plated on selective media to determine colony forming units per ml (CFU/ml). *A. actinomycetemcomitans* mono-culture strains are black bars and co-culture with *S. gordonii* are white bars. Error bars represent 1 standard error of the mean, n = 3.

Examination of aerobic metabolic end products of the *A. actinomycetemcomitans lctD*$^-$/*S. gordonii* co-culture revealed high levels of lactate, reminiscent of *S. gordonii* mono-cultures, indicating that as expected, the *A. actinomycetemcomitans lctD* mutant is unable to catabolize L-lactate in co-culture (Fig. 3.3A). Additionally, metabolite concentrations in anaerobic co-cultures were similar to *S. gordonii* mono-culture (Fig. 3.3B). It should be noted that these metabolites were measured from growing cells, not cell suspensions as in Figure 3.1. These data provide strong evidence that the inability to

use L-lactate, even when glucose is present, significantly inhibits *A. actinomycetemcomitans* growth and survival in co-culture.

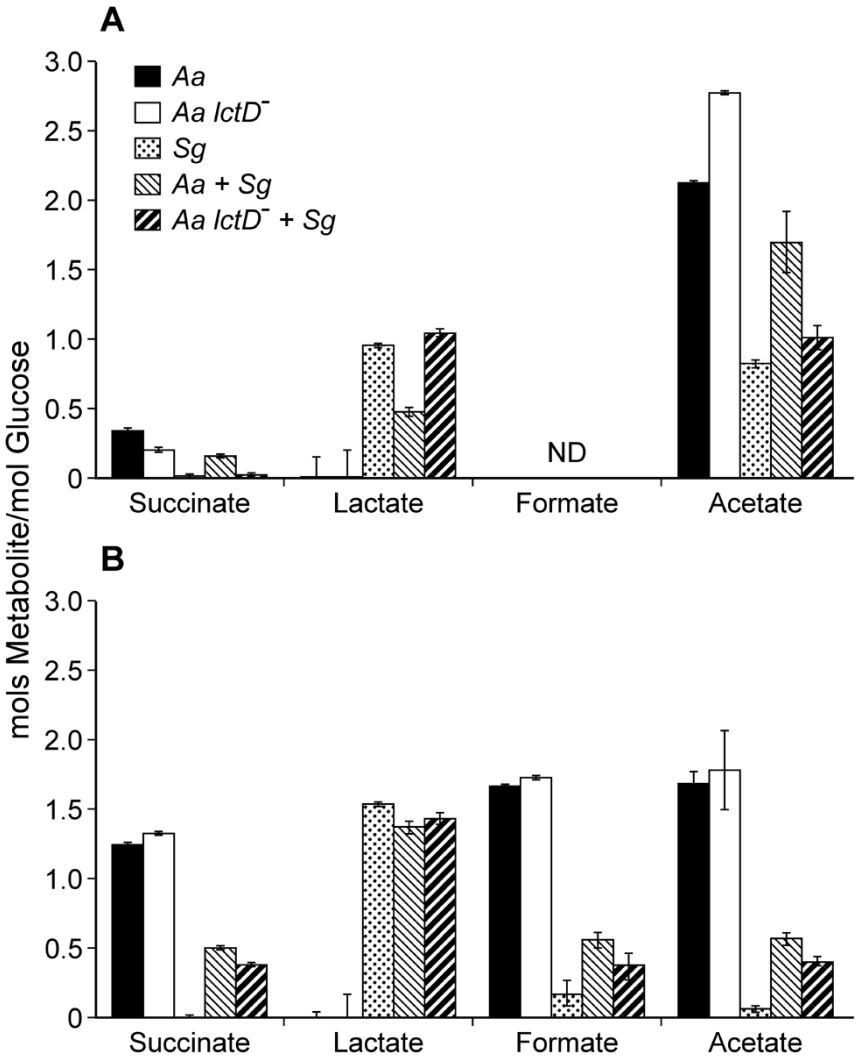

Figure 3.3. Metabolite production by *A. actinomycetemcomitans*, *A. actinomycetemcomitans lctD*-, and *S. gordonii* in aerobic or anaerobic mono- and co-cultures

Supernatants of the cultures used for CFU measurements in Fig. 3.2 were analyzed by HPLC for metabolite production from (A), aerobic or (B), anaerobic cultures. Data is presented as moles of metabolite produced/mole of glucose consumed. Error bars represent 1 standard error of the mean, n = 3. ND = No Data.

Interestingly, an approximate 7-fold increase in *S. gordonii* cell numbers were observed in the presence of *A. actinomycetemcomitans* aerobically, indicating that *A. actinomycetemcomitans* enhances *S. gordonii* proliferation under these co-culture conditions even when *A. actinomycetemcomitans* is unable to utilize L-lactate (Fig. 3.4). Importantly, the pH of the medium used in these experiments remained at neutrality; thus changes in cell numbers were not due to alterations in pH.

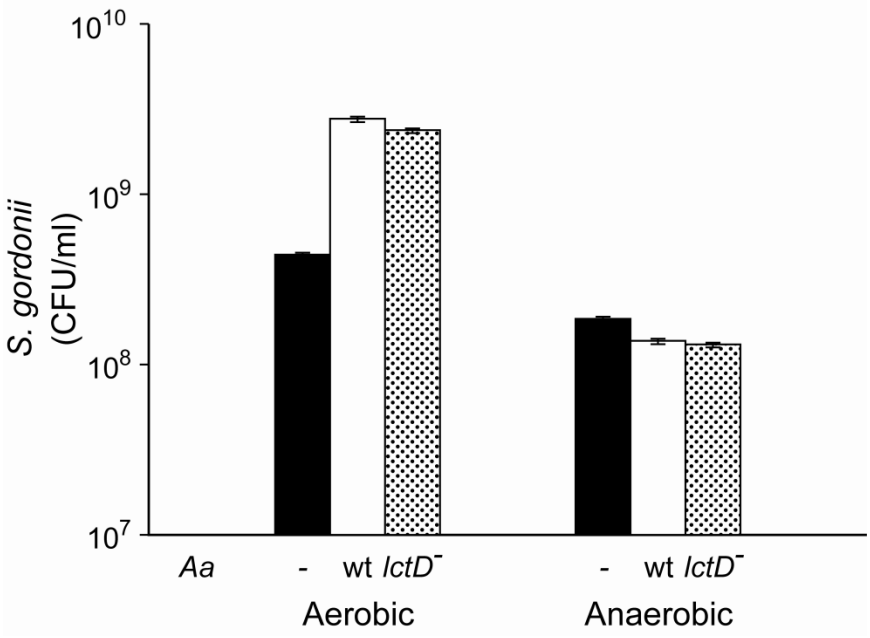

Figure 3.4. Growth of *S. gordonii* in mono- or co-culture with *A. actinomycetemcomitans* or *A. actinomycetemcomitans lctD*- in aerobic and anaerobic co-cultures

Strains were grown as mono- or co-cultures in 3 mM glucose aerobically or anaerobically for 10 or 12 h respectively, serially diluted, and plated on selective media to determine colony forming units per ml (CFU/ml). *S. gordonii* mono-cultures numbers are represented by black bars, co-culture numbers with *A. actinomycetemcomitans* are represented by white bars, and co-culture numbers with *A. actinomycetemcomitans lctD*- are represented by grey bars. Error bars represent 1 standard error of the mean, n = 3.

L-lactate consumption is required for co-culture growth of *A. actinomycetemcomitans in vivo*

The observation that L-lactate catabolism is critical for *A. actinomycetemcomitans* to establish co-culture with *S. gordonii in vitro* provides new insight into this model polymicrobial community; however, whether the requirement for this catabolic pathway extended to *in vivo* co-culture was not known. To examine the role of *A. actinomycetemcomitans* L-lactate catabolism for *in vivo* growth in mono- and co-culture,

we used a mouse thigh abscess model. This model has relevance as *A. actinomycetemcomitans* causes abscess infections outside of the oral cavity in close association with other bacteria [117] and has been used as a model system to examine pathogenesis of several oral bacteria [118, 119]. Using this model, bacterial survival and abscess formation was assessed for wt *A. actinomycetemcomitans* and *A. actinomycetemcomitans lctD*$^-$ during mono- and co-culture with *S. gordonii* (Fig. 3.5).

Unexpectedly, wt *A. actinomycetemcomitans* and the *lctD* mutant established similar infections in terms of cell number (Fig. 3.5A) and in abscess weight (Fig. 3.5B) indicating that host-derived L-lactate is not an important *in vivo* nutrient source during mono-culture infection. Interestingly, wt *A. actinomycetemcomitans* displayed a 10-fold increase in cell number when co-cultured with *S. gordonii*, while cell number of the *lctD* mutant changed >100-fold compared to the wild-type providing evidence that the ability to catabolize L-lactate is crucial for *A. actinomycetemcomitans* co-culture survival *in vivo*. These data also indicate that while not critical for mono-culture growth, L-lactate is an important energy source during co-culture infection. Unlike the *in vitro* experiments (Fig. 3.4), *S. gordonii* numbers were not statistically different in monoculture or in co-culture abscesses (2.7 x10^7 and 1.3 x 10^7 CFU/ml respectively; p = 0.15 via Mann-Whitney test) indicating that *S. gordonii* does not receive a benefit, at least in regard to cell number, from co-culture with *A. actinomycetemcomitans*. As a control, *in vivo* growth of the *A. actinomycetemcomitans apiA* mutant, which is hypersusceptible to killing by innate immunity, was examined. As expected, the *apiA* mutant exhibited a >250-fold changed in mono-culture *in vivo* survival, which was unchanged in the presence of *S. gordonii* (Fig. 3.5A).

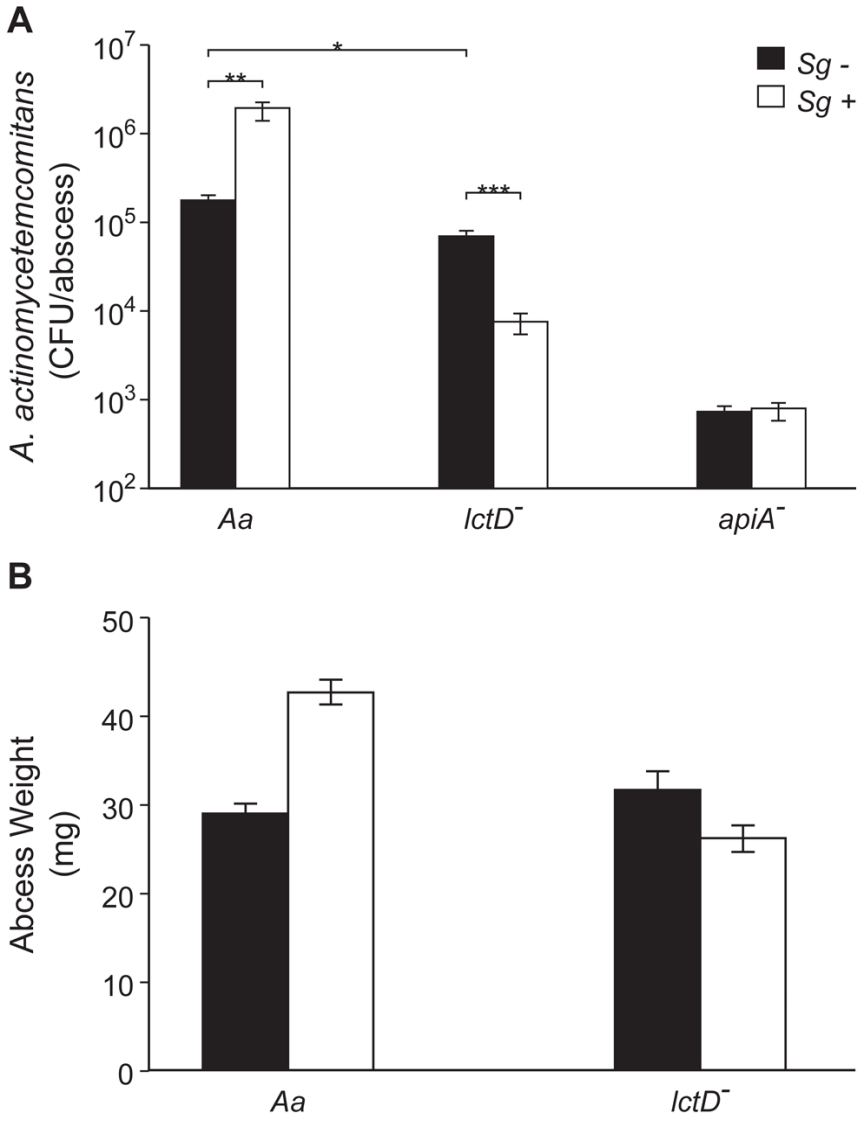

Figure 3.5. Persistence of *A. actinomycetemcomitans*, *A. actinomycetemcomitans lctD*-, and *A. actinomycetemcomitans apiA*- in mono- or co-culture in a murine abscess model

A. Bacterial colony forming units per abscess. Wilcoxon signed-rank test values are: * $p<0.02$, ** $p<0.01$, *** $p<0.008$. B. Abscess weights 6 days post-inoculation. Error bars represent 1 standard error of the mean, $n = 9$. $p<0.05$ for wt *A. actinomycetemcomitans* in mono- and co-culture via Student's t-test.

3.4 DISCUSSION

Microbes within polymicrobial infections often display synergistic interactions that result in enhanced colonization and persistence in the infection site [3, 95, 111, 117, 119-121]. Such interactions have been particularly noted in oral polymicrobial infections, although the molecular processes controlling these synergistic interactions are not well defined. Detailed mechanistic studies of the interactions required for enhanced persistence *in vivo* is a critical step towards a more comprehensive understanding of natural polymicrobial infections. In this study, we used a model polymicrobial infection [7, 31] to determine the importance of metabolic cross-feeding for establishing co-culture infections. Cross-feeding in polymicrobial populations has been reported in numerous studies [28, 122, 123], but its importance for establishing co-culture infections has not been investigated in depth. The methodology used in this study began with detailed studies of the metabolic pathways required for growth with the *in vivo* carbon sources glucose and L-lactate, followed by examination of the importance of specific catabolic pathways for establishing co-culture infections.

It is relevant to discuss the rationale for two *in vivo* experimental parameters: using a 'smooth' strain of *A. actinomycetemcomitans* in lieu of a 'rough' strain; and using a murine abscess model in lieu of a rat periodontal infection model [124, 125]. A "smooth" strain of *A. actinomycetemcomitans*, which displays impaired surface attachment, was used in this study [126]. As we were not investigating attachment or biofilm development, we opted to utilize a smooth strain that had undergone robust metabolic characterization, and feel this decision is justified as this bacterium clearly causes abscess infections in this model (Fig. 3.5). The murine abscess model was used for

several reasons. First, in addition to periodontal infections, *A. actinomycetemcomitans* causes abscess infections outside of the oral cavity that resemble, from a gross morphological standpoint, the abscess model infection [117]; thus the abscess model has clinical relevance. Second, the abscess model avoids complications arising from the normal flora, which are not completely eradicated in the periodontal rat infection models, and whose presence would make interpretation of metabolic interactions extraordinarily complex. Third, the abscess model allows direct, controlled inoculation with a finite number of cells that can be quantified throughout the infection by assessing colony forming units after removal of the entire abscess [111, 127, 128]. Finally, although the abscess model has primarily been used to study anaerobic pathogens [118, 119], it is also relevant for studying aerobic pathogens, demonstrated by the large abscesses [128] formed by the strict aerobe *Acinetobacter baumanii* [100, 129]. The presence of aerobic microenvironments in the abscess is also supported by our observations that the *S. gordonii spxB* mutant is significantly impaired for abscess formation (Fig. 3.6). The *spxB* gene encodes pyruvate oxidase which utilizes O_2 for biosynthesis of the virulence factor H_2O_2 [107]; thus its importance is limited to aerobic infections.

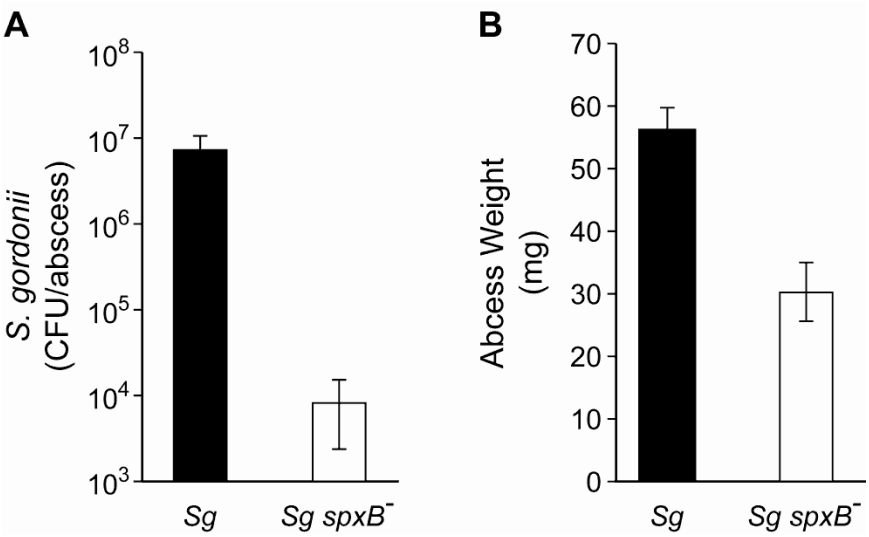

Figure 3.6. Survival of *S. gordonii* and *S. gordonii spxB*- in a murine abscess model

A. Number of bacteria recovered from each abscess expressed as colony forming units per abscess (CFU/abscess). Wilcoxon signed-rank test value, $p<0.03$. B. Abscess weights 6 days post-inoculation. Error bars represent 1 standard error of the mean, n = 4.

The observation that *A. actinomycetemcomitans* requires O_2 to catabolize L-lactate was surprising, as many oral bacteria grow on L-lactate anaerobically [28, 114]. These results also solve an apparent contradiction in the literature. It was reported by multiple sources [2, 100] that *A. actinomycetemcomitans* does not catabolize L-lactate, yet we recently provided evidence that several strains of *A. actinomycetemcomitans* grow aerobically with L-lactate as the sole energy source [7, 113]. Interrogation of the previous growth environments revealed that *A. actinomycetemcomitans* was grown under very low or O_2 free conditions; thus it is not surprising that significant growth was not observed in these studies. The O_2 dependency of L-lactate oxidation also highlights another facet of our *in vivo* data. In the murine abscess model, the *A. actinomycetemcomitans* wt and *lctD* mutant grew equally well in mono-culture (Fig 3.5). However, in co-culture only the survival of the *lctD* mutant was impaired. This result is reminiscent of our *in vitro* data

(Fig. 3.2) suggesting that O_2 dependent metabolism occurs in our model polymicrobial infection.

The observation that the terminal oxidase CydB is required for aerobic growth with L-lactate allows development of a new model for L-lactate consumption in *A. actinomycetemcomitans* (Fig. 3.7). Since L-lactate dehydrogenase (LctD) is necessary for lactate oxidation and does not use NAD^+ as an electron acceptor [113], anaerobic fermentation pathways that regenerate NAD^+ cannot act as electron acceptors for L-lactate oxidation. The model predicts that *A. actinomycetemcomitans* instead donates electrons directly to the quinone pool which in turn is re-oxidized by CydAB [130]. It should be noted that this does not rule out an unknown electron carrier between LctD and the membrane associated quinone.

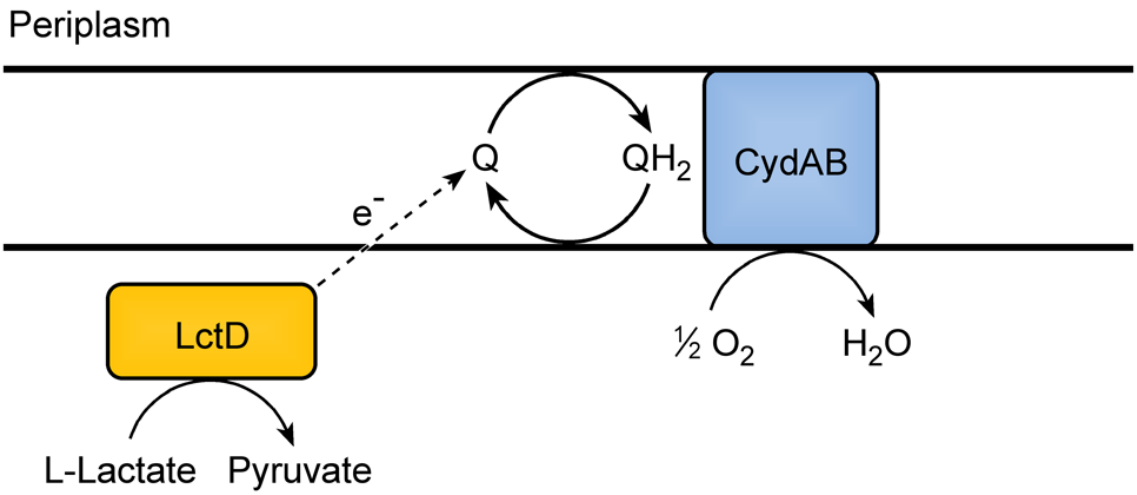

Figure 3.7. Model for electron transport during L-lactate oxidation in *A. actinomycetemcomitans*

A. actinomycetemcomitans requires O_2 for oxidation of L-lactate. LctD may donate electrons from L-lactate directly to the quinone pool or utilize an unknown intermediate electron carrier represented by the dotted arrow. The cytochrome oxidase CydAB ultimately donates the electrons to O_2.

The most exciting observation from these studies is that L-lactate catabolism is likely an important factor for *A. actinomycetemcomitans* to establish a polymicrobial, but not mono-culture, infection in a murine abscess model (Fig. 3.5). These data indicate that host-produced L-lactate is not a vital energy source for *A. actinomycetemcomitans* in mono-culture abscesses, but when *S. gordonii* is present, L-lactate catabolism becomes critical. We speculate that in the absence of *S. gordonii,* carbohydrates such as glucose are present in the infection site for *A. actinomycetemcomitans* growth. When *S. gordonii* is introduced, competition for these carbohydrates increases, and *A. actinomycetemcomitans* is likely at a disadvantage due to its relatively slow growth and catabolic rates compared to *S. gordonii* [7]. Thus, the ability to preferentially utilize L-lactate, the primary metabolite produced by *S. gordonii,* allows *A. actinomycetemcomitans* to avoid competition with *S. gordonii* for carbohydrates and consequently enhance its survival in the abscess. This model (Fig. 3.8) suggests that the importance of individual carbon catabolic pathways is dependent on the context of the infection, specifically if oral streptococci are present.

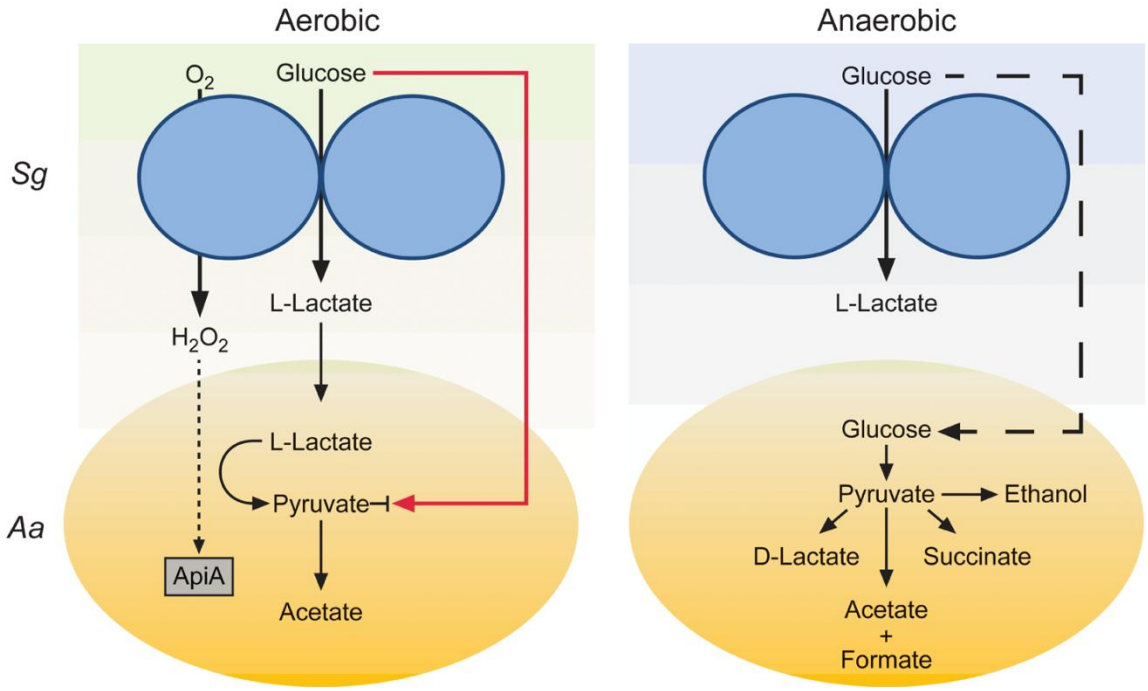

Figure 3.8. Model for enhanced persistence of *A. actinomycetemcomitans* during aerobic co-culture with *S. gordonii*

During co-culture aerobic growth with glucose, *S. gordonii* produces L-lactate and H_2O_2 which inhibit *A. actinomycetemcomitans* glucose uptake (red line) and induce *apiA* expression (dotted line) respectively. The production of L-lactate provides *A. actinomycetemcomitans* with a preferred carbon source for growth and reduces the need to compete with *S. gordonii* for glucose during aerobic co-culture. During anaerobic co-culture, *S. gordonii* also produces L-lactate but *A. actinomycetemcomitans* is unable to catabolize this carbon source due to the absence of O_2; thus requiring *A. actinomycetemcomitans* to compete directly with *S. gordonii* for glucose (dashed line).

Our work demonstrates that metabolic pathways required for *A. actinomycetemcomitans* proliferation during mono-culture infection are distinct from those required for co-culture infection with a common commensal. This study provides strong evidence that simply because elimination of a catabolic pathway does not elicit a virulence defect in mono-species infection does not preclude it from being important in polymicrobial infections. Since metabolic interactions can potentially occur in virtually

any polymicrobial infection, our results suggest that in some cases, the ability to cause infection will be as dependent on metabolic interactions as it is on known immune defense mechanisms and classical virulence factors. Our observations also have therapeutic implications, as development of small molecule inhibitors of metabolic pathways, particularly pathways restricted to prokaryotic pathogens, have promise as new therapeutic targets. Based on this study, efforts to develop such therapeutics will require a detailed understanding of how polymicrobial cross-feeding affects colonization and persistence in an infection site.

Chapter 4: Real time mapping of a H_2O_2 concentration profile across a polymicrobial bacterial biofilm using scanning electrochemical microscopy (SECM)*[3]

* This chapter is a collaborative effort between myself and the members of Dr. Alan Bard's laboratory at the University of Texas at Austin. In all cases, biological media preparation, cell preparation and any bacterial experiments were performed or prepared by myself. SECM calibration, measurements and operation were performed by members of the Bard laboratory. All participating members are credited in Liu *et al* [48].

4.1 INTRODUCTION

Streptococcus gordonii (*Sg*) is a member of the viridans group streptococci; Gram-positive oral microbes that are known to ferment sugars into lactic acid and produce hydrogen peroxide in the presence of oxygen [19]. The presence of these beneficial oral streptococci has been shown to improve oral health, by either competition with pathogens for nutrients in the oral cavity or by the production of inhibitory concentrations of hydrogen peroxide. Populations of viridans group streptococci negatively correlate with the presence of many notable oral pathogens [107, 131]. However, recent work has demonstrated that *in vitro Sg* can grow in co-culture with the opportunistic oral pathogen *Aggregatibacter actinomycetemcomitans* (*Aa*) [31]. *Aa* has been shown to preferentially utilize the *Sg* produced metabolite lactic acid as a primary carbon source, even when hexose sugars are present [7]. The primary mechanism for hydrogen peroxide detoxification in *Aa* is the *katA* enzyme [12]. Recent work has demonstrated that *katA* expression is induced by hydrogen peroxide as well as the induction of *apiA*, which encodes for an immunoprotective factor rendering *Aa* more resistant to the host immune system [30]. These studies demonstrated an induction of

[3] Liu, X., et al., *Real-time mapping of a hydrogen peroxide concentration profile across a polymicrobial bacterial biofilm using scanning electrochemical microscopy.* Proc Natl Acad Sci U S A, 2011. **108**(7): p. 2668-73.

gene expression in mixed species biofilms by *Sg*-produced hydrogen peroxide [31]. Because hydrogen peroxide is rapidly degraded by catalase and can also react with other biological materials, we sought to quantify local hydrogen peroxide concentrations in real-time to be utilized for future polymicrobial experiments between *Sg*, *Aa* and other oral bacteria.

Previous measurements of hydrogen peroxide have been performed using fluorescence, spectroscopy and other methods [19, 40, 132-134]. However, current techniques lack the ability of making a quantitative measurement of local hydrogen peroxide concentration at the surface of a biofilm. In this study, scanning electrochemical microscopy (SECM) was used to address this problem. SECM has the unique ability to set the exact distance from a sensing tip (an ultramicroelectrode （UME） of size ~ 10 to 25 μm diameter) to a substrate through a feedback approach curve [135] (tip current, i_T, vs. distance above substrate, d) and thus is able to measure the local concentration over a biofilm. Several studies concerned with the electrochemical measurement of hydrogen peroxide concentration have been reported [42-47], but none dealt with spatial mapping adjacent to a biofilm surface. In addition, SECM has the ability to scan over a substrate in the x-y direction and thus is able to record a unique spatial concentration profile over the surface. SECM has been used before in biological systems [136-141] to measure the local concentration over soft biological samples and for imaging. SECM is thus a new analytical tool to study not only the local peroxide concentration in a bacterial biofilm, but also to map the peroxide concentration spatially across two different species of bacteria located distally in a biofilm. This allows the determination of the actual peroxide concentration produced by *Sg*, but also the quantification of the effective peroxide concentration encountered by a neighboring organism such as *Aa*. This introduces SECM

for use in such real-time mapping of local peroxide concentration in a biofilm and determination of the consumption of peroxide in a polymicrobial biofilm during spatial scanning. This allows us to measure the effective concentration of hydrogen peroxide *in situ,* the flux of peroxide at the bacteria surface, and determine how it might shape polymicrobial interactions.

4.2 MATERIALS AND METHODS

Chemicals

Sulfuric acid (94-98%, trace metal grade), potassium nitrate, potassium chloride, agar purified grade) and o-phosphoric acid (85%) from Fisher Scientific (Fair Lawn, NJ) were used as received. Fresh solutions of hydrogen peroxide were made before each experiment by diluting a concentrated commercial aqueous solution (30% (v/v), Sigma-Aldrich GmbH, Steinheim, Germany). All solutions were prepared with deionized Milli-Q water.

Bacterial cultures and preparation

Streptococcus gordonii strain DL1, *Aggregatibacter actinomycetemcomitans* Y4 and *Aa* Y4 *katA*- containing an insertion mutant of the catalase-encoding gene *katA* [12] were used in our study. Broth cultures were grown by shaking at 150 RPM at 37 °C in a 5% CO_2 atmosphere unless specified otherwise. The growth medium included Tryptic soy broth + 5% yeast extract (TSBYE) or CDM [7].

Sg was inoculated from a single colony into 3 mL TSBYE broth and grown overnight to an approximate cell density of 3×10^9 cells/mL ($A_{600} = 3$). Cells were next diluted into 3 mL of TSBYE to a density of $A_{600} = 0.05$ and grown to a density of $A_{600} = 0.5$. 2 mL of cells were collected via centrifugation at 10,000 × g for 5 min and re-suspended in 1 mL phosphate buffered saline (PBS). 25 mm polycarbonate membranes (Whatman, 0.2 μm pore size) were aseptically transferred to the surface of a 100 mm TSAYE agar plate. 50 μL of the above cell suspension (~5 x 10^7 cells) was spotted directly onto the membrane surface and uniformly spread to cover the entire membrane using a sterile spreader. Cell suspensions were dried on the membranes for approximately

10 min in a laminar flow hood to form a colony biofilm. TSAYE plates and membranes containing bacterial biofilm were transferred back to 37 °C and 5% CO_2 environment for approximately 1 h.

Aa strains were grown overnight in 3 mL TSBYE to a cell density of A_{600} = 1; then diluted into 3 mL of TSBYE to a density of A_{600} = 0.05. Cells were then grown to a density of A_{600} = 0.5 and 2 mL were centrifuged as above and re-suspended in 1 mL of PBS. Cells were then diluted 1:10 in PBS buffer. 5 µL of cell suspension (corresponding to ~5×10^6 cells were spotted directly on the center of the *Sg* coated membrane prepared as above prior to the final 1 h incubation step at 37 °C. The polycarbonate membrane, as a result, had 25 mm diameter bacterial biofilm of *Sg* with a spot of 5 to 7 mm *Aa* in the middle. Biofilm preparations with the *katA*- mutant were performed identically.

Ultramicroelectrode fabrication

Gold (99.99+%) wire, 25 µm diameter, from Goodfellow (Devon, PA) was used to fabricate the SECM tip. First, it was fabricated by heat sealing the corresponding metal wire under vacuum in a borosilicate glass capillary. Then, it was polished and shaped conically by a wheel with 180-grid Carbimet paper disks and micropolishing cloth with 1.0, 0.3, and 0.05 µm alumina. The tip used in this study was sharpened to RG = 2, where RG is the ratio between the radius of the glass sheath and the radius of the active electrode surface. Before each experiment, the Au tip was polished with alumina paste (0.3 and 0.05 µm) on microcloth pads (Buehler, Lake Bluff, IL), sonicated for 15 min in water, and then electrochemically cleaned by cycling between 0.2 and 1.4 V in 0.1 M sulfuric acid for 40 cycles to a constant CV. 0.5 mm tungsten wire from Alfa Products

(Danvers, MA) was used as an auxiliary electrode. Ag|AgCl|3 M KCl was used as reference electrode to which all potentials for electrochemical experiments are referred.

Real-time electrochemical monitoring of hydrogen peroxide by SECM on *Sg* biofilm

An *Sg*-coated 25 mm polycarbonate membrane was prepared as described in the "Bacterial strains culture and preparation" section. The membrane was then transferred carefully from the agar plate onto a piece of double sided tape (3M: 34-8517-3569-5) fixed to the bottom of a 35 mm Petri dish (Becton Dickinson). The dish was later put on a home built copper heating plate on the CHI 920C SECM stage (CH Instruments, Austin, TX) to maintain a constant temperature of 37 °C. The experimental setup for SECM measurements is shown in Figure 4.1A,B. The biofilm was incubated for 1 h at 37 °C after adding 1.5 mL of CDM solution to the 35 mm Petri dish. During this period, an approach curve (tip current, i_T, vs. distance, d) was taken over the biofilm with oxygen as a mediator by holding the tip at -0.6 V (seen in Figure 4.1C). Tip-membrane distance was then fixed at 200 μm. The background was recorded at the same height by pulsing the tip from 0.55 to 0.80 V for 10 s. 15 μL of 1 M of glucose was added to the existing 1.5 mL of CDM buffer to make the final glucose concentration 10 mM. The hydrogen peroxide concentration over the biofilm was measured as a function of time by pulsing the tip at the same potential range of background recording every 5 min.

Y-scan and approach curve SECM experiment on a *Sg* and *Aa* co-culture biofilm

The biofilm sample was prepared by the same method as described in the "Bacterial strains culture and preparation" section. The only difference in this sample was a 5 to 7 mm diameter spot of *Aa* in the middle of the *Sg* biofilm. As shown in Figure 4.2A, the location of the *Aa* spot was marked on the outside of the Petri dish with a

marker. The same SECM imaging procedure was followed as before with the tip-substrate distance at 200 µm and the background current recorded at the same height. First, the growth of the hydrogen peroxide concentration was observed at d = 200 µm over the *Sg* area for 1 h. The tip was then scanned at 150 µm/s in the y-direction at d = 200 µm from *Sg-Aa-Sg* to record the peroxide concentration across the two different bacterial populations. Approach curves were performed using hydrogen peroxide as a mediator at three different points; one on *Sg* and one on *Aa* and another one again on *Sg*.

Fluorometric measurements of hydrogen peroxide

Hydrogen peroxide production was measured using the Amplex Red hydrogen peroxide assay kit (Invitrogen) using the manufacturer protocols. *Sg* was cultured as mentioned above and 5×10^7 cells were either spread onto a 25 mm polycarbonate membrane to form a biofilm and then placed in a 35 mm Petri dish or re-suspended directly in 1.5 mL of CDM + 10 mM glucose. Biofilm cells were covered with 1.5 mL CDM + 10 mM glucose. Aliquots were taken from each culture in triplicate at 2, 4 and 8 h then measured using the above assay kit on a BioTek Synergy MX (BioTek) fluorometric microplate reader at excitation / emission values of 530 nm and 590 nm, respectively. For *lux* reporter experiments we used the *Aa katA-lux* reporter strain (Chapter 2) in place of *Aa* wt in the biofilm overlay. *Aa katA-lux* was grown to the exponential phase and 5×10^8 cells were isolated via centrifugation at 10,000 × g for 10 min. Cells were resuspended in 5 µL TSBYE and placed onto the surface of the *Sg* biofilm prepared as above. Biofilms were incubated on the surface of a TSAYE plate at 37 ºC for ~1 h then image captures were exposed for 10 min in a Syngene G:BOX (Syngene) using the manufacturers software. Image sizes were scaled to the x-axis using Photoshop CS5.

Simulations

Simulations were performed with Comsol Multiphysics 3.3 on a 2.8 GHz Intel Pentium IV processor and 2 GB RAM desktop PC. Details about the simulation model are given in Appendix A.

4.3 RESULTS

Real time quantitative measurement of hydrogen peroxide produced by living *Sg* colony biofilms with SECM

Figure 4.1D shows the formation of hydrogen peroxide by a *Sg* colony biofilm [142] as a function of time (min) at 100 μm and 200 μm, respectively, above the film. Each concentration point in the plot corresponds to the chronoamperometric current due to hydrogen peroxide oxidation at a particular time, e.g. t = 30 min. The concentration was calculated from the current recorded at 10 s using the calibration curve shown in Appendix A figure A1.

For a pure *Sg* biofilm with the tip 100 μm away, the peroxide concentration increased initially for about 10 to 12 min and then tended to a quasi-steady-state concentration of ~1.4 mM. This behavior can be understood in terms of a substrate, the biofilm, with a sufficiently large area that diffusion from it can be considered linear. However, as is well known from the behavior of electrodes generating a species with a constant flux, diffusional behavior can only be maintained, even with careful isolation of the cell from vibrations, for a time of 5 to 10 min. At some stage natural convection begins and the current then tends to a steady state governed by the convection rate [143]. When the tip was placed at 200 μm above the membrane for the same biofilm, peroxide concentration was found to be 0.4 mM after 60 min.

To obtain the most relevant measurement of streptococcal released hydrogen peroxide, a relatively long monitoring time (8 h) for hydrogen peroxide generation from *Sg* was performed as shown in Figure 4.1E. After 8 h, the tip was raised to 1000 μm away from the membrane and hydrogen peroxide concentration at that region was found to be about 0.5 mM, much smaller than the steady-state concentration of hydrogen

peroxide closer to the membrane (e.g. ~1.6 mM), indicating that even with natural convection, there is a concentration profile of hydrogen peroxide away from the membrane. To show this, an approach curve was performed from 1000 μm away towards the membrane, as shown in Figure 4.1F. A gradual increase in tip current due to an increase of hydrogen peroxide concentration was observed over a distance of several hundred μm as the tip approached the membrane, indicating that somewhat higher hydrogen peroxide concentrations exist in the local area near the membrane. The sharp decrease of tip current at 1000 μm in Figure 4.1F is due to a blocking effect when the tip touched the membrane. The absolute value of peroxide concentration near the surface of the biofilm in Figure 4.1F was lower than that shown in Figure 4.1D. This difference might be due to a difference in time for data acquisition The current found through an approach curve over the 1000 μm distance was measured over a long duration compared to the 10 s pulse measurement (Figure 4.1D). However the bulk peroxide concentrations were the same in both the cases (Figure 4.1D and 4.1F).

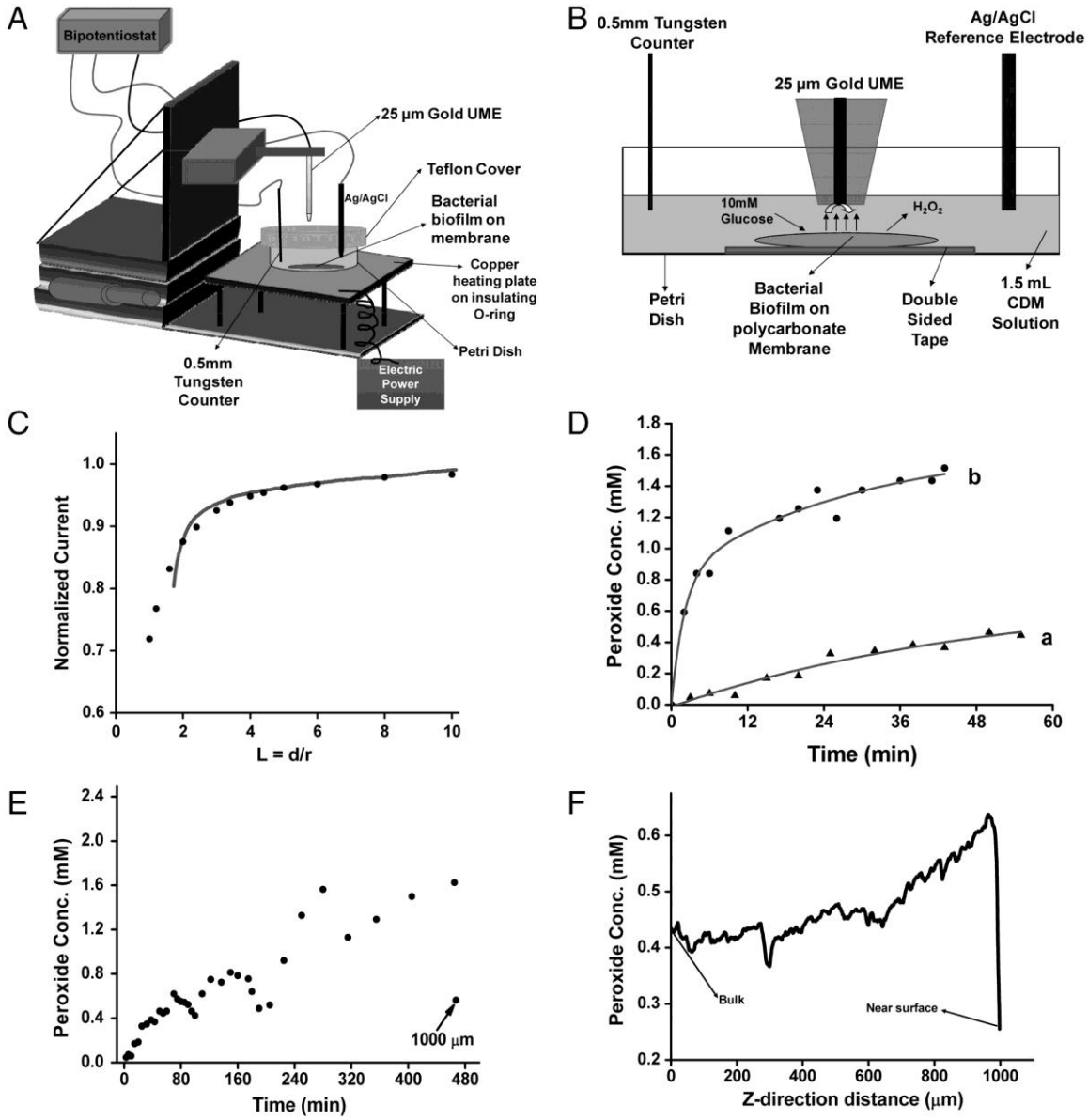

Figure 4.1. Hydrogen peroxide measurements in the z-axis and over time.

(A) Schematic diagram of SECM for real-time measurement of hydrogen peroxide formation in a bacterial biofilm. (B) Schematic diagram of an electrochemical experimental setup for A. (C) An approach curve (solid line) with oxygen as a mediator in CDM at 37 °C, the tip potential was held at -0.6 V, and the scan rate was 25 µm/s. The points represent the theoretical negative feedback approach curve above an electrically insulating surface. (D) Plots of the concentration of hydrogen peroxide produced by *Sg* in biofilm as a function of time at different distances between the Au UME and the biofilm (a, 200 µm, b, 100 µm). (E) Plot of hydrogen peroxide concentrations produced by a *Sg* biofilm as a function of time over 8 h. (F) An approach curve with hydrogen peroxide produced by a *Sg* biofilm as a mediator in CDM at 37 °C, the tip potential was held at 0.8 V, and the scan rate was 25 µm/s. The z-direction axis measures distance travelled from bulk to the surface, with the sharp drop indicating the surface position.

Y-scan and approach curve SECM experiments over *Sg* and *Aa* co-cultured bacterial biofilm

Figure 4.2B shows the results of a SECM y-scan over *Sg* only, *Sg* + *Aa* and *Sg* + *Aa katA*- biofilms. All currents were normalized for comparison purposes. The y-scan data obtained with the pure *Sg* biofilm shown in Figure 4.2B (green curve) is fairly constant, showing uniform behavior across the film. The *Sg* film modified with a 5 to 7 mm spot of *Aa* in the center (Figure 4.2B red curve), however, showed an evident current decrease (valley) over the *Aa* region on the membrane. The width of the valley was about 7000 μm, consistent with the diameter of the *Aa* spot made on the *Sg* biofilm (seen in Figure 4.2D). The current in the valley dropped to ~0.66 of the current for the *Sg* region. The blue curve in Figure 4.2B displays the y-scan over the *Aa katA*- mutant doped *Sg* biofilm. It shows a slight current dip over the *Aa katA*- mutant region as well; here the current dropped only to ~0.91 compared to *Sg*, indicating that a higher concentration of hydrogen peroxide is observed on the *Aa* mutant lacking catalase (*katA*) compared to wild-type *Aa*.

Approach curves were collected over the pure *Sg* region (y = 1000 μm) and the *Aa* region (y = 10,000 μm) in the same membrane, respectively (see Figure 4.2C). The approach curve over the *Sg* region showed a steady current increase as the tip approached the *Sg* membrane over a distance of 300 μm, indicating that a higher concentration of hydrogen peroxide was found near the *Sg* membrane. Over the *Aa* region, however, a current drop was observed as the tip moved closer to the *Aa* surface, showing a negative deviation from the usual negative feedback mode approach curve as a result of shielding because of consumption of hydrogen peroxide in the *Aa* region.

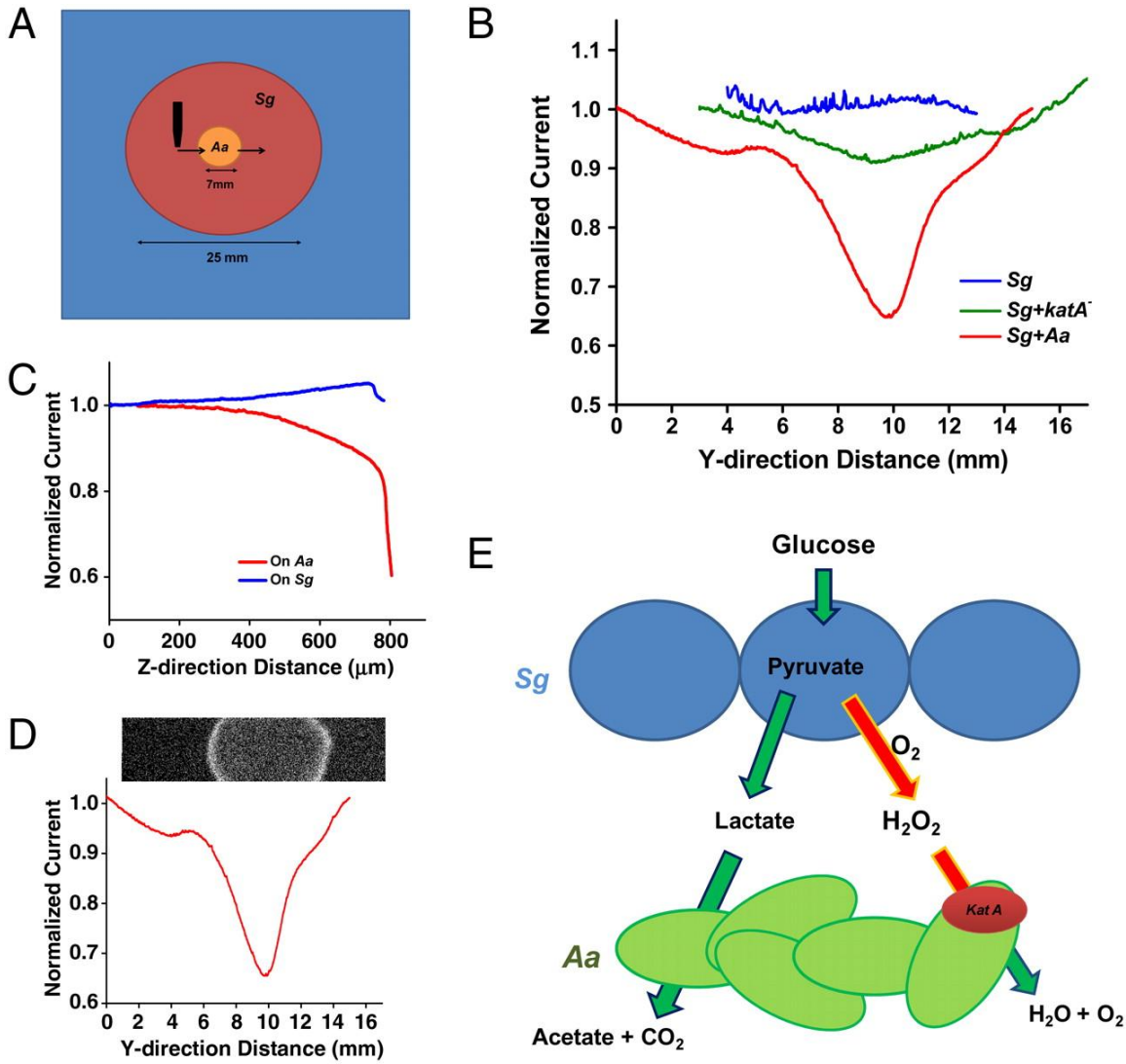

Figure 4.2. Spatial hydrogen peroxide measurement by SECM.

(A) Schematic diagram of tip scan across the region of a mixed species biofilm in the order of *Sg*-*Aa*-*Sg*. (B) Normalized current changes of an SECM y-scan over *Sg* alone, mutant *Aa* in an *Sg* film, and wild-type *Aa* in an *Sg* film, respectively, at 37 °C. Tip potential was held at 0.8 V, and scan rate was 150 μm/s. Green is pure *Sg*, blue is mutant *Aa* with *Sg*, red is wild *Aa* with *Sg*. (C) Approach curves for pure *Sg* and wild-type *Aa* region in an *Aa* + *Sg* biofilm (B, red curve). (D) Normalized current changes of an SECM y-scan over *Aa* + *Sg* biofilm extrapolated to identical biofilms using *Aa* carrying the *katA*-*lux* reporter vector. Light production (in white) is indicative of promoter response to hydrogen peroxide. (E) Model for the role of hydrogen peroxide in an *Sg* and *Aa* cocultured biofilm.

4.4 DISCUSSION

Real time quantitative measurement of local peroxide concentration produced by a *Sg* biofilm

Sg-produced hydrogen peroxide was measured with a SECM tip located ~100 to 200 μm above the biofilm in the experimental set up as shown in Figure 4.1A, B. The biofilm itself was 10 to 20 μm thick as measured by confocal laser scanning microscopy (Appendix A, figure A7). Although individual measurements were expected to be different because of biological variability (e.g., cell condition, number of the bacterial cells on the membrane), most concentration vs. time profiles we observed were very similar in shape to that shown in Fig. 4.1D. A quasi-steady-state hydrogen peroxide concentration of 1.4 mM was observed (Fig. 4.1D, curve b) at 100 μm away from biofilm, while only 0.4 mM peroxide concentration was recorded at 200 μm away for the same period of 60 min in the presence of 10 mM glucose as shown in Fig. 4.1D, curve a. As indicated earlier, this difference in hydrogen peroxide measurement may be due to mass transfer of hydrogen peroxide produced by the biofilm into the bulk phase by natural and induced convection. In addition, a slower response of hydrogen peroxide above the biofilm is observed at 200 μm, since it takes a much longer time to build up detectable hydrogen peroxide concentrations at this distance through diffusion and convection. This is supported by Fig. 4.1E where a higher hydrogen peroxide concentration (1.6 mM) is observed at 200 μm away for the same type of *Sg* biofilm when exposed to 10 mM glucose for 8 h.

Figure 4.3 shows the fitted simulated curve treating diffusion of peroxide from the film to the SECM tip could be fit to the experimental response by the biofilm upon exposure to 10 mM glucose. The simulated curve (the solid line) fit the experimental data for about 10 min, and then began to deviate because of the onset of natural

convection during measurement (not considered in the simulation model). However the response for the first 10 min could be used to predict the flux at the biofilm surface. As discussed previously, SECM was a very useful tool in measuring the local concentration of peroxide above the biofilm or 100 μm from the biofilm surface. But it still did not give the concentration or flux at the biofilm surface. With the aid of digital simulation, the exact peroxide flux at the biofilm surface can be calculated as in SECM experiments, when the tip-substrate distance is known. The details of the simulation model can be found in Appendix A. Briefly, the simulation assumes only diffusional mass transfer and a constant peroxide flux from the biofilm surface to a 25 μm SECM tip (RG=10) at a distance of 100 μm away from the surface. The fitted peroxide flux at the biofilm surface was determined to be 1.0×10^{-11} mol/cm^2/s. Assuming a dimension of each bacterium is 1.5 μm × 0.8 μm, the calculated bacterial density was 8.3×10^7/cm^2. So, approximately 1.2×10^{-19} mol (~70,000 molecules) of peroxide effluxed from a single bacterium at the film surface per second. This gives an important estimate of the amount of peroxide produced at the bacteria surface, which may be useful for elucidating the defense mechanism of a bacterial species or interactions with other bacterial species in terms of metabolite or peroxide concentration.

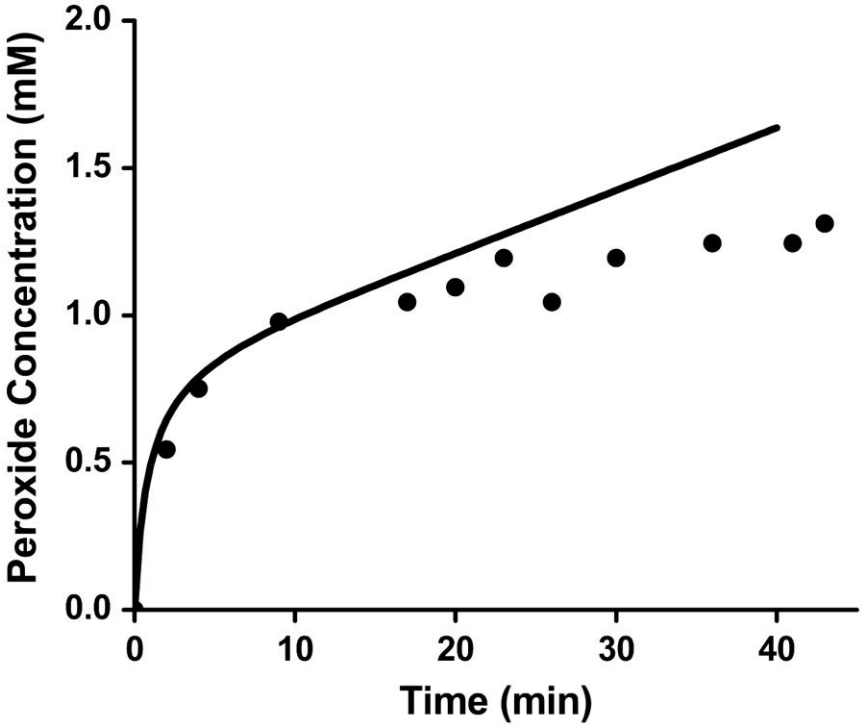

Figure 4.3. Modeling hydrogen peroxide flux at the biofilm surface.

The simulated (solid line) hydrogen peroxide metabolite efflux from a bacterial biofilm of *Sg* at a distance of 100 μm from surface compared to experimental measurements (dots). The diameter of the SECM tip used was 25 μm (RG = 10).

Interestingly, significantly lower concentrations (20-40 μM range) of peroxide are observed in Table 1 both for biofilm as well as cell suspensions when measured by taking aliquots of bulk solution using a commercial fluorometric assay. Similar bacterial numbers and incubation times in 1.5 mL of chemically defined medium (CDM) culture solution were used for the same time periods in both methods for comparison. Results suggest that the local peroxide concentration is significantly higher for a biofilm in comparison to the bulk phase and that SECM is an ideal analytical tool due to its ability to measure such concentrations close to the biofilm surface. However, it is difficult to

understand the results in terms of diffusion from the bacteria surface at times longer than about 10 min at most.

	Time (h)		
	2	4	8
Suspension fluorometric measurement	19.2 μM	20.2 μM	30.6 μM
Biofilm supernatant fluorometric measurement	21.0 μM	19.0 μM	30.6 μM
Biofilm electrochemical measurement (at 200 μm away)	0.7 mM	0.9 mM	1.6 mM

Table 4.1. Hydrogen peroxide measurement method comparisons.

A comparison of hydrogen peroxide production concentration from *Sg* by fluorometric and electrochemical measurement.

It is also important to carefully consider the conditions at which the metabolite concentration measurements are made before considering any of their effects on bacterial functions or their interactions with other bacterial species; especially for toxic molecules such as hydrogen peroxide. As observed from our SECM experiments, the *Sg* biofilm is able to produce a high enough peroxide concentration in the mM range, which should be able to inhibit the growth of many bacteria, but such conditions prevail only at a very close distance from the biofilm surface. The presence of higher peroxide concentrations close to the surface (~200 μm) is also observed in the hydrogen peroxide approach curve (shown in Fig. 4.1F). The sharp drop in current or peroxide concentration happens when the tip touches the surface and thus blocks any further diffusion of peroxide to the tip. Fluorescent dyes are available to detect reactive oxygen species such as hydrogen peroxide and superoxides in individual cells; however, such techniques only provide qualitative information about these metabolites. Thus, SECM has a significant advantage in measuring local concentrations spatially across a biofilm to elucidate how mass transfer affects this complex and dynamic biological system; existing biological analytical methods are unable to obtain such information.

KatA mediated decomposition of hydrogen peroxide in a mixed species biofilm

The y-direction SECM scan shown in Figure 4.2B (red curve) over co-cultured *Sg* and *Aa* wild type biofilms reveals a unique peroxide concentration profile across two different regions. The current from hydrogen peroxide oxidation at the tip while scanning over the *Aa* region, exhibits a lower concentration (a ~34 % decrease) based on the normalized currents at the deepest point, indicating that hydrogen peroxide is consumed by *Aa*. The reason for this consumption can be explained as shown in the model in Figure 4.2E. According to the proposed model, wild type *Sg* bacteria can produce hydrogen peroxide by metabolizing glucose in the presence of oxygen. In addition to lactic acid, which is another main metabolite, *Aa* is able to flourish in this environment by decomposing hydrogen peroxide using the KatA enzyme. This model has been validated in our experiments by performing y-scans over *Aa katA*-, which is unable to detoxify hydrogen peroxide in the presence of *Sg*. As shown in Figure 4.2B (blue curve), no significant decrease in y-scan current or concentration is noticed, thus confirming no hydrogen peroxide consumption by *Aa katA*-. The slight dip in y-scan current over the mutant *Aa* zone is, however, due to lower peroxide concentration over a void space created by the non-consuming and non peroxide producing mutant *Aa*. Since the *Aa* spot is surrounded by hydrogen peroxide producing *Sg* bacteria (Figure 4.2A), hydrogen peroxide can spill over from the surrounding area and subsequently fill the empty *Aa* spot. No dip in current is observed in Figure 4.2B (green curve) when the tip is scanned over the *Sg*-only bacterial biofilm as no spatial change in peroxide concentration in the y-direction is expected at a given height.

Discussion summary

By using SECM**,** we measured the local hydrogen peroxide concentration produced by *Sg* biofilms in real time and found it to be significantly different than suspension peroxide measurements. The concentration of hydrogen peroxide can reach 1.2 mM with the tip placed 100 μm away from the biofilm. A quasi-steady-state concentration was always observed, as hydrogen peroxide is likely decomposed by *Sg* to prevent injury by excessive hydrogen peroxide concentrations. Furthermore, we also measured local peroxide concentrations across *Sg* and *Aa* co-cultured biofilms with a one-directional scan SECM technique. Our results not only confirmed that *Aa* catalase activity was critical for decreasing local hydrogen peroxide concentration, but that this decomposition effect was only observed in the immediate vicinity of *Aa*. Quantitative investigation with these and other bacteria will help us to understand the mechanism of how hydrogen peroxide influences the ecology of mixed species communities.

Chapter 5: Pyocyanin Electrochemistry from a *Pseudomonas aeruginosa* Biofilm using SECM*

* This chapter is a collaborative effort between myself and the members of Dr. Alan Bard's laboratory at the University of Texas at Austin. In all cases, biological media preparation, cell preparation and any bacterial experiments were performed or prepared by myself. SECM calibration, measurements and operation were performed by Dipankar Koley of the Bard laboratory.

5.1 INTRODUCTION

P. aeruginosa is a Gram-negative bacterium whose dimensions are 0.5 to 0.8 μm by 1.5 to 3.0 μm. It is motile due to presence of a single polar flagellum and is generally found in soil and water environments. Most importantly, it is an opportunistic pathogen that primarily infects individuals with cystic fibrosis, neutropenia, AIDS, cancer and burn wounds. *P. aeruginosa* is a model organism for studying biofilms and cell-cell communication, also called quorum sensing (QS). At high cell densities, QS controlled signaling pathways induce *P. aeruginosa* to produce a distinguishing phenazine compound pyocyanin (PYO) in addition to several other phenazines that will be discussed later.

QS is the cell density-dependent regulation of bacterial gene expression. Gene expression is controlled in response to a bacterially-produced signal that increases in concentration as bacterial populations grow or as proximity between cells in a small volume decrease [144, 145]. [145, 146] QS plays an integral role in shaping bacterial behavior within a species (intra-species) or between other species (inter-species). Both Gram-positive and Gram-negative bacteria exhibit QS. A typical QS circuit diagram of

Gram-negative bacteria is shown in Figure 5.1. Gram-negative bacteria typically produce acyl homoserine lactone (AHL) signals (autoinducers) that are especially used for intra-species communication. AHL molecules consist of a homoserine lactone core and an acyl chain that can vary in length from C4 to C18, thereby conferring species-specificity (Figure 5.2). Bacteria produce AHL molecules via the LuxI synthase or its homologues, which catalyzes acylation and lactonization reactions between the substrates S-adenosylmethionine (SAM) and hexanoyl-ACP. AHLs diffuse into the extracellular environment when bacterial density is low, and when bacteria reach a high enough density, the signal reaches a threshold concentration whereby it binds its cytoplasmic receptor proteins (LuxR in the Figure 4.1 example), leading to changes in gene expression. When bound to its canonical ligand, receptor proteins bind to a consensus binding sequence (*lux* box), resulting in induction or repression of downstream genes. The LuxR protein is unstable in the absence of its respective AHL. In addition, LuxI is activated by the AHL-LuxR complex, which acts as a positive feedback control loop to synthesize more QS molecules.

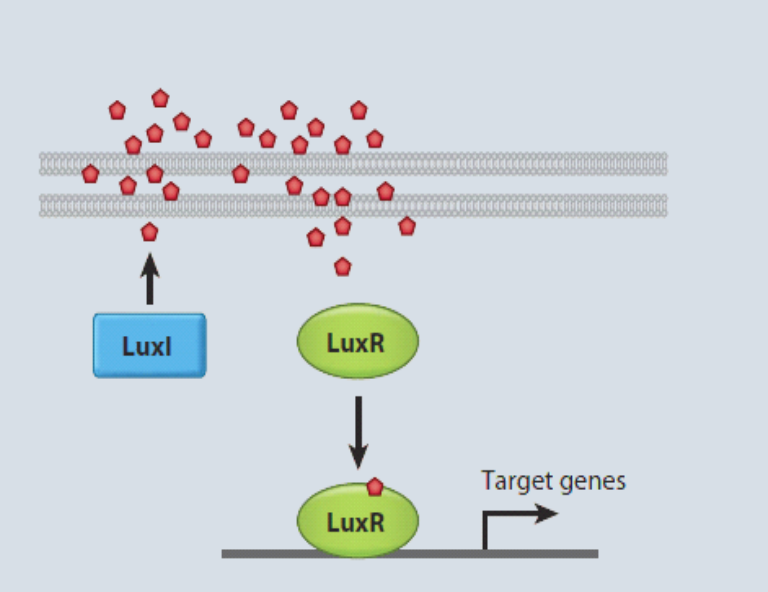

Figure 5.1. Schematic representation of a QS circuit of the Gram-negative bacteria *Vibrio fischeri*.

Red pentagons represent autoinducer molecules or acyl homoserine lactones (AHL). (Adapted from reference [145])

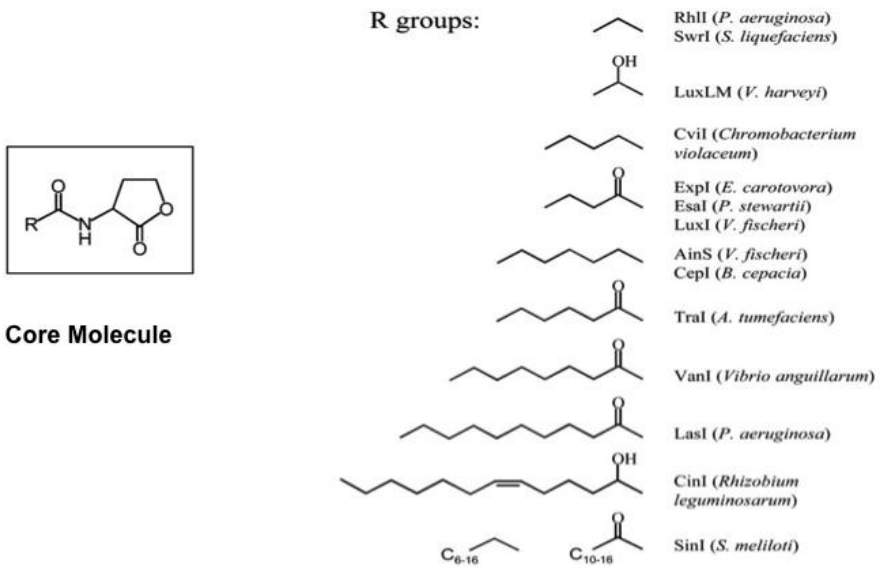

Figure 5.2. List of different autoinducers or (QS) molecules.

(*Left*) The core AHL molecule produced by Gram-negative bacteria. (*Right*) AHL side chain functional groups used by different bacterial species. The acyl variation of an AHL molecule is often unique to a particular bacterial species. (Adapted from reference [147])

The QS circuit for *P. aeruginosa* consists of two pairs of synthase/receptor units, LasI/R and RhlI/R. A detailed QS circuit diagram is shown in Figures 5.3 & 5.4. The AHLs C_{12}-AHL and C_4-AHL are produced in late exponential phase by LasI and RhlI, respectively. C_{12}-AHL upregulates the production of the Pseudomonas Quinolone Signal, or PQS, which induces C_4-AHL production via RhlI [146]. PQS upregulates the *phzA-G* genes, which produce phenazine derivative compounds which act as virulence factors and antimicrobials. One phenazine derivative, pyocyanin, plays a significant role in iron chelation as well as biofilm growth and morphology [148]. Pyocyanin is also hypothesized to act as an electron shuttle, moving electrons from the oxygen deficient biofilm core to the exterior oxygen rich environment [149].

In *P. aeruginosa*, quorum signals and their downstream effectors play important roles in biofilm formation. The schematic shown in Figure 5.5 denotes the basic steps involved in biofilm formation. Bacteria, when present in a low cell density (LCD) state, often exist as free-swimming planktonic organisms. At this stage, reversible attachment to a surface often occurs. As cell density increases, collisions between bacteria and the surface also rise, hence increasing the probability that cells will adhere. Here, the cells become irreversibly attached the surface. If favorable conditions exist, sufficient numbers of bacteria will adhere to the surface to form small, densely packed populations called microcolonies (third step) [150, 151].

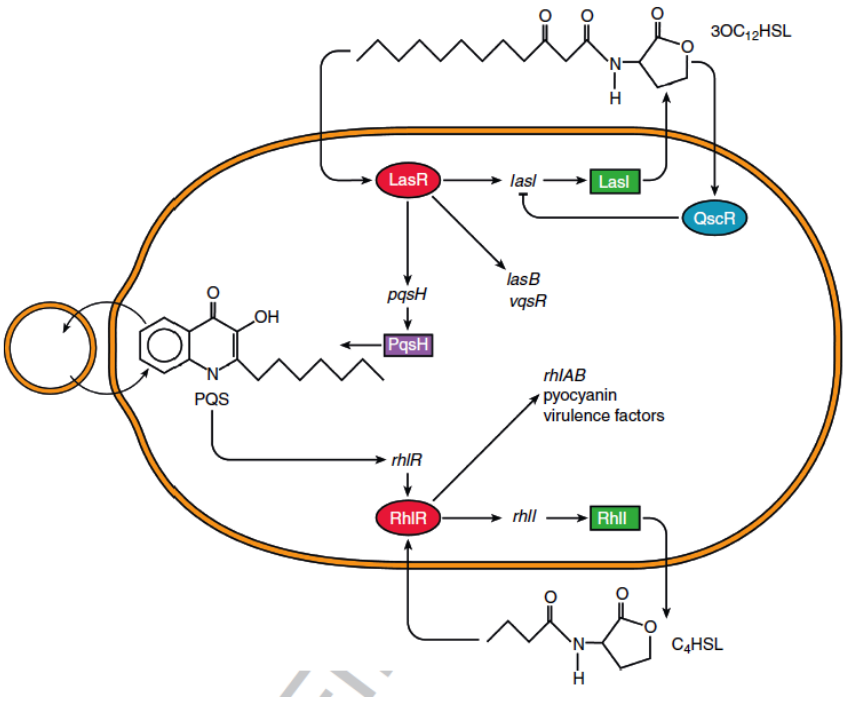

Figure 5.3. QS circuit for *P. aeruginosa*. (Adapted from reference [146]).

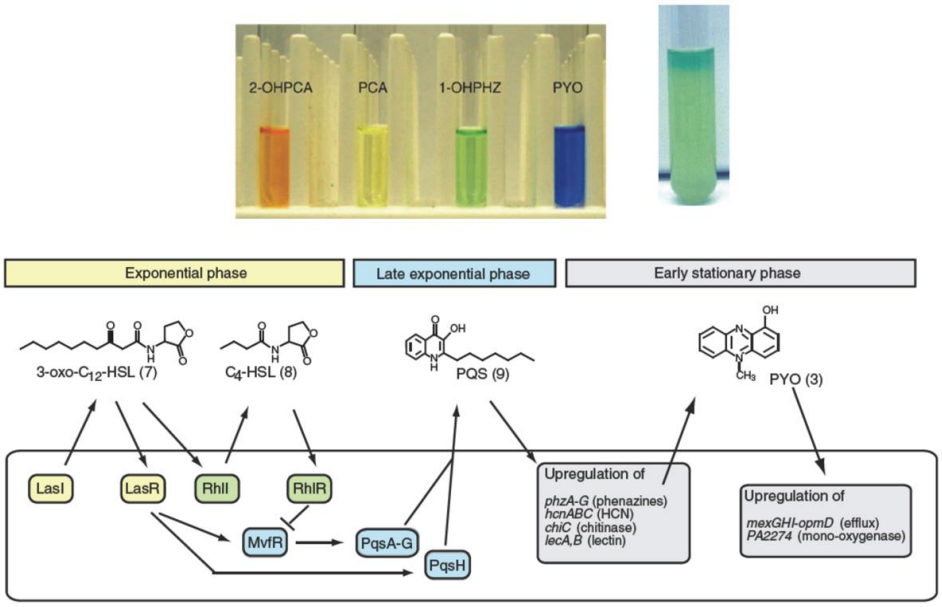

Figure 5.4. Phenazine characteristics and production.

(Top) The colored pigments of phenazine derivative compounds.(Bottom) QS diagram for *P. aeruginosa*. Acyl-HSL represents acyl homoserine lactones. (Adapted from reference [152])

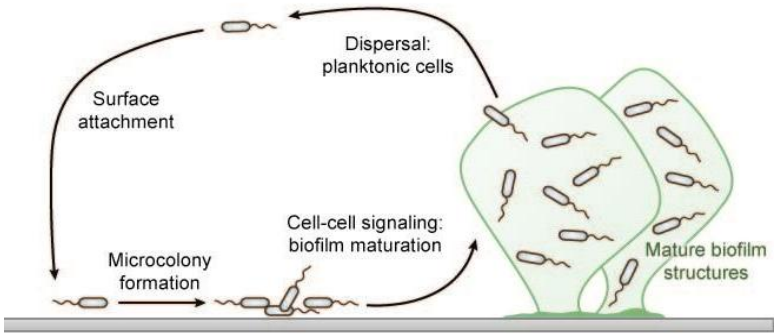

Figure 5.5. Schematic diagram of the different stages of *P. aeruginosa* biofilm formation. (Adapted from reference [153])

As the microcolony reaches high cell density, it activates QS pathways leading to the production of phenazines as well as the extracellular matrix (ECM). *P. aeruginosa* ECM is comprised of carbohydrate polymers, DNA, and protein, and the ECM helps establish the biofilm's three-dimensional architecture. At the final stage of development, the biofilm reaches a critical size and cells may disperse, ultimately liberating bacteria at the core of the matrix.

As previously mentioned, QS dependent signaling induces the production of phenazines. A detailed pathway illustrating phenazine synthesis is shown in Figure 5.6 [96, 152, 154, 155]. Briefly, a phenazine precursor, PCA, is produced from chorismate, and PCA is derivatized to produce more specific phenazines. Phenazines may serve as extracellular redox carriers, providing cells inside a biofilm with a mechanism to move electrons; as electron acceptors such as oxygen become limited at high cell densities, a soluble phenazine could act as an electron carrier.

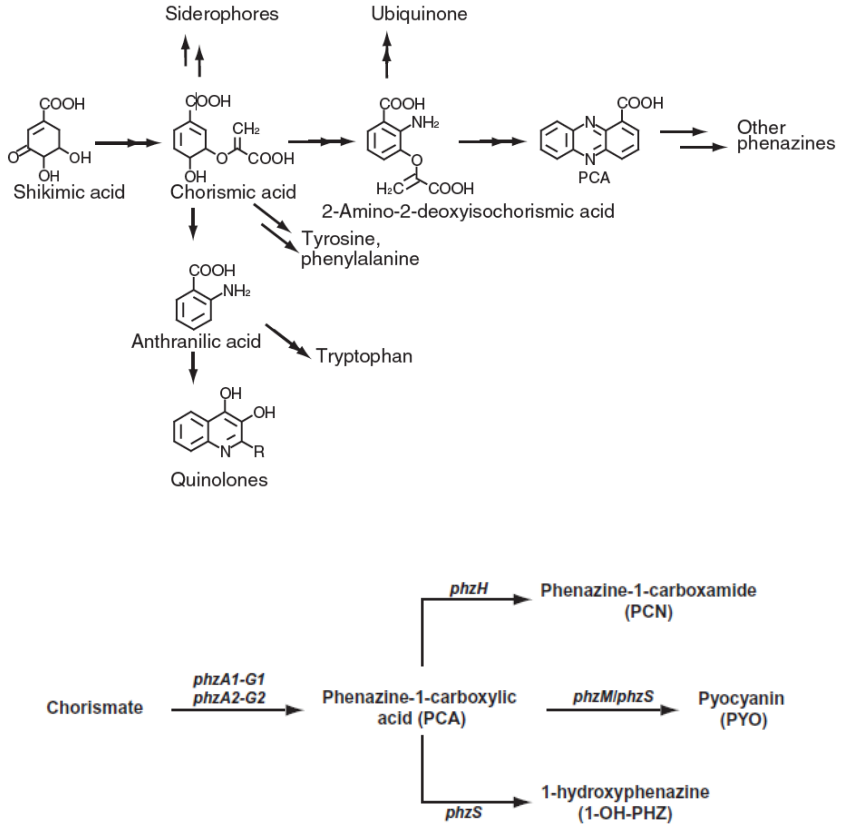

Figure 5.6. Phenazine biosynthesis pathways.

(*Top*) Schematic diagram of the phenazine synthesis pathway in *P. aeruginosa*. (*Bottom*) Phenazine production pathways from chorismate and the corresponding genes associated with them. (Adapted from reference [149, 153])

Phenazine derivatives, including pyocyanin have a wide variety of functions [154]. Particular attention has been given to the fact that several phenazines can generate reactive oxygen species (ROS). ROS generation can lend a powerful competitive

advantage to bacteria in the environment [156]. Pyocyanin has been studied as an antimicrobial compound for decades and is one of the primary pigments responsible for *P. aeruginosa*'s unique blue green color (Figure 5.4) [157]. Recent experiments have also demonstrated that phenazines can act as extracellular electron shuttles [149, 152]. These are hypothesized to either help dissipate electrons from bacteria when electron acceptors are limited (as may be the case in a dense biofilm environment) or to reduce and solublize certain metals *in situ* [158].

The structure and $E_{1/2}$ (half wave potential) of commonly found phenazine derivative compounds is shown in Table 5.1. Pyocyanin (PYO) shows two electron reversible Nernstian behavior in the pH range of 5 to 8. The $E_{1/2}$ of the reaction is -0.04 V (vs. NHE or normal hydrogen electrode/ standard electrode potential) or -0.68 V (vs. Hg/Hg_2SO_4) at pH 7.0. Since it is an outer sphere reaction, the $E_{1/2}$ position is independent of the type of electrodes (Pt, Au, glassy carbon or mercury electrode) used.

Chemical name (abbreviation)	Redox couple involving two-electron transfer	$E_{1/2}$ (vs. NHE) (mV)			
		pH 5	pH 6	pH 7	pH 8
pyocyanin (PYO)	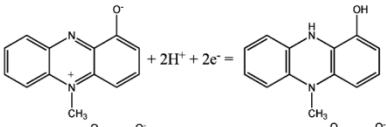	69	8	-40 (-34)[b]	-103
phenazine-1-carboxylate (PCA)	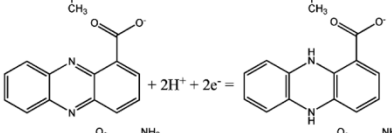	12	-60	-116 (-177)[c]	-
phenazine-1-carboxamide (PCN)	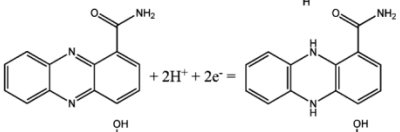	-8	-81	-140 (-115)[d]	-
1-hydroxyphenazine (1-OHPHZ)	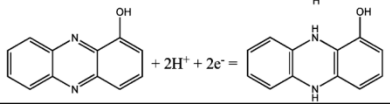	-57	-126	-174 (-172)[e]	-245

Table 5.1. List of electroactive phenazine derivative compounds and their respective half wave potentials. (Adapted from reference [159])

Iron is an essential nutrient for almost every bacterial species. In many environments, especially inside the body, iron is one of the limiting nutrients for invading bacteria. That is because *in vivo* free iron is essentially nonexistent and is scavenged and stored in hemoglobin and other iron binding proteins such as transferrin [160]. This is likely due to several reasons: first, ROS generated during aerobic respiration include hydrogen peroxide and the reaction of hydrogen peroxide with free, soluble ferrous iron yields the highly toxic hydroxyl radical. Thus, iron sequestration helps prevent generation of more potent ROS *in vivo*. Second, the sequestration of iron makes it inherently difficult for bacteria to proliferate after gaining access to an infection site. Many pathogenesis studies have demonstrated that impairing bacteria in iron transport renders them less virulent [161-163]. Bacteria have adapted and evolved many ways to obtain host iron, including the predation of other bacterial species and the liberation of iron from transferrin [160, 164]. In fact, it has been demonstrated that pyocyanin can reduce iron

and remove it from transferrin, allowing *P. aeruginosa* to grow using transferrin as an iron source [160].

P. aeruginosa has two primary ways to obtain iron from the environment. The first is siderophore mediated iron uptake. Siderophore mediated uptake allows *P. aeruginosa* to scavenge insoluble Fe (III) from its environment. Two siderophores, pyochelin and pyoverdine, are secreted from the cell, bind iron, and then subsequently contact a specific receptor on the cell exterior [148]. This process is very energy-dependent. Second, *P. aeruginosa* possesses a ferrous (*feo*) iron uptake system, allowing transport of soluble Fe (II) across the bacterial inner membrane.

5.2 RATIONALE

A biofilm is a complex three-dimensional structure comprised of bacteria and other microorganisms which can be found anywhere from rocks to dental plaques to burn wound infections. The properties of extremely high antibiotic resistance in biofilms make them an important phenomenon to study in a clinical setting. Besides being a model for biofilms and QS, *P. aeruginosa* poses a threat to immunocompromised individuals.

Currently quantitative studies on biofilm metabolism are lacking. To understand how cells communicate in their surrounding three-dimensional space, it is important to detect and spatially monitor metabolites quantitatively in real-time. Biofilms can be visually monitored using confocal microscopy, and bulk phase metabolite concentrations have been measured via HPLC and spectrophotometry. While these techniques are informative, they are also typically invasive and can involve several steps of extraction, separation, and measurement. Therefore we developed a technique that gives real time quantitative information about metabolite production in biofilms.

In this study, we used scanning electrochemical microscopy (SECM) to detect and quantify pyocyanin produced by a *P. aeruginosa* biofilm in real-time. Because pyocyanin is an electroactive compound, it is possible to directly detect its redox state, as it is produced by a biofilm. This gives us a unique opportunity to probe the local environment above the biofilm in dynamic or equilibrium conditions, which is beneficial for a biofilm behavioral study since *in situ* the local concentration is extremely relevant. Using this novel technique, we have shown that pyocyanin produced by a *P. aeruginosa* biofilm exists predominately in a reduced state and forms a layer above the biofilm in the order of

500 μm, even in the presence of oxygen. We have also demonstrated that in conditions where pyocyanin forms a substantial reducing layer, there is large proportion of Fe (II). We hypothesize that this Fe (II) enriched environment may be energetically favorable for the cell, not only for transport but by the ability to solubulize Fe (III), which may be inaccessible to the organism.

5.3 MATERIALS & METHODS

Materials

All the chemicals were used as purchased without any further purification. Pyocyanin (catalog no. R9532) and Potassium ferrocyanide were purchased from Sigma Aldrich. Falcon brand Petri dishes were used (catalog no 351008). 10 μm Pt wire was purchased from Good fellow. 18MΩ deionized water was used to prepare all the solutions (milli-Q water).

Preparation of Buffer

50/50 (v/v) mixture of MOPS and LB-broth was used as buffer in all of the experiments. pH of the buffer was adjusted to 7.2. MOPS buffer [27] contains 50 mM MOPS, 93 mM NH_4Cl, 2 mM KH_2PO_4, 1 mM $MgCl_2$, 3.6 μM $Fe_2(SO_4)_3$. LB-Broth buffer contains 5 g/L yeast extract, 10 g/L tryptone and 10 g/L NaCl. In select experiments cell supernatants were added. To generate supernatants, a *P. aeruginosa phzA1/2* mutant [96] was inoculated into 3 mL of LB-MOPS medium and grown overnight. The culture was then diluted in fresh LB-MOPS to approximately $1x10^9$ cells per mL (A600=1) and centrifuged in a 15mL tube at 7000xg for 10 min at 25°C. Supernatants were decanted and stored at 4°C until use.

Bacterial Culture & Biofilm Sample Preparation

Unless indicated wild-type *P. aeruginosa* PA14 was used. The *phzA1/2* mutant was generated previously [96] and all other *P. aeruginosa* mutants were obtained from the PA14 nonredundant transposon mutant library [165]. Unless specified, all planktonic

cultures were grown at 37°C in Luria-Bertani (LB) broth, shaking at 250 RPM. When necessary, gentamicin was used at 50 µg/mL. For biofilm formation, *P. aeruginosa* was grown planktonically overnight and resuspended to an A600 = 1. 5 µl of this suspension were added to the surface of a 25 mm polycarbonate membrane (Whatman #110606). Prior to inoculation, membranes were placed on a 100 mM petri dish containing LB agar + 100mM KNO_3. Membranes were then overlayed with a "stencil" made of Sylgard 184 PDMS (Dow Corning). PDMS stencils were fabricated by casting ~1.5 mL of PDMS into a 35 mm Petri dish with a 5 mm OD tube positioned flush with the center bottom of the well. Once polymerized the stencil was removed from the dish and the tubing was displaced leaving a 5 mm opening for biofilms to form. After inoculation, biofilms were allowed to form overnight at 37°C either aerobically or anaerobically in a Coy biofilm chamber with a 5% H_2, 10% CO_2, 85% N_2 atmosphere. Biofilms were then moved aerobically to room temperature where membranes were gently separated from the PDMS overlay. Films were transferred to the SECM apparatus mentioned in this section. Films were then overlayed with ~600 µL of LB-MOPS medium. LB-MOPS medium is a 1:1 ratio of LB medium and MOPS minimal medium with no added iron or carbon sources.

Measurement of pH and Pyocyanin Production by Planktonic Bacteria

1 mL of an overnight culture of *P. aeruginosa* was washed 2x in an equal volume of LB and the A600 determined. Washed cells were diluted into 50 ml of LB or LB-MOPS medium in a 250 ml Erlenmeyer flash and incubated at 37°C, shaking at 250 RPM. 1 ml was removed each hour for absorbance, pH and PYO measurements. Absorbance was measured at 600 nm to quantify cell growth. pH was determined by

calomel electrode and PYO concentration was determined by absorbance at 690 nm after chloroform extraction. Briefly, in a 1.5 ml polypropylene tube, 1ml of medium was extracted by addition of 500 µl chloroform and vortexed for 1 minute. Samples were centrifuged for 5 min at 14,000xg and the organic phase was transferred to a 3 mL glass vial. Chloroform was removed by an N_2 stream until no visible solvent remained. The contents of the vial were resuspended in 250 µL MOPS buffer (pH=7) and concentration was determined using the molar extinction coefficient of PYO at 690 nm (4130 M^{-1} cm^{-1}).

Detection of *phzA* Induction in a Colony Biofilm

phzA promoter fusions to GFP were a generous gift from Aimee Wessel, modified from her previous study [166]. These fusions were generated by replacement of the *rsaL* promoter region in vector pGJB5 with the *phzA1* promoter region creating pAW2, which was used here. *P. aeruginosa* containing pAW2 were used to form 5 mm colony biofilms described in "Bacterial culture and biofilm preparation". Biofilms were grown overnight anaerobically on LB agar +100mM NO_3 to ensure that *phzA* and other phenazines would not be induced at the beginning of the assay. At t=0 plates were transferred to aerobic incubation at 37°C. At 1 h intervals a 10 µL polypropylene micropipette tube was gently touched to an area of the biofilm and then used to aspirate 5 µL of PBS buffer onto a microscope slide. Samples were covered with a #1 25x25 mm coverslip and visualized for epifluoresence microscopy at 1000x magnification on a Nikon 50i microscope with a 100x 1.4NA PLAN APO lens, Nikon DS-2MBW digital camera and Nikon NiS-Elements D v3.0 software. All images were taken with a Gain of 1.0 and a 100 ms

exposure time. The brightest 4 cells in each field of view were used as representatives in the figure.

Determination of Fe(II) in the Presence of Pyocyanin (PYO)

Fe(II) measurements were performed as described by Viollier *et al* [167]. Briefly, ferrozine solution was added to samples, incubated for 5 min at 25°C allowing ferrozine to complex with Fe(II) and read for absorbance at 562 nm. After reading, the solution was acidified and reduced by addition of 1.4 M hydroxylamine in 2 M HCl to convert any Fe(III) to Fe(II) which complexed with ferrozine. Solutions were neutralized by the addition of ammonium acetate and read again at 562 nm. Initial readings were divided by final readings to determine the percentage Fe(II) present in each sample.

Electrochemical Measurements

All the electrochemical measurements were acquired using Scanning Electrochemical Microcopy (SECM) (CHI 920C, CH Instrument, Austin, Texas, USA). A 10 μm Pt electrode was used as SECM tip. Details about SECM tip fabrication can be found elsewhere [135]. 0.5 mm Tungsten wire and Hg/Hg_2SO_4 (Radiometer, Copenhagen) was used as counter and reference electrode respectively. All the potentials henceforth mentioned here were referred vs. Hg/Hg_2SO_4 (+0.64V vs. NHE).

Calibration Curve for Pyocyanin (PYO)

Biofilm was prepared as described in "Bacteria Culture & Biofilm Sample Preparation" section. After growing the *phzA1/2* mutant biofilm on a polycarbonate membrane in an anaerobic environment, it was carefully transferred on a 35 mm petri

dish (Falcon, catalog no. 351008). A PDMS stencil was carefully placed over the membrane, as shown in Figure 5.7. 500 μL of buffer was then added to fill the 1 cm diameter stencil chamber. The working UME (10 μm Pt), reference and counter electrodes were setup as shown in Figure 5.7 (*bottom*).

Aliquots of 1 mM PYO were then added to 500 μL of buffer to make 6, 10, 20, 50, 70 and 100 μM PYO solutions. Square wave voltammetry (SWV) was recorded at each PYO concentration in triplicate by 10 μm tip located in bulk solution. The parameters for SWV were as follows: Initial potential: -0.35 V, Final potential: -0.85 V, Increment Potential: 0.004 V, Amplitude: 0.025 V, Frequency: 5 Hz.

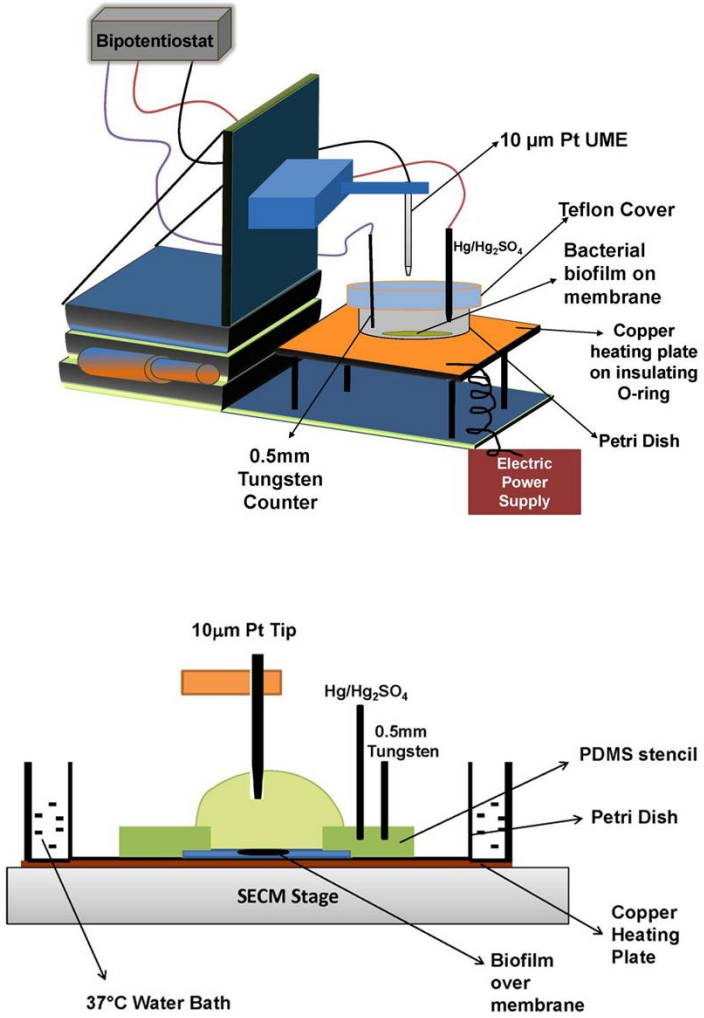

Figure 5.7. SECM Configuration.

(*Top*) Schematics of SECM experimental setup for biofilm experiment. (*Bottom*) Detail close-up experimental setup for biofilm experiment.

Real Time Quantitative Detection of Pyocyanin (PYO) using SECM

The 5 mm wild type *P. aeruginosa* biofilm was setup on an SECM stage as described in the previous section. The biofilm was gently washed twice with 500 μL of buffer (50/50 MOPS-LB mixture). Tip-substrate (biofilm) distance was then fixed at 20 μm with the aid of a negative feedback approach curve using 1 mM ferrocyanide as a redox mediator. The solution was then replaced by 500 μL of fresh buffer solution. Cells were additionally washed twice with buffer to remove any ferrocyanide in the solution. Finally, 600 μL of supernatant was added to the chamber and background current using square wave voltammetry (SWV), was measured by an SECM tip periodically. Once the background current was stabilized, the temperature of the water bath surrounding the Petri dish holding each sample was increased to 36°C using a copper heating plate connected to a Variac power supply. The temperature was constantly monitored by a thermocouple dipped inside the water bath located outside the Petri dish. The time was set to zero when the temperature reached 36°C. 200 μL of buffer was added to the chamber after 1.5 hr to compensate for water loss due to evaporation. SWV was recorded at every 10 min until 5 hr in the potential range of -0.35 to -0.85 V.

Mapping of Reduced / Oxidized Pyocyanin (PYO) Layer above a Biofilm using SECM

The biofilm was assembled on the SECM stage and an approach curve was performed to fix the tip-substrate distance as described in previous sections. Once the background was recorded, 125 μL of 1 mM PYO was added to 500 μL of buffer to make a 200 μM PYO solution. The biofilm was then incubated in the same solution for 30 min at 25°C. The tip was biased at -0.3 V (oxidizing reduced PYO at tip) and then moved in the z-direction towards the biofilm from 2000 μm away at the speed of 0.1 μm/0.02 sec

or 5 μm/sec. Similarly, the tip was biased at -0.8V (reducing oxidized PYO at tip) to map the z-direction oxidized PYO profile above the biofilm.

Electrochemical Imaging of a Biofilm using SECM

A 1 mm *P. aeruginosa* biofilm was used for electrochemical imaging using SECM. The biofilm was grown and assembled on the SECM stage as described in previous sections. The SECM stage tilt was fixed by performing a negative feedback approach curve using ferrocyanide as a redox mediator. PYO was then added to 500 μL buffer to prepare a 200 μM PYO solution. A feedback mode SECM image of a wild type biofilm was acquired at 25°C by biasing the tip at -0.3 V. The tip-substrate (biofilm) distance was kept constant at 20 μm (approx.). Scanning speed was maintained at 8 μm/0.02 sec.

5.4 RESULTS

Pyocyanin (PYO) Production by Planktonic Bacteria

To predict minimum incubation durations for our biofilm experiments, we first determined the incubation time necessary for PYO production in our media by planktonic cells. This was done because we could easily measure PYO in this setting and would provide us with an intial timeframe to approximate our biofilm measurements towards. Additionally, pH measurements were needed to determine what pH shifts we might expect during the duration of our measurements, this was necessary as pH changes affect electrochemical detection of PYO and other redox molecues. Data for PYO concentration along with a bacterial growth curve is given in Figure 5.8A. A detectable amount of PYO was observed at 4 h. A corresponding basic pH shift from 7.0 to 7.8 was also observed in Figure 5.8B.

Activation of QS Controlled Genes in a *P. aeruginosa* Colony Biofilm

To demonstrate that QS controlled gene activiation was occuring in our colony biofilm we utilized a previously constructed *phzA* promoter – GFP fusion reporter, which has been used to demonstrate the onset of QS dependent behavior [167]. Figure 5.9 shows that *phzA* promoter activity was observed in colony biofilms after transfer to fresh growth medium at a 5-6 h period.

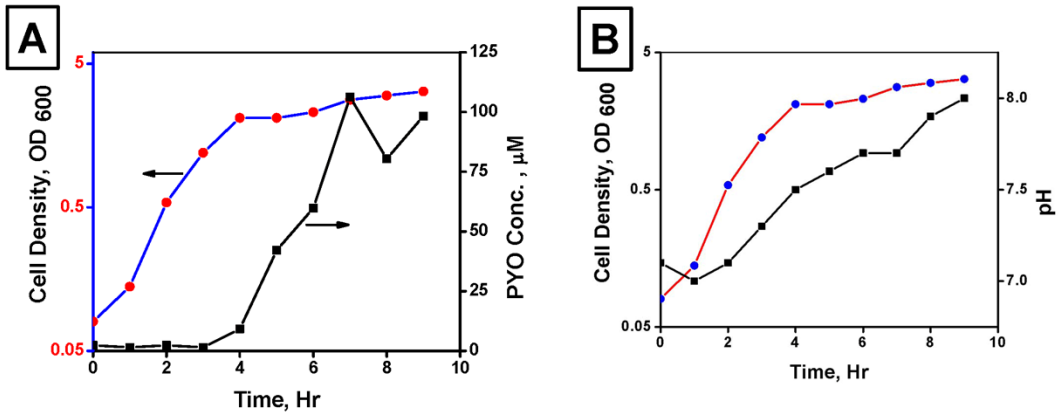

Figure 5.8. Planktonic cell PYO and pH measurements

(A) PYO concentration (black line), cell density (blue line) and (B) pH changes (black line) with cell density (red line) over time (hr). The Cell Density y-axis in both figures is plotted in logarithmic scale.

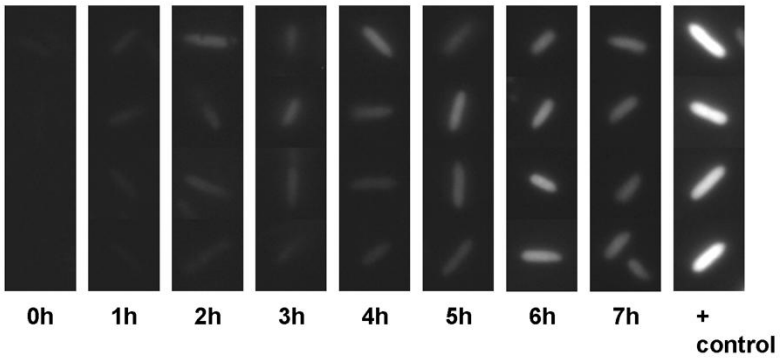

Figure 5.9. Activation of QS in a *P. aeruginosa* biofilm (5 mm).

An increase in brightness corresponds to QS activation. The cells were incubated in 50/50 MOPS-LB buffer at 37°C. Images were taken at 1000x magnification. + control cells were taken from an early stationary phase planktonic culture.

Real Time Quantitative Detection of Pyocyanin (PYO)

Figure 5.10 shows the real time quantitative detection of PYO produced from a *P. aeruginosa* 5 mm colony biofilm surface. Detectable amounts of PYO (~ 1 μM) were produced at 90 min. The local PYO concentration (or 20 μm away from the biofilm surface) produced by the biofilm was determined to be 28 μM after 7 hr. Figure 5.10 A shows gradual development of a characteristic PYO peak at -0.63V. The peak height was converted to PYO concentration by calibration curve (Figure B1 B). The time delay for the production of PYO was due to time required for accumulation of quorum signal to activate the QS circuit. Similar PYO production patterns were noticed for *P. aeruginosa* grown planktonically in a shaken incubator at 37°C (Figure 5.8A).

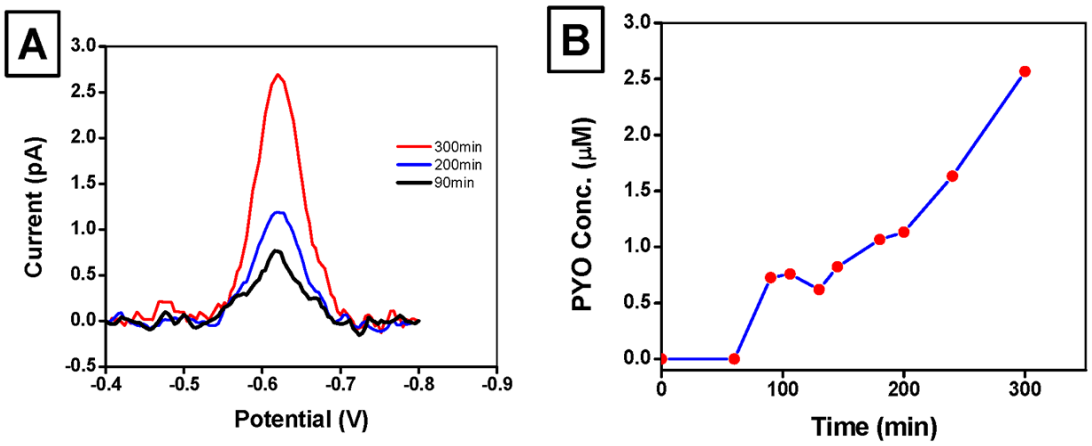

Figure 5.10. PYO production by a wt *P. aeruginosa* biofilm.

(A) Square wave voltammogram (SWV) of PYO produced by *P. aeruginosa* biofilm in presence of supernatant buffer at 36°C. (B) Plot of PYO concentration (μM) with respect to time (hr). Tip-substrate (biofilm) distance was 20 μm.

Spatial Mapping of Reduced/Oxidized Pyocyanin (PYO) above a Biofilm

During measurements of PYO production from colony biofilms, we noticed that PYO proximal to the biofilm was in a completely reduced state. To study this phenomenon, z-direction spatial mapping of the reduced and oxidized PYO ratio above the wild type *P. aeruginosa* biofilm at 36°C was measured and shown in Figure 5.11 A. The tip was biased at -0.3V (oxidizing at tip) and -0.8V (reducing at tip) while moving towards the biofilm to map the reduced and oxidized PYO respectively. Zero on the x-axis represents the surface of the biofilm. The height of the reduced PYO layer is observed to be 400 μm whereas the amount of reduced PYO was recorded to be 9 μM at 60 μm away.

To alleviate the problems of temporal variability of PYO produced by the biofilm, 200 μM oxidized PYO was added above a *phzA1/2* mutant biofilm (unable to produce phenazines including PYO [96]) to study the reduced layer behavior at different conditions. Figure 5.12 shows the z-direction spatial distribution of reduced PYO above the *phzA1/2* mutant biofilm in the presence of 200 μM PYO at 25°C and 36°C respectively. The height of the reduced PYO layer was measured to be 500 μm and 600 μm in height at 25°C and 36°C respectively. The profile at 25°C (Figure 5.12) shows no reduced PYO at 1500 μm and almost 50% of the added PYO is in the reduced form at ~60 μm from biofilm. However, at 100 μm ~5 times greater reduced PYO concentration were observed at 37°C compared to 25°C. Cyclic voltammograms (Figure 5.12 inset) at 37°C showed that all PYO was in reduced form at a distance of 100 μm; whereas PYO was in a 100% oxidized form at 1500 μm from the biofilm. In both of the reduced PYO profiles, a drop in PYO concentration is observed as the tip approaches 60 μm or closer above the biofilm. This is because when the tip is 2000 μm away from the biofilm the SECM instrument is operating in generation –collection mode but when the tip is within the reduced PYO layer zone it switches to feedback mode. When the tip moves even closer to the biofilm (i.e. 60 μm or less) the tip starts sensing the substrate or biofilm. As a result, the response at the tip ≤60 μm in distance depends on how fast the oxidized PYO at the tip is being reduced back by the biofilm. In this case the kinetics of PYO reduction by the biofilm is not fast enough to keep up with the rate of oxidation of PYO at the tip, hence the current drops at ≤60 μm. The z-direction oxidized PYO profile (Figure 5.13 A & B) complements the reduced profile. As observed in Figure 5.12, there is no oxidized PYO at 500 μm or less and the oxidized PYO layer resembles the enhanced negative feedback mode approach curve.

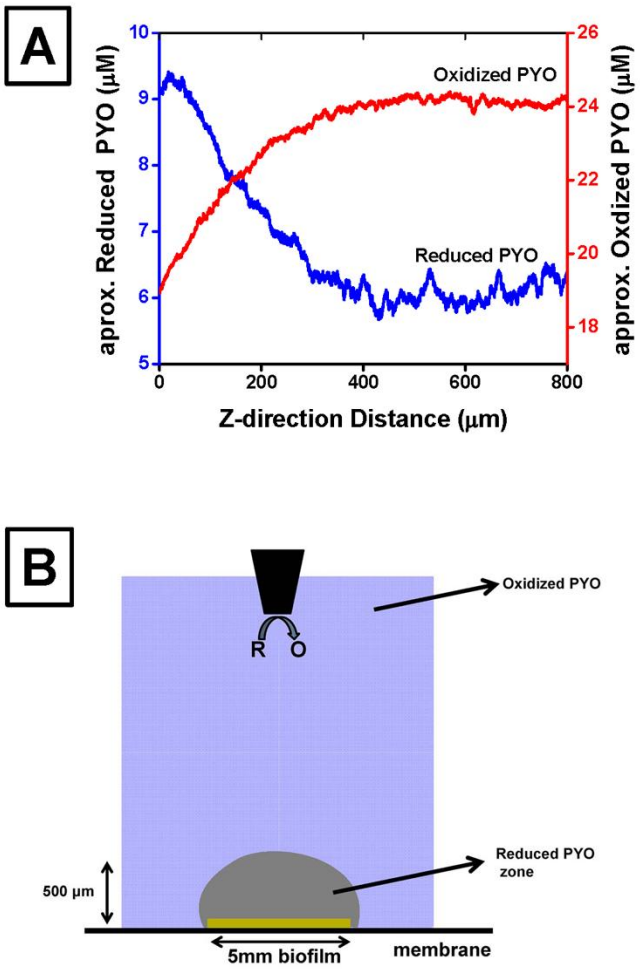

Figure 5.11. The detection of a reduced PYO layer.

(A) Z-direction profile of reduced and oxidized PYO concentrations produced by a *P. aeruginosa* wild type biofilm. Zero on the x-axis represents the surface of biofilm. (B) Schematic model of the reduced PYO layer above the biofilm. To spatially map the reduced and oxidized PYO profile, the tip was biased at -0.3V (oxidizing potential) and -0.8 V (reducing potential) respectively.

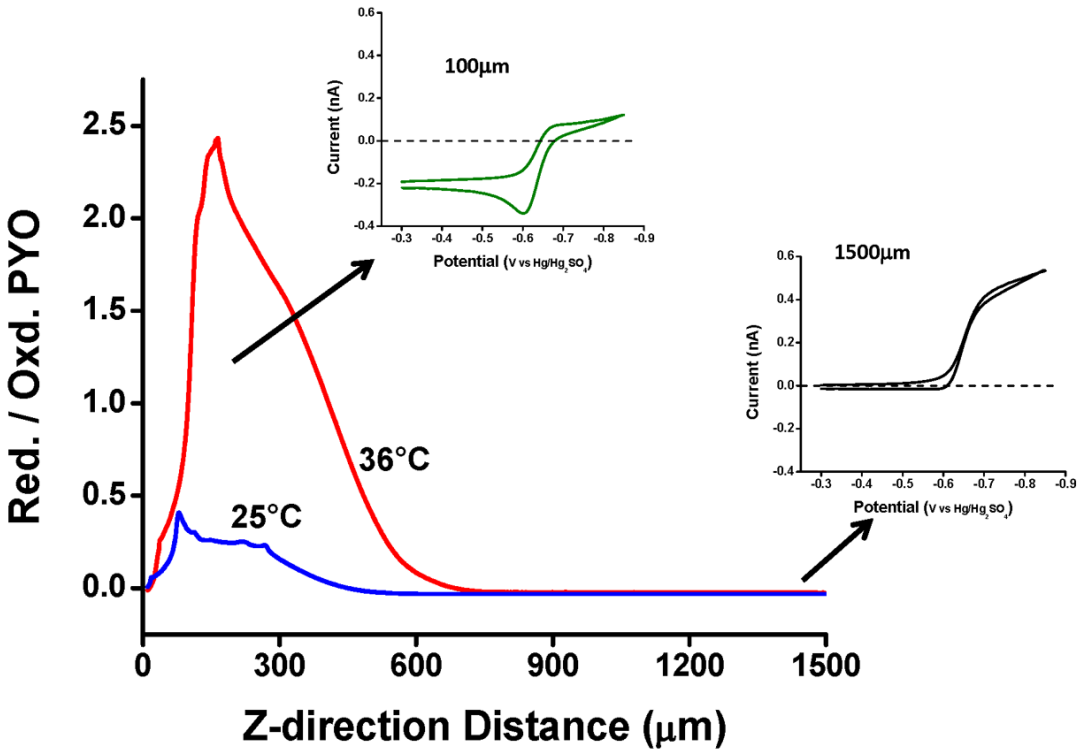

Figure 5.12: Temperature dependent reduced layer formation.

Z-direction reduced PYO profile above a *phzA1/2* biofilm at 25°C (blue line) and 36°C (red line). Cyclic voltammograms were taken at 1500 µm (black) and at 100 µm (green) at 36°C. The y-axis is normalized by 200 µM of added oxidized PYO.

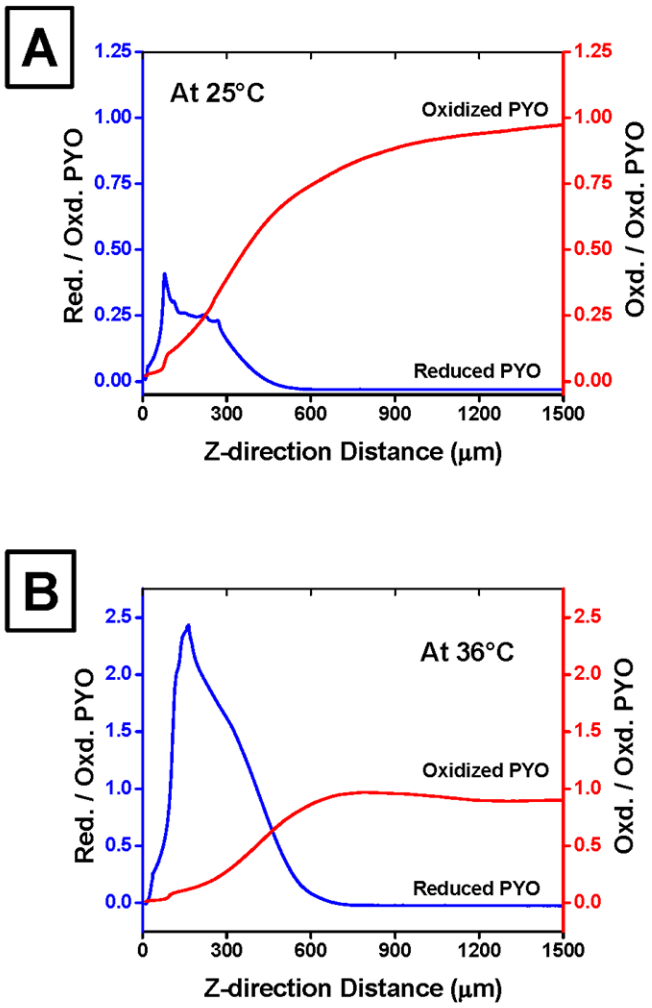

Figure 5.13. Reduced and Oxidized PYO profiles over a *P. aeruginosa* biofilm.

Z-direction reduced (blue line) and oxidized (red) PYO profiles above a *phzA1/2* mutant biofilm at (A) 25°C and (B) and 36°C respectively. Both y-axes are normalized by 200 μM of oxidized PYO added to the solution.

Determining the mechanism of PYO reduced layer development

We hypothesized that PYO reduced layer development was due to the flow of electrons from carbon source oxidation and that this flow could be diverted from PYO to NO_3 instead. To test this hypothesis we measured the reduced PYO layer above the *phzA1/2* mutant biofilm while adding either excess Fe(III) (100 μM ~10x the original concentration) to facilitate oxidation of PYO or NO_3 (100 mM) (Figure 5.14A) both in the presence of 200 μM PYO. The reduced PYO layer collapsed in the presence of excess NO_3 (100 mM) whereas the layer height decreased by 100 μm in the presence of excess (100 μM) Fe(III) in the buffer. However, the absolute value of the ratio of reduced/oxidized PYO remained the same. The oxidized PYO layer (Figure 5.14B) again showed a complimentary z-direction profile. For a *phzA1/2* mutant standard sample, the z-directional oxidized PYO profile confirmed the enhanced negative feedback or consumption of oxidized PYO above the biofilm. For the excess NO_3 sample, the oxidized PYO layer showed similar behavior to that of a negative feedback approach curve confirming the lack of any reduced PYO layer.

We used mutants impaired in PYO reduction (*fbcC* cytochrome bc1 mutant [168]) or aerobic NO_3 reduction (*napA* mutant) to explain how electron flow inside the cells effects a reduced PYO layer above the biofilm (Figure 5.15). The reduced PYO layer was 500 μm for both the *phzA1/2* mutant and the wild type *P. aeruginosa* biofilm, whereas the ratio of reduced/oxidized layer almost doubled for a *napA* mutant biofilm. This is hypothetically due to electron flow being diverted to PYO reduction instead of reduction of possible trace NO_3 concentrations present in LB-MOPS as seen in other complex media [169]. For the *fbcC* mutant biofilm, the reduced PYO layer was reported to be almost zero in comparison to the standard sample (*phzA1/2* mutant) explained by the fact

that cytochrome bc1 was reported to be the site at which PYO accepts electrons from *P. aeruginosa* [168]. A heat killed control biofilm showed no reduced PYO layer above the biofilm (Figure 5.14A).

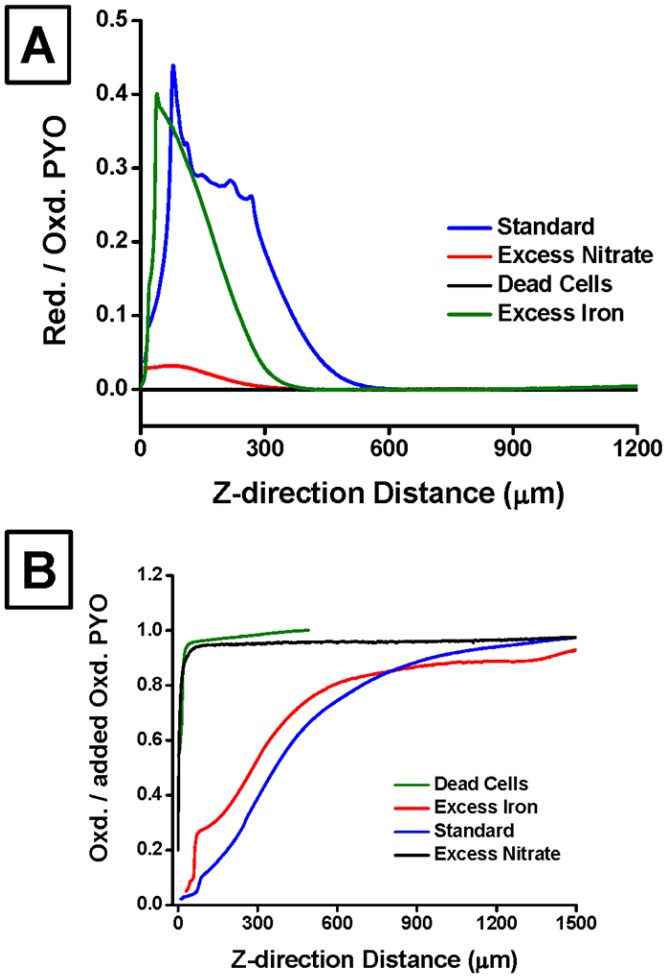

Figure 5.14. PYO layer measurements of a *phzA1/2* mutant biofilm in different media conditions.

(A) Z-direction reduced PYO profile above a *phzA1/*2 mutant biofilm. PYO was oxidizing at the tip while it approached the biofilm. (B) Z-direction oxidized PYO profile above the same set of biofilms. PYO was reducing at the tip in this experimental setup. In each experiment 200 μM of oxidized PYO was added at 25°C. Both reduced and oxidized PYO concentrations in the y-axis are normalized by 200 μM of oxidized PYO.

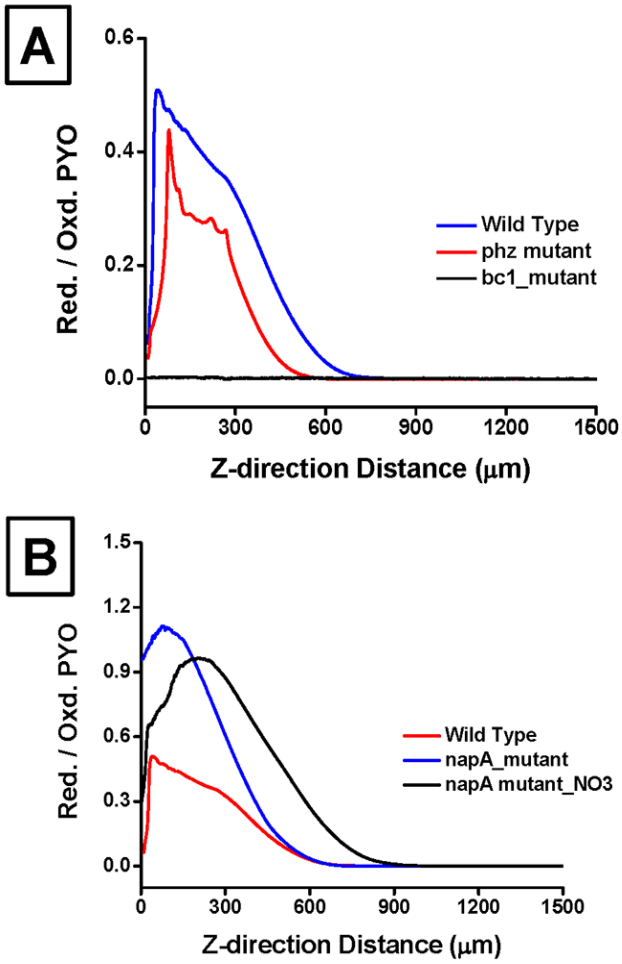

Figure 5.15. PYO layer measurements of different *P. aeruginosa* mutants.

(A) & (B) Z-direction profile of reduced PYO above biofilms of indicated *P. aeruginosa* mutants. The tip was held at -0.3V or at oxidizing potential of reduced PYO. In each experiment 200 μM of oxidized PYO was added at 25°C. Both reduced and oxidized PYO concentration in y-axis is normalized by 200 μM of oxidized PYO.

Reduction of Iron (III) in the Presence of Pyocyanin (PYO)

We hypothesized that a reduced PYO layer may enrich the local environment around a biofilm with Fe(II) by PYO-mediated reduction of Fe(III), even in the presence of oxygen. As demonstrated in Figure 5.14, the addition of excess Fe(III) modulated the reduced PYO layer height. Using a Ferrozine based Fe(II) assay we measured total Fe(II) percentages from media exposed to colony biofilms for 1hr. These data are presented in Figure 5.16. The data supports our model that a reduced PYO layer generated by the *phzA1/2* mutant biofilm indeed reduces the Fe(III) present in the solution. Henceforth, addition of NO_3 or the inactivation of cytochrome bc1 leads to a lower Fe(II) percentage, likely due to collapse of the reduced PYO layer above the biofilm (Figure 5.14 & 5.15). We also observed that the inhibition of the NapA-dependent NO_3 reduction pathway led to an increase in Fe(II) percentage. However, the *napA* mutant data showed more variability in Fe (III) reduction. This fits our data as reduced PYO layer formation in the *napA* mutant was sometimes more varied than the wild type or *phzA1/2* mutant biofilms (not shown).

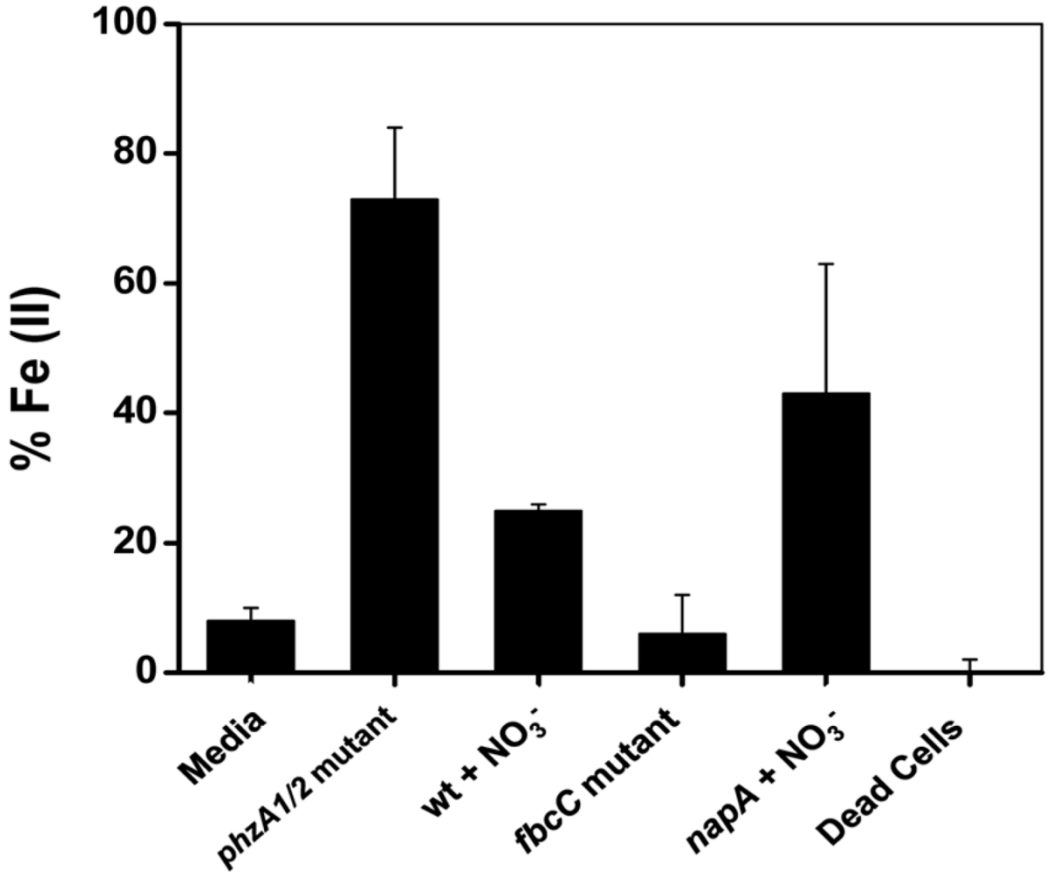

Figure 5.16: Percentage of Fe(II) in the presence of PYO treated biofilms.

250 μL of buffer was used in each experiment in standard 5 mm colony biofilms. Media used was LB-MOPS buffer with or without 100 mM NO_3 (+NO_3).

Electrochemical Imaging of a Biofilm

The property of *P. aeruginosa* biofilms to rapidly re-reduce PYO oxidized from the SECM tip allowed us to observe redox reactions from the biofilm to PYO as they occur. Measuring the reduction of oxidized PYO generated at the tip as it moved in the x and y axis over the biofilm surface enabled us to generate a "reactivity map" or electrochemical image of the biofilm itself. Figure 5.17 shows a constant height-mode

SECM image of a 1 mm diameter *P. aeruginosa* colony biofilm. The image (Figure 5.17 C) was taken in the presence of 200 μM exogenous PYO. The tip was held at -0.3 V (PYO oxidizing potential) while scanning over the biofilm at a distance of 60 μm from the polycarbonate membrane maintaining a constant speed of 8μm/0.02 sec (Figure 5.17 A). The false color contrast of the electrochemical image shows reactivity mapping of the biofilm for reducing oxidized PYO locally made by the tip just above the cells. The oxidized PYO diffused in the gap (tip-biofilm), where it is then reduced by cells, resulting in higher current (purple color) recorded by the tip as shown in Figure 5.17 C. Thus the image can be seen as a map of electron shuttling from the biofilm to PYO in real time. Since there is no reduced PYO (as shown in Figure 5.17 C) away from the biofilm, the current is almost zero (red color). Figure 5.17 B shows the x-direction scan over a 1 mm biofilm at 25°C and 36°C respectively. The fraction of reduced PYO at 37°C is almost five times higher than that observed at 25°C. This may be due to higher rates of electron transfer from biofilm to PYO in solution as observed in Figure 5.12.

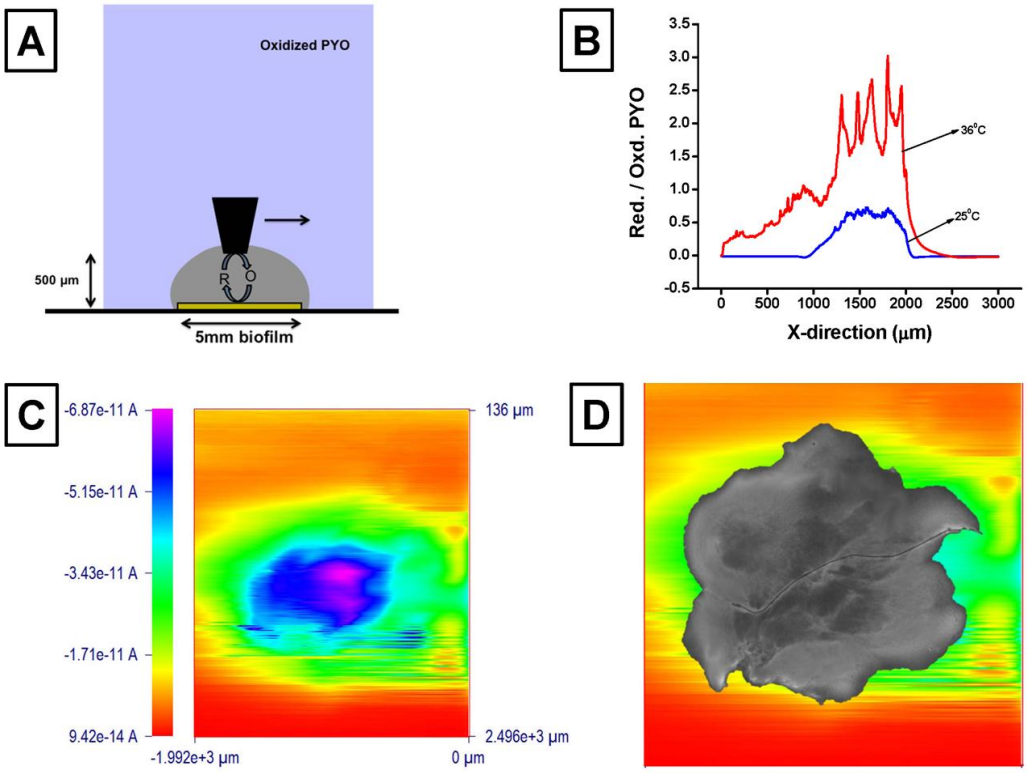

Figure 5.17. Electrochemical imaging of a *P. aeruginosa* biofilm.

(A) Schematic diagram of experimental setup for x-scan and SECM imaging. (B) x-direction scan over 1 mm biofilm at a height of 30 µm (C) Constant height SECM image of a 1 mm wild type *P. aeruginosa* biofilm. Blue and purple color represents the mapping of electron transport from the biofilm to reduce PYO in the solution above it. The tip was held at -0.3V to oxidize PYO. (D) Superimposed optical and SECM images of a 1 mm biofilm. Tip used: 10 µm Pt. Tip-substrate (biofilm) distance: 20-30 µm. Solution used: 200 µM oxidized PYO in 50/50 MOPS-LB buffer solution.

5.5 DISCUSSION

Our work initially sought to utilize SECM to directly measure PYO as it was produced from a *P. aeruginosa* biofilm. While carrying out measurements from colony biofilms, we observed that biofilm-produced PYO was entirely in the reduced form. In addition to reduced PYO proximal to the biofilm, the most surprising finding was the size of the reduced layer, extending hundreds of microns from the cell surface. The startling finding that such a large reduced layer was present led us to study and attempt to characterize this phenomenon.

To explain the unusual behavior of PYO reduced layer formation, we propose two models describing electron movement intra and extracellularly. The schematic diagrams of the proposed models for the intracellular and extracellular environment are shown in Figure 5.18. Figure 5.18 shows the flow of electrons from NADH to oxygen or the alternative electron acceptors NO_3 and/or PYO present outside the cell. Oxidation of a carbon source reduces NAD^+ to NADH, which subsequently donates electrons to the ubiquinone pool and onward to cytochrome bc1 and other electron carriers. When oxygen is present, it is reduced to generate maximum energy, as oxygen is the most negative potential redox couple (-1.2V vs. NHE) available. However, pyocyanin (PYO) has been hypothesized to short-circuit the electron transport chain at cytochrome bc1, diverting electron flow away from O_2 reduction towards PYO reduction [168]. Since PYO is produced only at high cell densities, a condition where O_2 may become limited due to cellular respiration, PYO may help alleviate electron acceptor limitation by acting as a soluble redox carrier.

When oxygen becomes limited in the presence of NO_3, electrons can be used to reduce NO_3 to NO_2 via either the *napA* or *narG* gene products. As this happens independently of cytochrome bc1, electron flow to PYO would compete with electron flow to NO_3 reduction. We have demonstrated that in the presence of high NO_3 concentrations, there is a decrease in PYO reduction, which diminishes the observed reduced layer in a NapA-dependent manner.

As PYO is reduced, it diffuses outside the cell and is oxidized in the presence of oxygen. Hence it provides the bacteria an alternative pathway for electron flow when oxygen becomes limiting and NO_3 is absent. One of the advantages of a reduced PYO layer is that *P. aeruginosa* can perform other physiologically relevant functions besides moving electrons to oxygen. One such function is to scavenge iron from its surroundings. Reduced PYO diffusing from a biofilm to the environment can reduce insoluble Fe(III) to soluble Fe(II). Fe(II) can then be transported using the highly efficient *feo* system (close proximity) or can be re-oxidized back to Fe(III) in presence of oxygen (further away from the biofilm). We hypothesized that Fe(III) concentrations could cause changes in the reduced layer, as PYO would donate electrons to Fe(III) and become oxidized more rapidly, abolishing the layer, if Fe(III) were in excess (Figure 5.18). We observed modulation of the reduced PYO layer on addition of excess Fe(III) in the solution. Thus, the reduced PYO layer contracts when iron is at high concentrations and grows when iron concentrations are low, providing a function for PYO to solubilize Fe(III) to Fe(II) in a volume much larger than the one occupied by the biofilm itself. This reduction would allow for the much more energy efficient uptake of Fe(II) over Fe(III) and could inhibit competition for iron by Fe(III) binding siderophores produced by *P. aeruginosa* and other species.

From our PYO CV data at 100 μm and 1500 μm above the biofilm (Figure 5.12) it is observed that oxygen is present in low concentrations within the reduced PYO layer. This may be due to reduced PYO donating electrons to oxygen or due to bacterial respiration. It has been demonstrated that *P. aeruginosa* cannot produce PYO in the absence of oxygen [170]. Thus at initial stages when oxygen concentration is high above a biofilm, PYO is produced due to activation of the QS circuit. Once PYO reaches a critical concentration, the oxygen concentration starts falling due to redox cycling of reduced PYO involving oxygen, ultimately leveling off PYO production.

Figure 5.18 also shows the proposed extracellular model for PYO redox cycling in the presence of oxygen. From Figure 5.18 it is apparent that the height of the reduced PYO layer depends on the complicated balance of kinetics of electron transport (kf) from the biofilm to PYO as well as the kinetics (k2) of PYO redox reactions with Fe(III) and the rate (k3) of Fe(II) oxidation to Fe(III) as well as the kinetics (k1) of reduced PYO reacting with oxygen. According to this model, the amount of reduced/oxidized PYO solely depends on kf or rate of heterogeneous electron transfer from biofilm to outside solution whereas the height of reduced PYO layer above biofilm depends on the kinetics balance of k1, k2 and k3 (Figure 5.14 and 5.15).

The model of electron flow to PYO and other terminal electron acceptors is confirmed by reduced PYO layer experiments performed with *P. aeruginosa* mutants as shown in Figure 5.18. As we can see the reduced PYO layer is abolished in a cytochrome bc1 mutant whereas the reduced layer is almost doubled in size when a *napA* mutant was used even in the presence of excess NO_3 (Figure 5.15). This is possibly due

to obstruction of electron flow to any trace NO_3 driving all electron flow through cyctochrome bc1 to reduce PYO, enlarging the layer.

Though *P. aeruginosa* is known to produce different siderophores (iron chelators) to scavenge Fe(III) from its surroundings, it is a very energy intensive process that involves an ATP-driven mechanism for active transport of Fe(III). Whereas, if reduced PYO is used to scavenge Fe(III) from its surroundings by reduction to Fe(II) and *feo* uptake it can serve three important functions: (a) to shuttle electrons from the core of the biofilm structure where oxygen is scarce to the outside environment (b) to scavenge Fe(III) and transport it using a more energy efficient Fe(II) transporter and (c) by producing PYO, it can kill other bacteria due to its antimicrobial properties and enhance competition in a multispecies environment. Previous studies have demonstrated that *P. aeruginosa* lyses other bacterial species as a means of obtaining iron [164]. It could be that while PYO is an antimicrobial, it acts synergistically with more powerful quinolone antibiotics produced by *P. aeruginosa*, as a means to ensure that iron freed from other bacteria remains in the easily transported Fe(II) form.

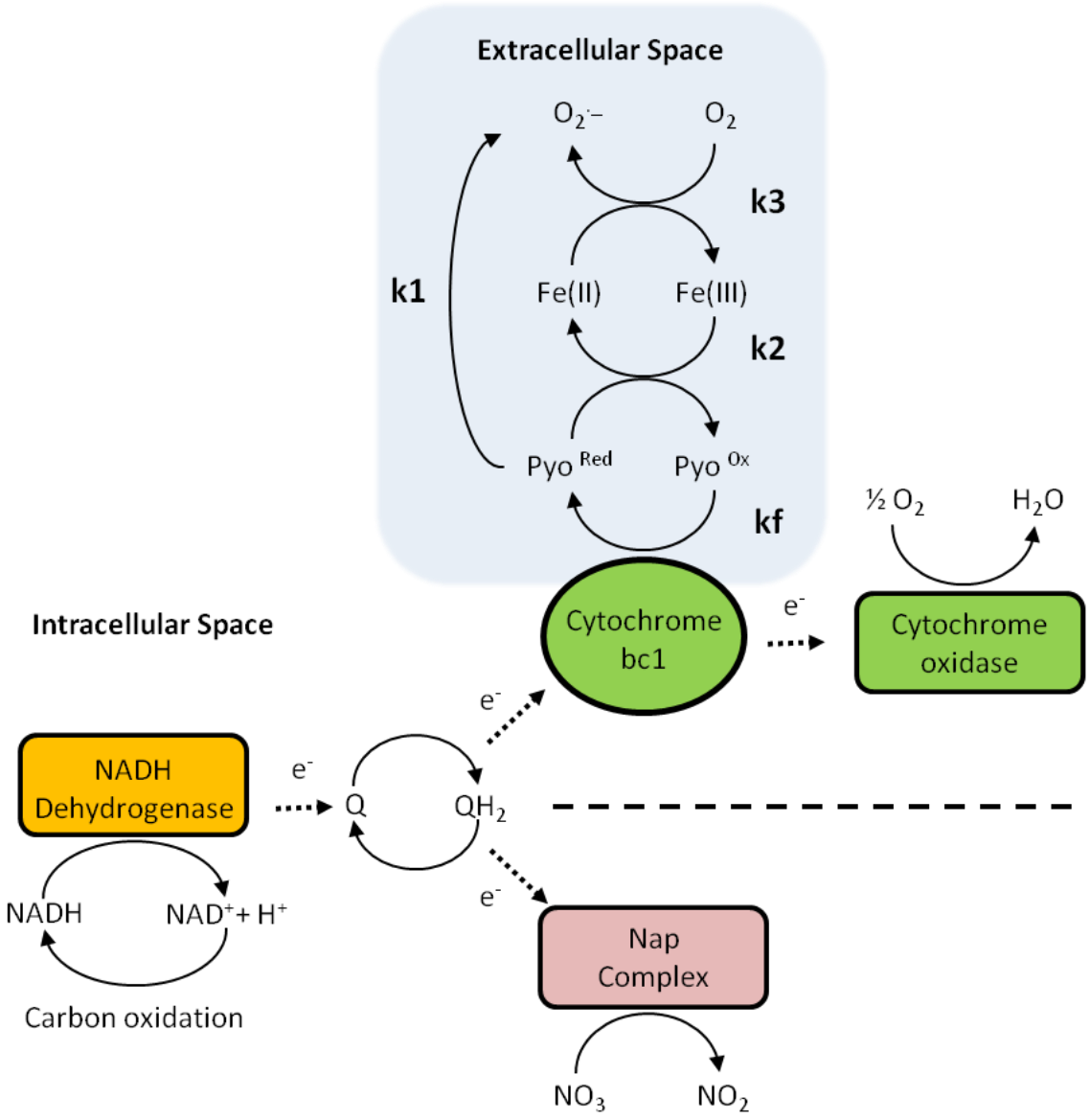

Figure 5.18. A proposed model to explain the generation and modulation of a reduced PYO layer.

Dotted arrows indicate electron transport between carriers. Additional electron transport molecules were omitted for clarity. The dashed line indicates a proposed branch point for electron flow between NO_3 or O_2 and PYO.

5.6 CONCLUSION

In studying the biofilm production of PYO by SECM we have made several discoveries including the ability to detect pyocyanin (PYO) concentrations as low as ≥ 3 μM by a novel application of square wave voltammetry (SWV). We have also demonstrated that PYO is reduced locally by a biofilm even in the presence of oxygen and that cells are able to maintain a 500 μm reduced PYO layer above the biofilm. We have also discovered a mechanism that may allow a *P. aeruginosa* biofilm to reduce iron over significant distances. This mechanism is reminiscent of recent findings by Newman et al [171] describing the ability of the phenazine PCA to reduce iron for *P. aeruginosa* utilization. We have also revealed an elegant mechanism that can expand or contract a volume of an iron reducing substrate dependent upon the iron concentration in the biofilms vicinity which functions to increase the concentration of soluble iron even in the presence of oxygen.

Appendix A: Collaborative data from Chapter 4.

*Chapter 4 results from a collaborative study whose participants are referenced here [48]. Methods and data presented here are solely credited to the other authors unless specifically noted with the exception that all biological samples and media were prepared by M.M.R.

A.1. Experimental methods and Results

Calibration Curves for H_2O_2 in CDM

Calibration curves for H_2O_2 were collected in the presence of a *Sg* biofilm. The conditions are described in detail in the Chapter 4 "Materials and methods" section. In order to be consistent with our real time measurements, we strictly followed the same procedure and carried out the calibration curve measurements in the same way. The *Sg* biofilm was incubated in 1.5 mL CDM for at least 1 h before different aliquots of H_2O_2 solution (0.03 %, v/v) were added into CDM solution to make H_2O_2 concentrations ranging from 0.06 mM to 1.6 mM. The H_2O_2 oxidation currents were measured by pulsing the Au ultramicroelectrode (UME) from 0.55 V to 0.80 V, 5 min after H_2O_2 was added each time. No glucose was added to the CDM so that *Sg* cells in the biofilm would not produce any extra H_2O_2 during calibration measurements.

Figure A1 shows the results obtained in the presence of a *Sg* biofilm. A linear relationship ($I=-0.299C-0.0069$, $R^2=0.99533$) between the current and H_2O_2 concentration was observed at H_2O_2 concentrations smaller than 1.0 mM (Figure S2). As concentration goes above 1.0 mM, the curve levels off and deviates from the linear portion. Most of the H_2O_2 concentrations obtained in our real time *in vitro* measurements

were within 1 mM, so we used the linear portion of the calibration curve to calculate H_2O_2 concentration (Figure A2).

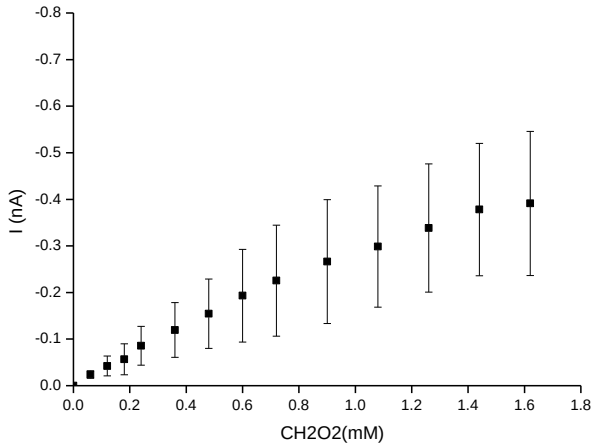

Figure A1.

Calibration curve for H_2O_2 with concentrations ranging from 0.06 ~ 1.6 mM in CDM with a *Sg* biofilm at 37 °C. Error bars were calculated based on three independent measurements.

In order to test if our calibration curve was working properly, we intentionally added 0.5 mM H_2O_2 to a 1.5 mL *Sg* biofilm suspended in CDM in a Petri dish, and the current response was measured to be 0.15 nA, which corresponds to 0.5 mM based on the calibration curve in Figure A2. This indicated that our calibration curve was indeed valid for our experiments.

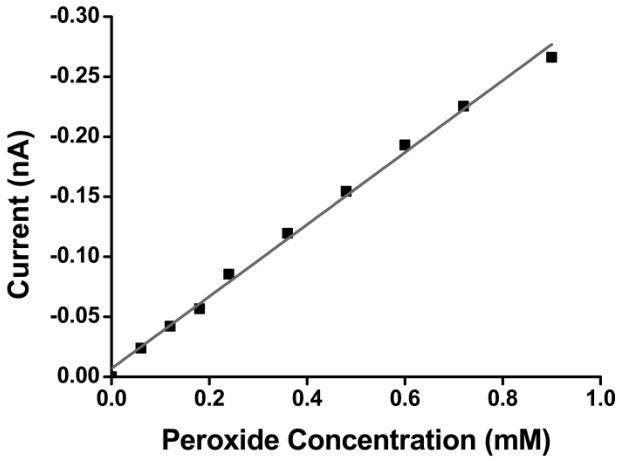

Figure A2.

Calibration curve for H_2O_2 over the concentration range from 0.06 ~ 1.0 mM in CDM with a *Sg* biofilm at 37 °C.

Stability Tests

Stability is a very important issue since we normally need to run the experiments for a long duration. Because CDM is a defined culture medium with many components, and the temperature needs to be maintained at ~37 °C during the experimental process, in such conditions, the SECM tip (Au UME) is prone to contamination, and H_2O_2 tends to decompose as well. As a result, a current decay is usually observed as time proceeds. To make sure that our measurements were valid during this long duration, we carried out a series of stability tests.

Figure A3 shows the results of stability tests performed in the absence of *Sg*. The current response for 0.2 mM H_2O_2 in 1.5 mL CDM with 10 mM glucose was measured as a function of time. As shown in Figure A3, the H_2O_2 oxidation current decreases slowly with time. After 30 min, the current decreased only ~20%, which means that the tip has relatively good stability in low H_2O_2 concentration.

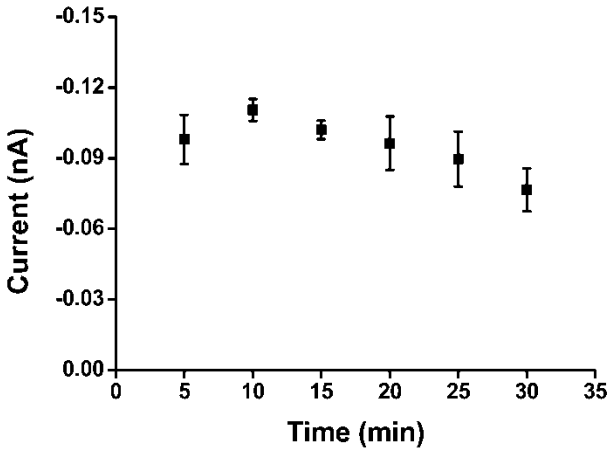

Figure A3.

Amperometric current of Au UME as a function of time in 0.2 mM H2O2 CDM solution at 37 °C. Error bars were calculated based on at least three independent measurements.

Another stability test was carried out in the presence of a *Sg* biofilm. A relatively high H_2O_2 concentration (0.6 mM) was tested this time. H_2O_2 current was measured every 5 min up to 35 min, and the result is shown in Figure A4. The current of H_2O_2 decreased gradually with time. The rate for the current decay is faster (43% current drop in first 20 min) in the presence of *Sg* cells.

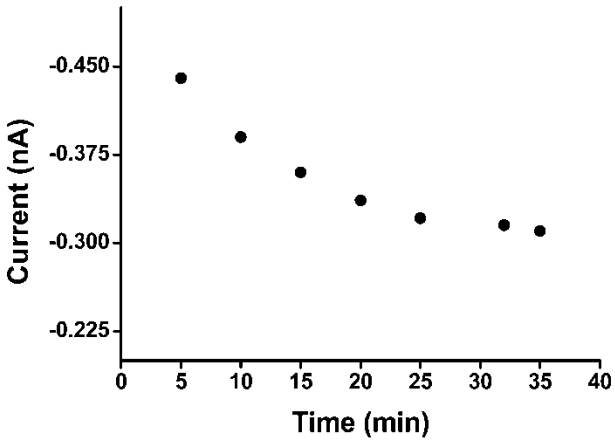

Figure A4.

Current response of 0.6 mM H_2O_2 as a function of time in the presence of a *Sg* biofilm.

Effect of the Number of *Sg* Bacteria on H_2O_2 Current Response

We also tested to see if the amount of *Sg* cells would affect H_2O_2 measurements. In this experiment, 0.5 mM H_2O_2 was added to 1.5 mL CDM solution. The current response of 0.5 mM H_2O_2 was measured 10 min later each time when one aliquot of 0.5 mL of *Sg* suspension (2.5×10^8 *Sg* cells) was added into the above solution. To make the concentration of H_2O_2 constant during the measurements, extra H_2O_2 was added (28 μl 0.03% H_2O_2) each time to compensate the volume change due to the addition of 0.5 mL *Sg* suspension. A total of 4 aliquots of *Sg* suspension were added, and it was found that the current responses did not show any significant changes (Figure A5). This indicated that the number of *Sg* did not significantly affect H_2O_2 detection.

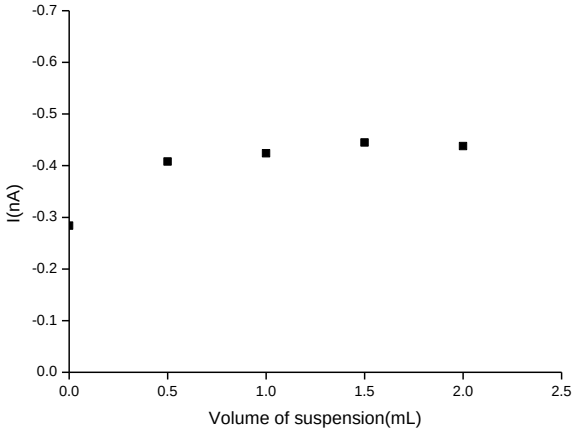

Figure A5.

Effect of *Sg* numbers on H_2O_2 detection. 1.0 mL of *Sg* suspension contain 5×10^8 *Sg* cells.

Simulation

Since the electroactive species hydrogen peroxide or P moved toward and away from the electrode surface only because of a concentration gradient, Fick's second law of diffusion was used in the simulation. The concentration of species P was given as C(r,z,t) and the diffusion equation in cylindrical coordinates was described as

$$\frac{\partial c}{\partial t} = D\left(\frac{\partial^2 c}{\partial r^2} + \frac{1}{r}\frac{\partial c}{\partial r} + \frac{\partial^2 c}{\partial z^2}\right)$$

Where, r and z are the coordinates as shown in Figure A6; t represents time; C and D represent the concentration and diffusion coefficient of species P.

The simulation model described above was solved by a finite element method in 2D axial symmetry dimension where the mesh was increased in exponential grid fashion to generate a two-dimensional grid. A finer mesh distribution was used at the regions where sharp changes in the concentration gradients were noticed.

Initially the peroxide concentration in the solution was zero and the flux in the bulk boundary was set as zero. The diffusion coefficient of peroxide in the solution was taken as 1.5×10^{-9} m^2/s. The peroxide generated from the biofilm surface was assumed to be a constant flux problem. Henceforth, the flux ($mol/m^2/sec$) value was adjusted at the biofilm surface to fit the experimental peroxide response curve or peroxide concentration vs. time (s) measured by SECM tip. The 25 µm tip (RG=10) was located 100 µm away from the substrate to record peroxide concentration and was held at diffusion controlled potential to avoid kinetic complications. The current at the electrode was calculated as

$$I_{tip} = \int_{r=0}^{r=a} 2\pi nFD\, r\, \frac{\partial c}{\partial z}\, dr$$

Where, n = 1; F= 96485 C/mol; and $D = 1.5\times10^{-9}$ m^2/s; a = tip radius, m. The current obtained by the simulation was converted to peroxide concentration using the same calibration curve used in experimental peroxide measurement.

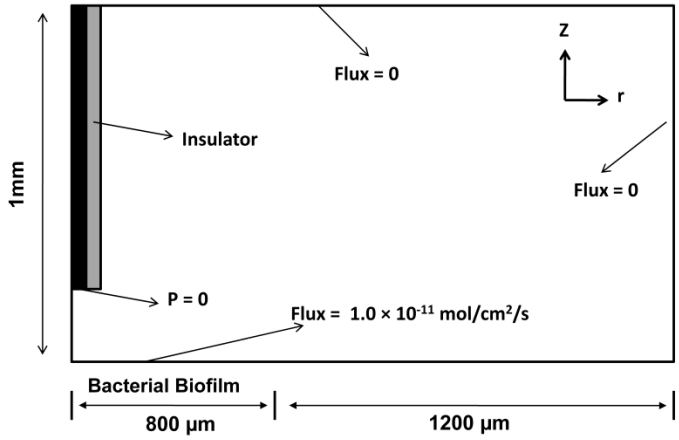

Figure A6.

The schematic diagram of Comsol Multiphysics model used for simulation.

Confocal laser scanning microscopy*

*All work in this section was performed by M.M.R.

Cells were grown and prepared as described above, except for the replacement of *Aa* Y4 with a constitutive GFP-producing *Aa* Y4 strain. Membranes were stained in 3 mL of PBS containing 60 µM propidium iodide and incubated for 10 min prior to rinsing in PBS 3x at 3 mL each. Membranes were then resuspended in 3 mL PBS and observed through a 40x water immersion lens with an Olympus FV1000 confocal microscope. Excitation was performed using a 488 nm Ar laser and green and red channels were separated using standard filter settings. Micrographs were acquired at 400x magnification in 1 µm z-axis step sizes. Image processing was performed using Imaris software.

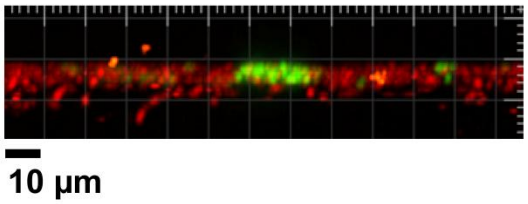

Figure A7.

Confocal laser scanning micrograph of a mixed species biofilm. *S. gordonii* (red) and *Aa* (green) were co-cultured in a colony biofilm. Green and red channel fluorescence are due to *Aa* GFP expression and propidium iodide staining respectively. Images were taken at 400x magnification with a z-step interval of 1 µm.

Appendix B: Collaborative data from Chapter 5*

*This work was done in collaboration with Dipankar Koley from Dr. Al Bard's lab at the University of Texas. D.K. performed all SECM measurements and assisted with the draft preparations and editing of chapter 5 of this dissertation. In all cases, any biological samples or biological media used were prepared by M.M.R.

B.1. Experimental methods and Results

Calibration Curve for Pyocyanin (PYO)

Square wave voltammograms (SWV) at different concentrations (6 to 100 μM) of added PYO in supernatant buffer are shown in Figure B1 A. Figure B1 B shows a calibration curve for PYO in the range of 6-100 μM in supernatant buffer solution in presence of *Δphz* mutant biofilm. The calibration curves (Figure B1 C & D) show a linear relationship in the range of 6-200 μM PYO in presence of 50/50 MOPS-LB buffer in presence of *Δphz* mutant biofilm. The equation for figure B, C and D is y=mx+c where, y represents SWV peak height (pA) and x corresponds to PYO concentration (μM) in their corresponding buffer. The calibration curve equations used are as follows:

Biofilm in supernatant buffer solution:

Y = (1.06e-12*X) – 2.08e-12

Biofilm in 50/50 MOPS-LB buffer (low concentration range, 6-30 μM):

Y = (1.46e-12*X)-3.14e-12

Biofilm in 50/50 MOPS-LB buffer (high concentration range, 30-200 μM):

Y = (0.91e-12*X) + 5.63e-12

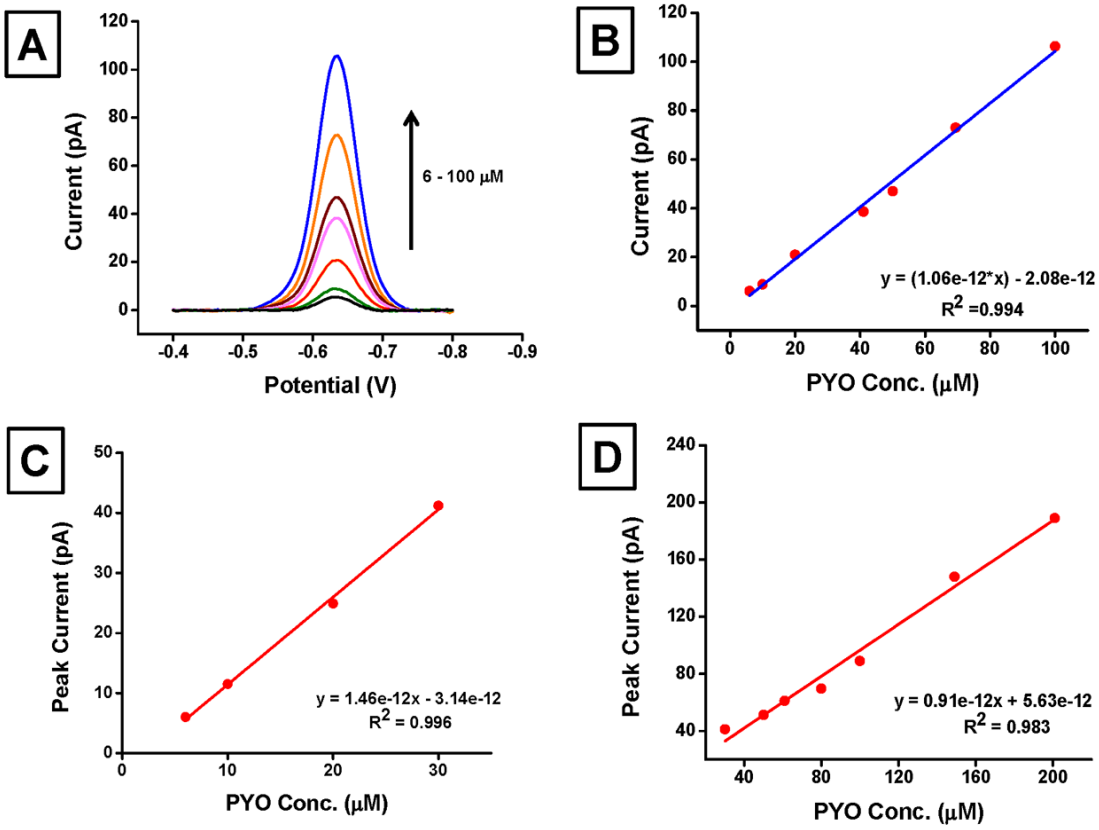

Figure B1. Square Wave Voltammetry for SECM.

(A) & (B) Square wave voltammogram (SWV) and calibration curve at different concentration (6 to 100 µM) of PYO in the presence of supernatant buffer solution. (C) Calibration curve at varying concentrations of PYO in the range of 6-30 µM in 50/50 MOPS-LB buffer solution. (D) Calibration curve at varying concentrations of PYO in the range of 30 - 200 µM in 50/50 MOPS-LB buffer solution. Working electrode: 10 µm Pt. Reference electrode: Hg/Hg_2SO_4.

References

1. Meyer, D.H. and P.M. Fives-Taylor, *Oral pathogens: from dental plaque to cardiac disease.* Curr Opin Microbiol, 1998. **1**(1): p. 88-95.
2. Slots, J., H.S. Reynolds, and R.J. Genco, *Actinobacillus actinomycetemcomitans in human periodontal disease: a cross-sectional microbiological investigation.* Infect Immun, 1980. **29**(3): p. 1013-20.
3. Kozarov, E.V., et al., *Human atherosclerotic plaque contains viable invasive Actinobacillus actinomycetemcomitans and Porphyromonas gingivalis.* Arterioscler Thromb Vasc Biol, 2005. **25**(3): p. e17-8.
4. Kroes, I., P.W. Lepp, and D.A. Relman, *Bacterial diversity within the human subgingival crevice.* Proc Natl Acad Sci U S A, 1999. **96**(25): p. 14547-52.
5. Paster, B.J., et al., *Bacterial diversity in human subgingival plaque.* J Bacteriol, 2001. **183**(12): p. 3770-83.
6. Bergey, D.H., N.R. Krieg, and J.G. Holt, *Bergey's manual of systematic bacteriology*. 1984, Baltimore: Williams & Wilkins. 4 v. (xxvii, 2648 p.).
7. Brown, S.A. and M. Whiteley, *A novel exclusion mechanism for carbon resource partitioning in Aggregatibacter actinomycetemcomitans.* J Bacteriol, 2007. **189**(17): p. 6407-14.
8. Biswas, S., D.F. Duperon, and F.S. Chebib, *Study of crevice fluid in relation to periodontal disease in children. II. Effect of age, sex and gingival inflammation on crevice fluid protein, carbohydrate, total calcium, phosphate and nitrogen.* J Periodontal Res, 1977. **12**(4): p. 265-78.
9. Ohta, H., K. Fukui, and K. Kato, *Effect of bicarbonate on the growth of Actinobacillus actinomycetemcomitans in anaerobic fructose-limited chemostat culture.* J Gen Microbiol, 1989. **135**(12): p. 3485-95.
10. Courts, F.J., et al., *Detection of functional complement components in gingival crevicular fluid from humans with periodontal diseases.* J Dent Res, 1977. **56**(3): p. 327-31.
11. Nathan, C.F., et al., *Extracellular cytolysis by activated macrophages and granulocytes. II. Hydrogen peroxide as a mediator of cytotoxicity.* J Exp Med, 1979. **149**(1): p. 100-13.
12. Thomson, V.J., et al., *Direct selection of IS903 transposon insertions by use of a broad-host-range vector: isolation of catalase-deficient mutants of Actinobacillus actinomycetemcomitans.* J Bacteriol, 1999. **181**(23): p. 7298-307.
13. Miyasaki, K.T., et al., *Oxidative and nonoxidative killing of Actinobacillus actinomycetemcomitans by human neutrophils.* Infect Immun, 1986. **53**(1): p. 154-60.
14. Genco, R.J. and J. Slots, *Host responses in periodontal diseases.* J Dent Res, 1984. **63**(3): p. 441-51.

15. Jenkinson, H.F. and R.J. Lamont, *Oral microbial communities in sickness and in health.* Trends Microbiol, 2005. **13**(12): p. 589-95.
16. Fine, D.H., et al., *How we got attached to Actinobacillus actinomycetemcomitans: A model for infectious diseases.* Periodontol 2000, 2006. **42**: p. 114-57.
17. Kaplan, J.B., et al., *Genes involved in the synthesis and degradation of matrix polysaccharide in Actinobacillus actinomycetemcomitans and Actinobacillus pleuropneumoniae biofilms.* J Bacteriol, 2004. **186**(24): p. 8213-20.
18. Chhatwal, R.H.a.S., *Molecular Biology of Streptococci*. 2007, Wymondham, U.K: Horizon Scientific Press.
19. Barnard, J.P. and M.W. Stinson, *Influence of environmental conditions on hydrogen peroxide formation by Streptococcus gordonii.* Infect Immun, 1999. **67**(12): p. 6558-64.
20. Kolenbrander, P.E., et al., *Communication among oral bacteria.* Microbiol Mol Biol Rev, 2002. **66**(3): p. 486-505, table of contents.
21. Costerton, J.W., P.S. Stewart, and E.P. Greenberg, *Bacterial biofilms: a common cause of persistent infections.* Science, 1999. **284**(5418): p. 1318-22.
22. Martinez, L.R. and A. Casadevall, *Cryptococcus neoformans cells in biofilms are less susceptible than planktonic cells to antimicrobial molecules produced by the innate immune system.* Infect Immun, 2006. **74**(11): p. 6118-23.
23. Singh, P.K., et al., *A component of innate immunity prevents bacterial biofilm development.* Nature, 2002. **417**(6888): p. 552-5.
24. Walker, T.S., et al., *Enhanced Pseudomonas aeruginosa biofilm development mediated by human neutrophils.* Infect Immun, 2005. **73**(6): p. 3693-701.
25. Suzuki, T., et al., *Presence of activated eosinophils, high IgE and sCD23 titers in gingival crevicular fluid of patients with adult periodontitis.* J Periodontal Res, 1995. **30**(3): p. 159-66.
26. Burmolle, M., et al., *Enhanced biofilm formation and increased resistance to antimicrobial agents and bacterial invasion are caused by synergistic interactions in multispecies biofilms.* Appl Environ Microbiol, 2006. **72**(6): p. 3916-23.
27. Whiteley, M., et al., *Gene expression in Pseudomonas aeruginosa biofilms.* Nature, 2001. **413**(6858): p. 860-4.
28. Egland, P.G., R.J. Palmer, Jr., and P.E. Kolenbrander, *Interspecies communication in Streptococcus gordonii-Veillonella atypica biofilms: signaling in flow conditions requires juxtaposition.* Proc Natl Acad Sci U S A, 2004. **101**(48): p. 16917-22.
29. Yang, H.W., et al., *Relationship of Actinobacillus actinomycetemcomitans serotypes to periodontal condition: prevalence and proportions in subgingival plaque.* Eur J Oral Sci, 2005. **113**(1): p. 28-33.
30. Asakawa, R., et al., *Outer membrane protein 100, a versatile virulence factor of Actinobacillus actinomycetemcomitans.* Mol Microbiol, 2003. **50**(4): p. 1125-39.
31. Ramsey, M.M. and M. Whiteley, *Polymicrobial interactions stimulate resistance to host innate immunity through metabolite perception.* Proc Natl Acad Sci U S A, 2009. **106**(5): p. 1578-83.

32. Kraig, E., T. Dailey, and D. Kolodrubetz, *Nucleotide sequence of the leukotoxin gene from Actinobacillus actinomycetemcomitans: homology to the alpha-hemolysin/leukotoxin gene family.* Infect Immun, 1990. **58**(4): p. 920-9.
33. Haubek, D., et al., *Early-onset periodontitis in Morocco is associated with the highly leukotoxic clone of Actinobacillus actinomycetemcomitans.* J Dent Res, 2001. **80**(6): p. 1580-3.
34. Socransky, S.S., et al., *Microbial complexes in subgingival plaque.* J Clin Periodontol, 1998. **25**(2): p. 134-44.
35. Chen, Z., et al., *Purification and characterization of a 50-kDa cysteine proteinase (gingipain) from Porphyromonas gingivalis.* J Biol Chem, 1992. **267**(26): p. 18896-901.
36. Nakayama, K., et al., *Construction and characterization of arginine-specific cysteine proteinase (Arg-gingipain)-deficient mutants of Porphyromonas gingivalis. Evidence for significant contribution of Arg-gingipain to virulence.* J Biol Chem, 1995. **270**(40): p. 23619-26.
37. Nelson, D., et al., *Purification and characterization of a novel cysteine proteinase (periodontain) from Porphyromonas gingivalis. Evidence for a role in the inactivation of human alpha1-proteinase inhibitor.* J Biol Chem, 1999. **274**(18): p. 12245-51.
38. Jansen, H.J., D. Grenier, and J.S. Van der Hoeven, *Characterization of immunoglobulin G-degrading proteases of Prevotella intermedia and Prevotella nigrescens.* Oral Microbiol Immunol, 1995. **10**(3): p. 138-45.
39. Labbe, S. and D. Grenier, *Characterization of the human immunoglobulin G Fc-binding activity in Prevotella intermedia.* Infect Immun, 1995. **63**(7): p. 2785-9.
40. Kreth, J., et al., *Competition and coexistence between Streptococcus mutans and Streptococcus sanguinis in the dental biofilm.* J Bacteriol, 2005. **187**(21): p. 7193-203.
41. Noble, R.W. and Q.H. Gibson, *The reaction of ferrous horseradish peroxidase with hydrogen peroxide.* J Biol Chem, 1970. **245**(9): p. 2409-13.
42. Wang, X., et al., *A Novel Hydrogen Peroxide Biosensor Based on the Synergistic Effect of Gold-Platinum Alloy Nanoparticles/Polyaniline Nanotube/Chitosan Nanocomposite Membrane.* Electroanalysis, 2009. **21**(7): p. 819-825.
43. Mao, L., et al., *Continuous on-line measurement of cerebral hydrogen peroxide using enzyme-modified ring-disk plastic carbon film electrode.* Anal Chem, 2002. **74**(15): p. 3684-9.
44. Liu, X. and J.L. Zweier, *A real-time electrochemical technique for measurement of cellular hydrogen peroxide generation and consumption: evaluation in human polymorphonuclear leukocytes.* Free Radic Biol Med, 2001. **31**(7): p. 894-901.
45. Horrocks, B.R., et al., *Scanning electrochemical microscopy. 24. Enzyme ultramicroelectrodes for the measurement of hydrogen peroxide at surfaces.* Anal Chem, 1993. **65**(24): p. 3605-14.
46. Wittstock, G. and W. Schuhmann, *Formation and Imaging of Microscopic Enzymatically Active Spots on an Alkanethiolate-Covered Gold Electrode by*

Scanning Electrochemical Microscopy. Analytical Chemistry, 1997. **69**(24): p. 5059-5066.
47. Wilhelm, T. and G. Wittstock, *Analysis of interaction in patterned multienzyme layers by using scanning electrochemical microscopy.* Angew Chem Int Ed Engl, 2003. **42**(20): p. 2248-50.
48. Liu, X., et al., *Real-time mapping of a hydrogen peroxide concentration profile across a polymicrobial bacterial biofilm using scanning electrochemical microscopy.* Proc Natl Acad Sci U S A, 2011. **108**(7): p. 2668-73.
49. Ebersole, J.L., D. Cappelli, and M.N. Sandoval, *Subgingival distribution of A. actinomycetemcomitans in periodontitis.* J Clin Periodontol, 1994. **21**(2): p. 65-75.
50. Ficara, A.J., et al., *A comparison of the glucose and protein content of gingival fluid from diabetics and nondiabetics.* J Periodontal Res, 1975. **10**(3): p. 171-5.
51. Marcotte, H. and M.C. Lavoie, *Oral microbial ecology and the role of salivary immunoglobulin A.* Microbiol Mol Biol Rev, 1998. **62**(1): p. 71-109.
52. Yamaguchi, M., et al., *Non-invasive monitoring of gingival crevicular fluid for estimation of blood glucose level.* Med Biol Eng Comput, 2004. **42**(3): p. 322-7.
53. Loesche, W.J., et al., *Relationship between oxygen tension and subgingival bacterial flora in untreated human periodontal pockets.* Infect Immun, 1983. **42**(2): p. 659-67.
54. Ohta, H., et al., *Microaerophilic property of Actinobacillus actinomycetemcomitans in fructose-limited chemostat cultures.* FEMS Microbiol. Lett., 1996. **136**: p. 191-196.
55. Syed, S.A. and W.J. Loesche, *Bacteriology of human experimental gingivitis: effect of plaque age.* Infect Immun, 1978. **21**(3): p. 821-9.
56. Hillman, J.D. and M. Shivers, *Interaction between wild-type, mutant and revertant forms of the bacterium Streptococcus sanguis and the bacterium Actinobacillus actinomycetemcomitans in vitro and in the gnotobiotic rat.* Arch Oral Biol, 1988. **33**(6): p. 395-401.
57. Mintz, K.P. and P.M. Fives-Taylor, *impA, a gene coding for an inner membrane protein, influences colonial morphology of Actinobacillus actinomycetemcomitans.* Infect Immun, 2000. **68**(12): p. 6580-6.
58. Ausubel, F.M., *Short protocols in molecular biology : a compendium of methods from Current protocols in molecular biology*. 5th ed. 2002, New York: Wiley. 2 v. (various pagings).
59. Ramsey, M.M. and M. Whiteley, *Pseudomonas aeruginosa attachment and biofilm development in dynamic environments.* Mol Microbiol, 2004. **53**(4): p. 1075-87.
60. Schuster, M., et al., *Identification, timing, and signal specificity of Pseudomonas aeruginosa quorum-controlled genes: a transcriptome analysis.* J Bacteriol, 2003. **185**(7): p. 2066-79.

61. Lloyd, A.L., B.J. Marshall, and B.J. Mee, *Identifying cloned Helicobacter pylori promoters by primer extension using a FAM-labelled primer and GeneScan analysis.* J Microbiol Methods, 2005. **60**(3): p. 291-8.
62. Frackman, S., M. Anhalt, and K.H. Nealson, *Cloning, organization, and expression of the bioluminescence genes of Xenorhabdus luminescens.* J Bacteriol, 1990. **172**(10): p. 5767-73.
63. Galli, D.M., J.L. Polan-Curtain, and D.J. LeBlanc, *Structural and segregational stability of various replicons in Actinobacillus actinomycetemcomitans.* Plasmid, 1996. **36**(1): p. 42-8.
64. Sreenivasan, P.K., et al., *Transformation of Actinobacillus actinomycetemcomitans by electroporation, utilizing constructed shuttle plasmids.* Infect Immun, 1991. **59**(12): p. 4621-7.
65. Mintz, K.P., C. Brissette, and P.M. Fives-Taylor, *A recombinase A-deficient strain of Actinobacillus actinomycetemcomitans constructed by insertional mutagenesis using a mobilizable plasmid.* FEMS Microbiol Lett, 2002. **206**(1): p. 87-92.
66. Fong, K.P., L. Gao, and D.R. Demuth, *luxS and arcB control aerobic growth of Actinobacillus actinomycetemcomitans under iron limitation.* Infect Immun, 2003. **71**(1): p. 298-308.
67. Yue, G., et al., *A second Aggregatibacter actinomycetemcomitans autotransporter adhesin exhibits specificity for buccal epithelial cells in humans and Old World primates.* Infect Immun, 2007. **75**(9): p. 4440-8.
68. Wang, Q., et al., *Sensing wetness: a new role for the bacterial flagellum.* EMBO J, 2005. **24**(11): p. 2034-42.
69. Christensen, B.B., et al., *Molecular tools for study of biofilm physiology.* Methods Enzymol, 1999. **310**: p. 20-42.
70. Walters, M.C., 3rd, et al., *Contributions of antibiotic penetration, oxygen limitation, and low metabolic activity to tolerance of Pseudomonas aeruginosa biofilms to ciprofloxacin and tobramycin.* Antimicrob Agents Chemother, 2003. **47**(1): p. 317-23.
71. Chang, W., et al., *Global transcriptome analysis of Staphylococcus aureus response to hydrogen peroxide.* J Bacteriol, 2006. **188**(4): p. 1648-59.
72. Mostertz, J., et al., *Transcriptome and proteome analysis of Bacillus subtilis gene expression in response to superoxide and peroxide stress.* Microbiology, 2004. **150**(Pt 2): p. 497-512.
73. Palma, M., et al., *Transcriptome analysis of the response of Pseudomonas aeruginosa to hydrogen peroxide.* J Bacteriol, 2004. **186**(1): p. 248-52.
74. Stohl, E.A., A.K. Criss, and H.S. Seifert, *The transcriptome response of Neisseria gonorrhoeae to hydrogen peroxide reveals genes with previously uncharacterized roles in oxidative damage protection.* Mol Microbiol, 2005. **58**(2): p. 520-32.
75. Zeller, T., et al., *Transcriptome and physiological responses to hydrogen peroxide of the facultatively phototrophic bacterium Rhodobacter sphaeroides.* J Bacteriol, 2005. **187**(21): p. 7232-42.

76. Zheng, M., et al., *DNA microarray-mediated transcriptional profiling of the Escherichia coli response to hydrogen peroxide.* J Bacteriol, 2001. **183**(15): p. 4562-70.
77. Komatsuzawa, H., et al., *Identification of six major outer membrane proteins from Actinobacillus actinomycetemcomitans.* Gene, 2002. **288**(1-2): p. 195-201.
78. El Tahir, Y. and M. Skurnik, *YadA, the multifaceted Yersinia adhesin.* Int J Med Microbiol, 2001. **291**(3): p. 209-18.
79. Zheng, M., F. Aslund, and G. Storz, *Activation of the OxyR transcription factor by reversible disulfide bond formation.* Science, 1998. **279**(5357): p. 1718-21.
80. Hishinuma, S., et al., *OxyR regulated the expression of two major catalases, KatA and KatB, along with peroxiredoxin, AhpC in Pseudomonas putida.* Environ Microbiol, 2006. **8**(12): p. 2115-24.
81. Toledano, M.B., et al., *Redox-dependent shift of OxyR-DNA contacts along an extended DNA-binding site: a mechanism for differential promoter selection.* Cell, 1994. **78**(5): p. 897-909.
82. Sugita, N., et al., *Differential expression of CR3, Fc epsilon RII and Fc gamma RIII on polymorphonuclear leukocytes in gingival crevicular fluid.* J Periodontal Res, 1993. **28**(5): p. 363-72.
83. Neeleman, C., et al., *Resistance to both complement activation and phagocytosis in type 3 pneumococci is mediated by the binding of complement regulatory protein factor H.* Infect Immun, 1999. **67**(9): p. 4517-24.
84. Hoffmann, O.M., D. Becker, and J.R. Weber, *Bacterial hydrogen peroxide contributes to cerebral hyperemia during early stages of experimental pneumococcal meningitis.* J Cereb Blood Flow Metab, 2007. **27**(11): p. 1792-7.
85. Duane, P.G., et al., *Identification of hydrogen peroxide as a Streptococcus pneumoniae toxin for rat alveolar epithelial cells.* Infect Immun, 1993. **61**(10): p. 4392-7.
86. Takeuchi, O., et al., *Differential roles of TLR2 and TLR4 in recognition of gram-negative and gram-positive bacterial cell wall components.* Immunity, 1999. **11**(4): p. 443-51.
87. Kruidenier, L. and H.W. Verspaget, *Review article: oxidative stress as a pathogenic factor in inflammatory bowel disease--radicals or ridiculous?* Aliment Pharmacol Ther, 2002. **16**(12): p. 1997-2015.
88. Boveris, A. and B. Chance, *The mitochondrial generation of hydrogen peroxide. General properties and effect of hyperbaric oxygen.* Biochem J, 1973. **134**(3): p. 707-16.
89. Boveris, A., N. Oshino, and B. Chance, *The cellular production of hydrogen peroxide.* Biochem J, 1972. **128**(3): p. 617-30.
90. Root, R.K., et al., *H2O2 release from human granulocytes during phagocytosis. I. Documentation, quantitation, and some regulating factors.* J Clin Invest, 1975. **55**(5): p. 945-55.
91. Finlay, B.B. and R.E. Hancock, *Can innate immunity be enhanced to treat microbial infections?* Nat Rev Microbiol, 2004. **2**(6): p. 497-504.

92. Brown, S.A., K.L. Palmer, and M. Whiteley, *Revisiting the host as a growth medium.* Nat Rev Microbiol, 2008. **6**(9): p. 657-66.
93. Brouqui, P. and D. Raoult, *Endocarditis due to rare and fastidious bacteria.* Clin Microbiol Rev, 2001. **14**(1): p. 177-207.
94. Kuramitsu, H.K., et al., *Interspecies interactions within oral microbial communities.* Microbiol Mol Biol Rev, 2007. **71**(4): p. 653-70.
95. Bakaletz, L.O., *Developing animal models for polymicrobial diseases.* Nat Rev Microbiol, 2004. **2**(7): p. 552-68.
96. Dietrich, L.E., et al., *The phenazine pyocyanin is a terminal signalling factor in the quorum sensing network of Pseudomonas aeruginosa.* Mol Microbiol, 2006. **61**(5): p. 1308-21.
97. Ciantar, M., et al., *Development of an in vitro microassay for glucose quantification in submicrolitre volumes of biological fluid.* J Periodontal Res, 2002. **37**(2): p. 79-85.
98. Serra, E., et al., *Lactate dehydrogenase activity in gingival crevicular fluid during orthodontic treatment.* Am J Orthod Dentofacial Orthop, 2003. **124**(2): p. 206-11.
99. Lamster, I.B., et al., *Evaluation and modification of spectrophotometric procedures for analysis of lactate dehydrogenase, beta-glucuronidase and arylsulphatase in human gingival crevicular fluid collected with filter-paper strips.* Arch Oral Biol, 1985. **30**(3): p. 235-42.
100. Bergey, D.H., *Bergey's Manual of Determinitive Bacteriology*. 9th Edition ed, ed. J.G. Holt. 1994, Baltimore: Williams & Wilkins.
101. Dzink, J.L., et al., *Gram negative species associated with active destructive periodontal lesions.* J Clin Periodontol, 1985. **12**(8): p. 648-59.
102. Kreth, J., J. Merritt, and F. Qi, *Bacterial and host interactions of oral streptococci.* DNA Cell Biol, 2009. **28**(8): p. 397-403.
103. Moore, W.E., et al., *Bacteriology of severe periodontitis in young adult humans.* Infect Immun, 1982. **38**(3): p. 1137-48.
104. Cook, G.S., J.W. Costerton, and R.J. Lamont, *Biofilm formation by Porphyromonas gingivalis and Streptococcus gordonii.* J Periodontal Res, 1998. **33**(6): p. 323-7.
105. Kononen, E., et al., *Population-based study of salivary carriage of periodontal pathogens in adults.* J Clin Microbiol, 2007. **45**(8): p. 2446-51.
106. Sirinian, G., et al., *Periodontopathic bacteria in young healthy subjects of different ethnic backgrounds in Los Angeles.* J Periodontol, 2002. **73**(3): p. 283-8.
107. Kreth, J., Y. Zhang, and M.C. Herzberg, *Streptococcal Antagonism In Oral Biofilms: Streptococcus sanguinis and Streptococcus gordonii interference with Streptococcus mutans.* J Bacteriol, 2008.
108. Kovach, M.E., et al., *Four new derivatives of the broad-host-range cloning vector pBBR1MCS, carrying different antibiotic-resistance cassettes.* Gene, 1995. **166**(1): p. 175-6.
109. Ho, S.N., et al., *Site-directed mutagenesis by overlap extension using the polymerase chain reaction.* Gene, 1989. **77**(1): p. 51-9.

110. Talasniemi, J.P., et al., *Analytical investigation: assay of D-lactate in diabetic plasma and urine.* Clin Biochem, 2008. **41**(13): p. 1099-103.
111. Mastropaolo, M.D., et al., *Synergy in polymicrobial infections in a mouse model of type 2 diabetes.* Infect Immun, 2005. **73**(9): p. 6055-63.
112. Nuttall, F.Q., M.A. Khan, and M.C. Gannon, *Peripheral glucose appearance rate following fructose ingestion in normal subjects.* Metabolism, 2000. **49**(12): p. 1565-71.
113. Brown, S.A. and M. Whiteley, *Characterization of the L-lactate dehydrogenase from Aggregatibacter actinomycetemcomitans.* PLoS One, 2009. **4**(11): p. e7864.
114. Kolenbrander, P., *The genus Veillonella*, in *The Prokaryotes*, M. Dworkin, Editor. 2006, Springer New York. p. 1022-1040.
115. Chen, C., et al., *Genome sequence of Aggregatibacter actinomycetemcomitans serotype c strain D11S-1.* J Bacteriol, 2009. **191**(23): p. 7378-9.
116. Chen, C., et al., *Genome sequence of naturally competent Aggregatibacter actinomycetemcomitans serotype a strain D7S-1.* J Bacteriol, 2010. **192**(10): p. 2643-4.
117. Kaplan, A.H., et al., *Infection due to Actinobacillus actinomycetemcomitans: 15 cases and review.* Rev Infect Dis, 1989. **11**(1): p. 46-63.
118. Ebersole, J.L., et al., *Comparative virulence of periodontopathogens in a mouse abscess model.* Oral Dis, 1995. **1**(3): p. 115-28.
119. Kesavalu, L., S.C. Holt, and J.L. Ebersole, *Virulence of a polymicrobic complex, Treponema denticola and Porphyromonas gingivalis, in a murine model.* Oral Microbiol Immunol, 1998. **13**(6): p. 373-7.
120. Nagashima, H., A. Takao, and N. Maeda, *Abscess forming ability of streptococcus milleri group: synergistic effect with Fusobacterium nucleatum.* Microbiol Immunol, 1999. **43**(3): p. 207-16.
121. Chen, P.B., et al., *Host responses induced by co-infection with Porphyromonas gingivalis and Actinobacillus actinomycetemcomitans in a murine model.* Oral Microbiol Immunol, 1996. **11**(4): p. 274-81.
122. Periasamy, S. and P.E. Kolenbrander, *Aggregatibacter actinomycetemcomitans builds mutualistic biofilm communities with Fusobacterium nucleatum and Veillonella species in saliva.* Infect Immun, 2009. **77**(9): p. 3542-51.
123. Schultz, J.E. and J.A. Breznak, *Cross-Feeding of Lactate Between Streptococcus lactis and Bacteroides sp. Isolated from Termite Hindguts.* Appl Environ Microbiol, 1979. **37**(6): p. 1206-10.
124. Kesavalu, L., et al., *Rat model of polymicrobial infection, immunity, and alveolar bone resorption in periodontal disease.* Infect Immun, 2007. **75**(4): p. 1704-12.
125. Fine, D.H., et al., *Colonization and persistence of rough and smooth colony variants of Actinobacillus actinomycetemcomitans in the mouths of rats.* Arch Oral Biol, 2001. **46**(11): p. 1065-78.
126. Fine, D.H., et al., *Tenacious adhesion of Actinobacillus actinomycetemcomitans strain CU1000 to salivary-coated hydroxyapatite.* Arch Oral Biol, 1999. **44**(12): p. 1063-76.

127. Han, G., et al., *Nitric oxide releasing nanoparticles are therapeutic for Staphylococcus aureus abscesses in a murine model of infection.* PLoS One, 2009. **4**(11): p. e7804.
128. Fetiye, K., et al., *Comparison in a rat thigh abscess model of imipenem, meropenem and cefoperazone-sulbactam against Acinetobacter baumannii strains in terms of bactericidal efficacy and resistance selection.* Ann Clin Microbiol Antimicrob, 2004. **3**: p. 2.
129. Dworkin, M. and S. Falkow, *The prokaryotes : a handbook on the biology of bacteria*. 3rd ed. 2006, New York ; [London]: Springer. v. < 1-6 >.
130. Yamada, H., E. Takashima, and K. Konishi, *Molecular characterization of the membrane-bound quinol peroxidase functionally connected to the respiratory chain.* FEBS J, 2007. **274**(3): p. 853-66.
131. De Stoppelaar, J.D., J. Van Houte, and O. Backer Dirks, *The relationship between extracellular polysaccharide-producing streptococci and smooth surface caries in 13-year-old children.* Caries Res, 1969. **3**(2): p. 190-9.
132. Jakubovics, N.S., et al., *Role of hydrogen peroxide in competition and cooperation between Streptococcus gordonii and Actinomyces naeslundii.* FEMS Microbiol Ecol, 2008. **66**(3): p. 637-44.
133. Garcia-Mendoza, A., et al., *Evaluation of the capacity of oral streptococci to produce hydrogen peroxide.* J Med Microbiol, 1993. **39**(6): p. 434-9.
134. Seki, M., et al., *Hydrogen peroxide production in Streptococcus pyogenes: involvement of lactate oxidase and coupling with aerobic utilization of lactate.* J Bacteriol, 2004. **186**(7): p. 2046-51.
135. Bard, A.J. and M.V. Mirkin, *Scanning electrochemical microscopy*. 2001, New York: Marcel Dekker. x, 650 p.
136. Zhan, D., et al., *Scanning electrochemical microscopy. 58. Application of a micropipet-supported ITIES tip to detect Ag+ and study its effect on fibroblast cells.* Anal Chem, 2007. **79**(14): p. 5225-31.
137. Nunes Kirchner, C., M. Trauble, and G. Wittstock, *Diffusion and reaction in microbead agglomerates.* Anal Chem, 2010. **82**(7): p. 2626-35.
138. Cai, C., et al., *Scanning electrochemical microscopy of living cells. 3. Rhodobacter sphaeroides.* Anal Chem, 2002. **74**(1): p. 114-9.
139. Liu, B., S.A. Rotenberg, and M.V. Mirkin, *Scanning electrochemical microscopy of living cells: different redox activities of nonmetastatic and metastatic human breast cells.* Proc Natl Acad Sci U S A, 2000. **97**(18): p. 9855-60.
140. Fan, F.R. and A.J. Bard, *Imaging of biological macromolecules on mica in humid air by scanning electrochemical microscopy.* Proc Natl Acad Sci U S A, 1999. **96**(25): p. 14222-7.
141. Zhan, D., F.R. Fan, and A.J. Bard, *The Kv channel blocker 4-aminopyridine enhances Ag+ uptake: a scanning electrochemical microscopy study of single living cells.* Proc Natl Acad Sci U S A, 2008. **105**(34): p. 12118-22.

142. Anderl, J.N., M.J. Franklin, and P.S. Stewart, *Role of antibiotic penetration limitation in Klebsiella pneumoniae biofilm resistance to ampicillin and ciprofloxacin.* Antimicrob Agents Chemother, 2000. **44**(7): p. 1818-24.
143. Bard, A.J., *Effect of Electrode Configuration and Transition Time in Solid Electrode Chronopotentiometry.* Analytical Chemistry, 1961. **33**(1): p. 11-15.
144. Fuqua, C., S.C. Winans, and E.P. Greenberg, *Census and consensus in bacterial ecosystems: the LuxR-LuxI family of quorum-sensing transcriptional regulators.* Annu Rev Microbiol, 1996. **50**: p. 727-51.
145. Miller, M.B. and B.L. Bassler, *Quorum sensing in bacteria.* Annu Rev Microbiol, 2001. **55**: p. 165-99.
146. Schaechter, M., *Encyclopedia of microbiology*. 3rd ed. 2009, Amsterdam ; Boston: Elsevier/Academic Press.
147. Taga, M.E. and B.L. Bassler, *Chemical communication among bacteria.* Proc Natl Acad Sci U S A, 2003. **100 Suppl 2**: p. 14549-54.
148. Banin, E., M.L. Vasil, and E.P. Greenberg, *Iron and Pseudomonas aeruginosa biofilm formation.* Proc Natl Acad Sci U S A, 2005. **102**(31): p. 11076-81.
149. Price-Whelan, A., L.E. Dietrich, and D.K. Newman, *Pyocyanin alters redox homeostasis and carbon flux through central metabolic pathways in Pseudomonas aeruginosa PA14.* J Bacteriol, 2007. **189**(17): p. 6372-81.
150. Ma, L., et al., *Assembly and development of the Pseudomonas aeruginosa biofilm matrix.* PLoS Pathog, 2009. **5**(3): p. e1000354.
151. O'Toole, G.A. and R. Kolter, *Flagellar and twitching motility are necessary for Pseudomonas aeruginosa biofilm development.* Mol Microbiol, 1998. **30**(2): p. 295-304.
152. Price-Whelan, A., L.E. Dietrich, and D.K. Newman, *Rethinking 'secondary' metabolism: physiological roles for phenazine antibiotics.* Nat Chem Biol, 2006. **2**(2): p. 71-8.
153. West, S.A., et al., *The Social Lives of Microbes.* Annual Review of Ecology, Evolution and Systematics, 2007. **38**: p. 53-77.
154. Pierson, L.S., 3rd and E.A. Pierson, *Metabolism and function of phenazines in bacteria: impacts on the behavior of bacteria in the environment and biotechnological processes.* Appl Microbiol Biotechnol, 2010. **86**(6): p. 1659-70.
155. Mentel, M., et al., *Of two make one: the biosynthesis of phenazines.* Chembiochem, 2009. **10**(14): p. 2295-304.
156. Hassan, H.M. and I. Fridovich, *Mechanism of the antibiotic action pyocyanine.* J Bacteriol, 1980. **141**(1): p. 156-63.
157. Fordos, M.-J., *Recherches sur la matiere colorante des suppurations bleues: pyocyanine.* Comptes rendus hebdomadaires des séances del'Académie des sciences, 1860. **51**: p. 215-217.
158. Newman, D.K. and R. Kolter, *A role for excreted quinones in extracellular electron transfer.* Nature, 2000. **405**(6782): p. 94-7.

159. Wangt, Y. and D.K. Newman, *Redox reactions of phenazine antibiotics with ferric (hydr)oxides and molecular oxygen.* Environ Sci Technol, 2008. **42**(7): p. 2380-6.
160. Cox, C.D., *Role of pyocyanin in the acquisition of iron from transferrin.* Infect Immun, 1986. **52**(1): p. 263-70.
161. Sokol, P.A. and D.E. Woods, *Relationship of iron and extracellular virulence factors to Pseudomonas aeruginosa lung infections.* J Med Microbiol, 1984. **18**(1): p. 125-33.
162. Bearden, S.W. and R.D. Perry, *The Yfe system of Yersinia pestis transports iron and manganese and is required for full virulence of plague.* Mol Microbiol, 1999. **32**(2): p. 403-14.
163. Velayudhan, J., et al., *Iron acquisition and virulence in Helicobacter pylori: a major role for FeoB, a high-affinity ferrous iron transporter.* Mol Microbiol, 2000. **37**(2): p. 274-86.
164. Mashburn, L.M., et al., *Staphylococcus aureus serves as an iron source for Pseudomonas aeruginosa during in vivo coculture.* J Bacteriol, 2005. **187**(2): p. 554-66.
165. Liberati, N.T., et al., *An ordered, nonredundant library of Pseudomonas aeruginosa strain PA14 transposon insertion mutants.* Proc Natl Acad Sci U S A, 2006. **103**(8): p. 2833-8.
166. Connell, J.L., et al., *Probing prokaryotic social behaviors with bacterial "lobster traps".* MBio, 2010. **1**(4).
167. Viollier, E., et al., *The ferrozine method revisited: Fe(II)/Fe(III) determination in natural waters.* Applied Geochemistry, 2000. **15**(6): p. 785-790.
168. Price-Whelan, A., *Physiology and mechanisms of pyocyanin reduction in Pseudomonas aeruginosa*, in *Biology*. 2009, California Institute of Technology: Pasadena, CA.
169. Palmer, K.L., S.A. Brown, and M. Whiteley, *Membrane-bound nitrate reductase is required for anaerobic growth in cystic fibrosis sputum.* J Bacteriol, 2007. **189**(12): p. 4449-55.
170. Schertzer, J.W., S.A. Brown, and M. Whiteley, *Oxygen levels rapidly modulate Pseudomonas aeruginosa social behaviours via substrate limitation of PqsH.* Mol Microbiol, 2010. **77**(6): p. 1527-38.
171. Wang, Y., et al., *Phenazine-1-carboxylic acid promotes bacterial biofilm development via ferrous iron acquisition.* J Bacteriol, 2011.